



UNIVERSIDAD DE INVESTIGACIÓN DE TECNOLOGÍA EXPERIMENTAL YACHAY

Escuela de Ciencias Físicas y Nanotecnología

**TÍTULO: *Ab initio* studies of bulk and (001)
surfaces of the metal halide double perovskite
 $\text{Cs}_2\text{Au}_2\text{Cl}_6$**

Trabajo de integración curricular presentado como requisito para
la obtención del título de Físico

Autor:

Vizcaino Rojas Anthony Myron

Tutor:

Ph. D. Pinto Esparza Henry

Urcuquí, Octubre 2022

Urququí, 6 de septiembre de 2022

SECRETARÍA GENERAL
ESCUELA DE CIENCIAS FÍSICAS Y NANOTECNOLOGÍA
CARRERA DE FÍSICA
ACTA DE DEFENSA No. UITEY-PHY-2022-00020-AD

En la ciudad de San Miguel de Urququí, Provincia de Imbabura, a los 6 días del mes de septiembre de 2022, a las 10:00 horas, en el Aula S_CAN de la Universidad de Investigación de Tecnología Experimental Yachay y ante el Tribunal Calificador, integrado por los docentes:

Presidente Tribunal de Defensa	Dr. GUEVARA GRANIZO, MARCO VINICIO , Ph.D.
Miembro No Tutor	LAGOS LLAGUNO, DANIEL ALEJANDRO , Ph.D.
Tutor	Dr. PINTO ESPARZA, HENRY PAUL , Ph.D.

Se presenta el(la) señor(ita) estudiante **VIZCAINO ROJAS, ANTHONY MYRON**, con cédula de identidad No. **1004384739**, de la **ESCUELA DE CIENCIAS FÍSICAS Y NANOTECNOLOGÍA**, de la Carrera de **FÍSICA**, aprobada por el Consejo de Educación Superior (CES), mediante Resolución **RPC-SO-39-No.456-2014**, con el objeto de rendir la sustentación de su trabajo de titulación denominado: **Ab initio studies of bulk and (001) surfaces of the metal halide double perovskite Cs₂Au₂Cl₆** , previa a la obtención del título de **FÍSICO/A**.

El citado trabajo de titulación, fue debidamente aprobado por el(los) docente(s):

Tutor	Dr. PINTO ESPARZA, HENRY PAUL , Ph.D.
--------------	---------------------------------------


Y recibió las observaciones de los otros miembros del Tribunal Calificador, las mismas que han sido incorporadas por el(la) estudiante.


Previamente cumplidos los requisitos legales y reglamentarios, el trabajo de titulación fue sustentado por el(la) estudiante y examinado por los miembros del Tribunal Calificador. Escuchada la sustentación del trabajo de titulación, que integró la exposición de el(la) estudiante sobre el contenido de la misma y las preguntas formuladas por los miembros del Tribunal, se califica la sustentación del trabajo de titulación con las siguientes calificaciones:

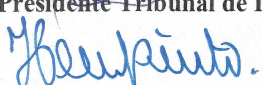
Tipo	Docente	Calificación
Miembro Tribunal De Defensa	LAGOS LLAGUNO, DANIEL ALEJANDRO , Ph.D.	8,0
Presidente Tribunal De Defensa	Dr. GUEVARA GRANIZO, MARCO VINICIO , Ph.D.	9,0
Tutor	Dr. PINTO ESPARZA, HENRY PAUL , Ph.D.	10,0

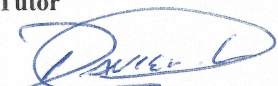
Lo que da un promedio de: **9 (Nueve punto Cero)**, sobre 10 (diez), equivalente a: **APROBADO**


Para constancia de lo actuado, firman los miembros del Tribunal Calificador, el/la estudiante y el/la secretario ad-hoc.


VIZCAINO ROJAS, ANTHONY MYRON
Estudiante


Dr. GUEVARA GRANIZO, MARCO VINICIO , Ph.D.
Presidente Tribunal de Defensa


Dr. PINTO ESPARZA, HENRY PAUL , Ph.D.
Tutor


LAGOS LLAGUNO, DANIEL ALEJANDRO , Ph.D.
Miembro No Tutor


CIFUENTES TAFUR, EVELYN CAROLINA
Secretario Ad-hoc

AUTORÍA

Yo, ANTHONY MYRON VIZCAINO ROJAS, con cédula de identidad 1004384739, declaro que las ideas, juicios, valoraciones, interpretaciones, consultas bibliográficas, definiciones y conceptualizaciones expuestas en el presente trabajo; así cómo, los procedimientos y herramientas utilizadas en la investigación, son de absoluta responsabilidad de la autora del trabajo de integración curricular. Así mismo, me acojo a los reglamentos internos de la Universidad de Investigación de Tecnología Experimental Yachay.

Urcuquí, Octubre 2022.



Anthony Myron Vizcaino Rojas

CI: 1004384739

AUTORIZACIÓN DE PUBLICACIÓN

Yo, ANTHONY MYRON VIZCAINO ROJAS, con cédula de identidad 1004384739, cedo a la Universidad de Investigación de Tecnología Experimental Yachay, los derechos de publicación de la presente obra, sin que deba haber un reconocimiento económico por este concepto. Declaro además que el texto del presente trabajo de titulación no podrá ser cedido a ninguna empresa editorial para su publicación u otros fines, sin contar previamente con la autorización escrita de la Universidad.

Asimismo, autorizo a la Universidad que realice la digitalización y publicación de este trabajo de integración curricular en el repositorio virtual, de conformidad a lo dispuesto en el Art. 144 de la Ley Orgánica de Educación Superior.

Urcuquí, Octubre 2022.

A handwritten signature in blue ink, appearing to read 'Anthony', with a stylized flourish extending to the right.

Anthony Myron Vizcaino Rojas
CI: 1004384739

Acknowledgements

I express my sincere gratitude to my tutor Henry Pinto for being my guide, teacher, and friend during my time at Yachay Tech. Thank you for your unconditional support and for opening the doors to his research group, where I have met great colleagues who inspire me to keep going.

I thank my parents and family, who have always supported me, and motivated me to continue even in difficult times. Finally, I want to thank my closest friends who were along with me on the university path and have been by my side, although our ways have separated. Those memories will always be with me, like when we did homework or other things besides academic responsibilities, like the creation of the AEFN-YT and Optica Student Chapter, where I lived great adventures with extraordinary people.

Thank you very much to all of you!.

Resumen

Las perovskitas son un material que ha adquirido especial importancia en los últimos años debido a sus potenciales aplicaciones en la industria de generación de energía debido a sus propiedades electrónicas; ya existe evidencia de su uso y funcionamiento en esta industria como paneles solares, piezoeléctricos. Actualmente, se está estudiando en profundidad para sacar todo el potencial de este material, ya que existen diferentes tipos de perovskitas para sintetizar e investigar.

Sin embargo, este trabajo se basa en estudios recientes sobre la doble perovskita de halogenuros metálicos $\text{Cs}_2\text{Au}_2\text{Cl}_6$, profundizando en su análisis mediante la construcción de modelos atómicos utilizando su estructura completa y sus estructura con defectos de cloro, que es el átomo más fácil de extraer de este compuesto. Este estudio realiza la descripción de estos modelos atómicos usando la Teoría Funcional de la Densidad con SCAN como funcional para calcular las propiedades electrónicas. Los resultados obtenidos se presentan a través de imágenes de densidad parcial de estados (PDOS) para cada capa con la descripción de la contribución de cada elemento e imágenes STM para los modelos que presentaron banda prohibida. Además, también se presentan imágenes de UPS con la posición de los picos, el cálculo de la función de trabajo y el potencial de ionización de cada modelo de superficie A y B.

Se encontró que de todos los modelos presentados, solo los modelos 14a-2clv, 14b-2clv2B y 14a son aisladores. Todos los demás modelos atómicos muestran un comportamiento metálico en su capa más externa, lo que puede permitir que este material se utilice en futuras aplicaciones tecnológicas.

Palabras Clave: Teoría Funcional de la Densidad, materiales en capas, estructura electrónica, VASP, PDOS, STM, UPS, potencial de ionización, función trabajo

Abstract

Perovskites are a material that has acquired special importance in recent years due to their potential applications in the energy generation industry from renewable resources due to their electronic properties. There is already evidence of their use and operation in this industry as piezoelectric, solar panels. Currently, it is being studied in-depth to get the full potential of this material due to there are different types of perovskites to be synthesized and investigated.

However, this work is based on recent studies on the metal halide double perovskite $\text{Cs}_2\text{Au}_2\text{Cl}_6$, deepening its analysis by building atomic models using its complete structure and its structure with chlorine defects, which is the atom that is easier to extract from this compound. This study performs the description of these atomic models using Density Functional Theory with SCAN as a functional to calculate the electronic properties. The obtained results are presented through images of the partial density of states (PDOS) for each layer with the description of the contribution of each element and STM images for the models that presented band gap. Furthermore, UPS images with the position of the peaks, the work function calculation and the ionization potential of each model surface A and B are also presented.

It was found that of all the models presented, only models l4a-2clv, l4b-2clv2B, and l4a are insulators. All the other atomic models show metallic behaviour in their outermost layer, which may allow this material to be used in future technological applications.

Keywords: Density-Functional Theory, layered materials, electronic structure, VASP, PDOS, STM, UPS, ionization potential, work function

Contents

Acknowledgements	v
Resumen	vii
Abstract	ix
List of Figures	xv
List of Tables	xxi
1 Introduction	1
1.1 Problem Statement	1
1.2 General and Specific Objectives	2
2 Theoretical Background	3
2.1 Many-Body Schrödinger Equation	3
2.2 Atomic Units	5
2.3 The Born-Oppenheimer Approximation	5
2.4 Density Functional Theory	6
2.5 Hohenberg-Kohn theorems	7
2.5.1 Theorem 1: Uniqueness	7
2.5.2 Theorem 2: Variational Principle	7
2.6 Kohn-Sham theory	7
2.7 Exchange-correlation functionals	8
2.8 Vienna ab initio Simulation Package (VASP)	9
2.8.1 Periodic systems and plane waves	9
2.8.2 Cut-off energy E_{cut}	10
2.8.3 K-points Sampling	10
2.8.4 Pseudopotentials	11

2.8.5	The Projector Augmented-Wave (PAW) Method	11
3	Methodology	13
3.1	VASP working principle	13
3.1.1	VASP inputs	13
3.1.2	VASP outputs	14
3.2	Scanning Tunneling Microscopy STM	15
3.3	Tersoff-Hamann approximation	15
3.4	Ultraviolet Photoelectron Spectroscopy UPS	16
3.5	Point Defects in Solids	16
4	Results & Discussion	19
4.1	Bulk metal halide double perovskite $\text{Cs}_2\text{Au}_2\text{Cl}_6$	19
4.2	The $\text{Cs}_2\text{Au}_2\text{Cl}_6$ (001) surface	22
4.3	Four layers thickness surface A (14a)	23
4.3.1	Simulated constant current (STM) images for $\text{Cs}_2\text{Au}_2\text{Cl}_6$ (14a)	25
4.3.2	Simulated Ultraviolet Photoelectron Spectroscopy (UPS)	26
4.3.3	Work Function (ϕ) and Ionization potential	26
4.4	Four layers thickness surface B (14b)	27
4.4.1	Simulated constant current (STM) images for $\text{Cs}_2\text{Au}_2\text{Cl}_6$ (14b)	29
4.4.2	Simulated Ultraviolet Photoelectron Spectroscopy (UPS)	30
4.4.3	Work Function (ϕ)	30
4.5	Chlorine Vacancies for $\text{Cs}_2\text{Au}_2\text{Cl}_6$ surface A	31
4.5.1	Surface A with one chlorine vacancy (14a-clv)	31
4.5.2	Surface A with two chlorine vacancies (14a-2clv)	34
4.5.3	Surface A with one A-type chlorine vacancy at the subsurface (14a-sclvA)	37
4.5.4	Surface A with one B-type chlorine vacancy at the subsurface (14a-sclvB)	40
4.5.5	Vacancy Energy Formation	42
4.5.6	Work Function (ϕ)	43
4.6	Chlorine Vacancies for $\text{Cs}_2\text{Au}_2\text{Cl}_6$ surface B	43
4.6.1	Surface B with one A-type chlorine vacancy (14b-clvA)	44
4.6.2	Surface B with one B-type chlorine vacancy (14b-clvB)	46
4.6.3	Surface B with two A-type chlorine vacancies (14b-2clvA)	49
4.6.4	Surface B with two B-type chlorine vacancies (14b-2clvB)	51
4.6.5	Vacancy Energy Formation	54
4.6.6	Work Function (ϕ)	55
5	Conclusions & Outlook	57

A	Appendix A: Input and output files examples	59
B	Appendix B: Atomic and electronic structure of $\text{Cs}_2\text{Au}_2\text{Cl}_6$ with 6 layers	63
C	Appendix C: Detailed computed PDOS for all the surfaces	67
D	Appendix D: Computed work functions (ϕ) for vacancies	77
	Bibliography	83

List of Figures

3.1	Inelastic mean Free Path for $\text{Cs}_2\text{Au}_2\text{Cl}_6$	16
4.1	Simulated crystal structure of $\text{Cs}_2\text{Au}_2\text{Cl}_6$ perovskite. In this figure, the yellow, green and violet spheres represent the Au, Cl and Cs atoms, respectively. Two gold atoms are not equivalent, the atom identified as Au(1) has a +1 oxidation state, and the atom identified as Au(2) has a +3 oxidation state. The atoms are identified according to the positions presented in Table 4.1. The black line represents the unit cell.	19
4.2	Cut-off energy for bulk $\text{Cs}_2\text{Au}_2\text{Cl}_6$. The energies start to converge at 650 eV, according to the $< 1\text{meV/atom}$ criteria.	20
4.3	k-points mesh convergence for bulk $\text{Cs}_2\text{Au}_2\text{Cl}_6$. The energies begin to converge at $0.035\ 2\pi\text{\AA}^{-1}$ according to the $< 1\text{meV/atom}$ criteria. However, it is possible to use upper k points to get more accurate results.	20
4.4	SCAN computed equation of state for $\text{Cs}_2\text{Au}_2\text{Cl}_6$. The blue line represents the Birch-Murnaghan equation of state fit, and the red dots represent the computed energies' value.	21
4.5	SCAN computed PDOS of bulk $\text{Cs}_2\text{Au}_2\text{Cl}_6$ perovskite. The vertical black line represents the Fermi level shifted to 0 eV. The green, yellow and violet represent respectively the chlorine, gold and cesium contribution. The overlapping result in different shades of purple or yellow represents the contribution of more than one atomic species.	21
4.6	Atomic structure and SCAN computed PDOS for outermost layers of $\text{Cs}_2\text{Au}_2\text{Cl}_6$ surface A (I4a). a) Side view of the atomic structure with four layers, L1 is the surface layer, and L4 is the last layer. It is important to notice that one layer is composed as shown. b) Top view of the surface layer. The black line represents the unit cell. c) PDOS of the outermost layers. The Fermi level is shifted to 0 eV and is represented by the vertical black line. The red lines (1 and 2) represent the range of integrated energies to obtain the STM images.	24

4.7	Computed STM images, line scan and relative height for $\text{Cs}_2\text{Au}_2\text{Cl}_6$ (I4a) surface. These images were computed for a supercell of $2 \times 2 \times 1$, where $V_{bias} = -1.10$ V (left) and $V_{bias} = 1.0$ V (right) correspond to occupied states and in both images is superimposed the top view of the atomic structure of the surface. The red box represents the unit cell, and at the bottom, there is a side view of the atomic structure of the surface. On the sides of the images it is presented in relative height, which was calculated in the diagonal direction	25
4.8	Computed UPS spectrum for $\text{Cs}_2\text{Au}_2\text{Cl}_6$ (I4a) surface using 115 eV photons. The strongest contribution is from the gold and chlorine atoms, which form the largest peak. The Fermi level is shifted to 0 eV and is represented by the vertical black line.	26
4.9	SCAN computed work function for $\text{Cs}_2\text{Au}_2\text{Cl}_6$ surface A (I4a). The blue line represents the average potential in the z-direction, and the horizontal red dotted line is the Fermi level E_F	27
4.10	Work Function and the potential inside the material for $\text{Cs}_2\text{Au}_2\text{Cl}_6$	27
4.11	Atomic structure and SCAN computed PDOS for outermost layers of $\text{Cs}_2\text{Au}_2\text{Cl}_6$ surface B (I4b). a) Side view of the atomic structure with four layers, L1 is the surface layer, and L4 is the last layer. It is important to notice that one layer is composed as shown. b) Top view of the surface layer. The black line represents the unit cell. c) PDOS of the outermost layers. The Fermi level is shifted to 0 eV and is represented by the vertical black line. The red lines (1 and 2) represent the range of integrated energies to obtain the STM images.	28
4.12	Computed STM images, line scan and relative height for $\text{Cs}_2\text{Au}_2\text{Cl}_6$ (I4a) surface (I4b). These images were computed for a supercell of $2 \times 2 \times 1$, where $V_{bias} = -0.85$ V (left) correspond to an occupied state and the $V_{bias} = 1.80$ V (right) is at an unoccupied state. In both images is superimposed the top view of the atomic structure of the surface. The red box represents the unit cell, and at the bottom, there is a side view of the atomic structure of the surface. On the sides of the images it is presented in relative height, which was calculated in the diagonal direction.	29
4.13	Computed UPS spectrum for $\text{Cs}_2\text{Au}_2\text{Cl}_6$ (I4b) surface using 115 eV photons. The strongest contribution is from the gold and chlorine atoms. The Fermi level is shifted to 0 eV and is represented by the vertical black line.	30
4.14	SCAN computed work function for $\text{Cs}_2\text{Au}_2\text{Cl}_6$ surface B (I4b). The blue line represents the average potential in the z-direction, and the horizontal red dotted line is the Fermi level E_F	31
4.15	SCAN computed atomic and electronic structure for outermost layers of $\text{Cs}_2\text{Au}_2\text{Cl}_6$ with four layers of thickness and one chlorine vacancy (I4a-clv). a) Side view of the atomic structure after relaxation, L1 is the surface layer, and L4 is the last layer. b) Top view of the surface. The black line represents the unit cell. c) PDOS of the outermost layers. The Fermi level is shifted to 0 eV and is represented by the vertical black line.	32
4.16	SCAN computed spin-polarized PDOS of the surface layer for $\text{Cs}_2\text{Au}_2\text{Cl}_6$ surface A with one chlorine vacancy (I4a-clv). The Fermi level is shifted to 0 eV and is represented by the vertical black line. . .	33

4.17	Computed UPS spectrum for $\text{Cs}_2\text{Au}_2\text{Cl}_6$ surface A with one chlorine vacancy (14a-clv). The strongest contribution is from the chlorine atoms. The Fermi level is shifted to 0 eV and is represented by the vertical black line.	34
4.18	SCAN computed atomic and electronic structure for outermost layers of $\text{Cs}_2\text{Au}_2\text{Cl}_6$ with four layers of thickness and two chlorine vacancies (14a-2clv). a) Side view of the atomic structure after relaxation, L1 is the surface layer, and L4 is the last layer. b) Top view of the surface. The black line represents the unit cell. c) PDOS of the outermost layers. The Fermi level is shifted to 0 eV and is represented by the vertical black line. The red lines (1 and 2) represent the range of integrated energies to obtain the STM images.	35
4.19	Computed STM images, line scan and relative height for $\text{Cs}_2\text{Au}_2\text{Cl}_6$ (14a-2clv). These images were computed for a supercell of $2 \times 2 \times 1$, where $V_{bias} = -0.35$ V. (left) correspond to an occupied state and the $V_{bias} = 2.4$ V. (right) is at an unoccupied state. In both images is superimposed the top view of the atomic structure of the surface. The red box represents the unit cell, and at the bottom, there is a side view of the atomic structure of the surface. On the sides of the images it is presented in relative height, which was calculated in the diagonal direction.	36
4.20	Computed UPS spectrum for $\text{Cs}_2\text{Au}_2\text{Cl}_6$ surface A with two chlorine vacancies (14a-2clv). The strongest contribution is from the gold and chlorine atoms. The Fermi level is shifted to 0 eV and is represented by the vertical black line.	37
4.21	SCAN computed atomic and electronic structure for outermost layers of $\text{Cs}_2\text{Au}_2\text{Cl}_6$ with four layers of thickness and one chlorine vacancy at the subsurface (14a-sclvA). a) Side view of the atomic structure after relaxation, L1 is the surface layer, and L4 is the last layer. b) Top view of the surface. The black line represents the unit cell. c) PDOS of the outermost layers. The Fermi level is shifted to 0 eV and is represented by the vertical black line.	38
4.22	SCAN computed spin-polarized PDOS of the surface layer for $\text{Cs}_2\text{Au}_2\text{Cl}_6$ surface A with one chlorine vacancy at the subsurface(14a-sclvA). The Fermi level is shifted to 0 eV and is represented by the vertical black line.	39
4.23	Computed UPS spectrum for $\text{Cs}_2\text{Au}_2\text{Cl}_6$ surface A with one chlorine vacancy at the subsurface (14a-sclvA). The strongest contribution is from the gold and chlorine atoms. The Fermi level is shifted to 0 eV and is represented by the vertical black line.	40
4.24	SCAN computed atomic and electronic structure for outermost layers of $\text{Cs}_2\text{Au}_2\text{Cl}_6$ with four layers of thickness and one chlorine vacancy at the subsurface of the case B (14a-sclvB). a) Side view of the atomic structure after relaxation, L1 is the surface layer, and L4 is the last layer. b) Top view of the surface. The black line represents the unit cell. c) PDOS of the outermost layers. The Fermi level is shifted to 0 eV and is represented by the vertical black line.	41
4.25	Computed UPS spectra for $\text{Cs}_2\text{Au}_2\text{Cl}_6$ surface A with one chlorine vacancy at the subsurface (14a-sclvB). The strongest contribution is from the gold and chlorine atoms. The Fermi level is shifted to 0 eV and is represented by the vertical black line.	42

4.26	SCAN computed atomic and electronic structure for outermost layers of $\text{Cs}_2\text{Au}_2\text{Cl}_6$ with four layers of thickness and one chlorine vacancy (l4b-clvA). a) Side view of the atomic structure after relaxation, L1 is the surface layer, and L4 is the last layer. b) Top view of the surface. The black line represents the unit cell. c) PDOS of the outermost layers. The Fermi level is shifted to 0 eV and is represented by the vertical black line.	45
4.27	Computed UPS spectra for $\text{Cs}_2\text{Au}_2\text{Cl}_6$ surface B with one chlorine vacancy at the surface (l4b-clvA). The strongest contribution is from the gold and chlorine atoms. The Fermi level is shifted to 0 eV. and is represented by the vertical black line.	46
4.28	SCAN computed atomic and electronic structure for outermost layers of $\text{Cs}_2\text{Au}_2\text{Cl}_6$ with four layers of thickness and one chlorine vacancy (l4b-clvB). a) Side view of the atomic structure after relaxation, L1 is the surface layer, and L4 is the last layer. b) Top view of the surface. The black line represents the unit cell. c) PDOS of the outermost layers. The Fermi level is shifted to 0 eV and is represented by the vertical black line.	47
4.29	SCAN computed spin-polarized PDOS of the surface layer for $\text{Cs}_2\text{Au}_2\text{Cl}_6$ surface B with one chlorine vacancy at the subsurface(l4b-clvB). The Fermi level is shifted to 0 eV and is represented by the vertical black line.	48
4.30	Computed UPS spectra for $\text{Cs}_2\text{Au}_2\text{Cl}_6$ surface B with one chlorine vacancy at the surface (l4b-clvB). The strongest contribution is from the gold and chlorine atoms. The Fermi level is shifted to 0 eV. and is represented by the vertical black line.	49
4.31	SCAN computed atomic and electronic structure for outermost layers of $\text{Cs}_2\text{Au}_2\text{Cl}_6$ with four layers of thickness and two chlorine vacancies (l4b-2clvA). a) Side view of the atomic structure after relaxation, L1 is the surface layer, and L4 is the last layer. b) Top view of the surface. The black line represents the unit cell. c) PDOS of the outermost layers. The Fermi level is shifted to 0 eV and is represented by the vertical black line.	50
4.32	Computed UPS spectra for $\text{Cs}_2\text{Au}_2\text{Cl}_6$ surface B with two chlorine vacancies at the surface (l4b-2clvA). The strongest contribution is from the gold and chlorine atoms. The Fermi level is shifted to 0 eV. and is represented by the vertical black line.	51
4.33	SCAN computed atomic and electronic structure for outermost layers of $\text{Cs}_2\text{Au}_2\text{Cl}_6$ with four layers of thickness and two chlorine vacancies (l4b-2clvB). a) Side view of the atomic structure after relaxation, L1 is the surface layer, and L4 is the last layer. b) Top view of the surface. The black line represents the unit cell. c) PDOS of the outermost layers. The Fermi level is shifted to 0 eV and is represented by the vertical black line. The red lines (1 and 2) represent the range of integrated energies to obtain the STM images.	52

4.34	Computed STM images, line scan and relative height for $\text{Cs}_2\text{Au}_2\text{Cl}_6$ (l4b-2clvB). These images were computed for a supercell of $2 \times 2 \times 1$, where $V_{bias} = -0.85$ V. (left) correspond to an occupied state and the $V_{bias} = 1.0$ V. (right) is at an unoccupied state. In both images is superimposed the top view of the atomic structure of the surface. The red box represents the unit cell, and at the bottom, there is a side view of the atomic structure of the surface. On the sides of the images, it is presented the relative height, which was calculated in the diagonal direction.	53
4.35	Computed UPS spectra for $\text{Cs}_2\text{Au}_2\text{Cl}_6$ surface B with two chlorine vacancies at the surface (l4b-2clvB). The strongest contribution is from the gold and chlorine atoms. The Fermi level is shifted to 0 eV and is represented by the vertical black line.	54
A.1	INCAR file example. It is possible to observe several tags with their assigned value for electronic relaxation, functionals, and dipole corrections to be used in the calculations. These tags determine what to do and how to do the calculations in VASP. ¹	59
A.2	POSCAR file example. At the top, we have the name of our system. Next is the scaling constant, which scales the lattice vectors. From the third to the fifth line, the lattice vectors are presented. Below we have the species of atoms present in our system; something important point is that the order in which they are presented must be the same order in which they are found in the POTCAR file to avoid errors. The next line shows the number of atoms for each species mentioned in the previous line. The next two lines represent the restrictions on the movement of the atoms and the way the atomic coordinates are presented; in this case, we use direct(fractional) coordinates. Finally, all the atomic positions are presented, accompanied by their respective movement restriction. ² . . .	60
A.3	K-POINTS file example. As a first-line, we have our study system. Next, we have that the k points are 0, which will cause the mesh to be generated automatically. Below we have to generate a Gamma-centered mesh. The fourth line shows the number of desired subdivisions for our case. Furthermore, the last line is used when we want to perform a mesh shift. ³	60
A.4	DOSCAR file example. DOSCAR file is an output file. In its first line, we have the number of ions (including empty spheres), number of ions, 0 (not partial DOS) or 1 (partial DOS). The next line has the unit cell's volume along with the basis vectors' length (a,b,c). The third line presents the initial temperature. Below we have the system's name as given by the tag SYSTEM in the INCAR file. In the sixth line, values correspond to the energy range given by the DOS, the number of grid points, the Fermi energy level, and 1 as a value. Then all this is followed by the columns energy, DOS, integrated DOS. ⁴	61
A.5	OSZICAR file example. OSZICAR file is an output file which gives information about convergence speed and the current step. In the first line, we have N, which represents the number of electronic steps, E is the current free energy, dE is the change in the free energy from the last to the current step and d eps is the change in the band structure energy. ⁵	61

B.1	SCAN computed atomic and electronic structure for outermost layers of $\text{Cs}_2\text{Au}_2\text{Cl}_6$ with six layers thickness type A (16a). a) Side view of the atomic structure after relaxation, L1 is the surface layer, and L4 is the last layer. b) Top view of the surface. The black line represents the unit cell. c) PDOS of the outermost layers. The Fermi level is shifted to 0 eV and is represented by the vertical black line.	64
B.2	SCAN computed atomic and electronic structure for outermost layers of $\text{Cs}_2\text{Au}_2\text{Cl}_6$ with six layers thickness type B (16b). a) Side view of the atomic structure after relaxation, L1 is the surface layer, and L4 is the last layer. b) Top view of the surface. The black line represents the unit cell. c) PDOS of the outermost layers. The Fermi level is shifted to 0 eV and is represented by the vertical black line.	65
C.1	Detailed PDOS for $\text{Cs}_2\text{Au}_2\text{Cl}_6$ surface A (14a) computed with SCAN, where the states of each orbital are shown. On the horizontal axis are the $E - E_F$, and on the vertical are states/eV.	67
C.2	Detailed PDOS for $\text{Cs}_2\text{Au}_2\text{Cl}_6$ surface B (14b) computed with SCAN, where the states of each orbital are shown. On the horizontal axis are the $E - E_F$, and on the vertical are states/eV.	68
C.3	Detailed PDOS for $\text{Cs}_2\text{Au}_2\text{Cl}_6$ surface A with one A-type chlorine vacancy (14a-clv) computed with SCAN, where the states of each orbital are shown. On the horizontal axis are the $E - E_F$, and on the vertical are states/eV.	69
C.4	Detailed PDOS for $\text{Cs}_2\text{Au}_2\text{Cl}_6$ surface A with two A-type chlorine vacancies at the surface (14a-2clv) computed with SCAN, where the states of each orbital are shown. On the horizontal axis are the $E - E_F$ and on the vertical are states/eV.	70
C.5	Detailed PDOS for $\text{Cs}_2\text{Au}_2\text{Cl}_6$ surface A with one A-type chlorine vacancy at the sub surface (14a-sclvA) computed with SCAN, where the states of each orbital are shown. On the horizontal axis are the $E - E_F$, and on the vertical are states/eV.	71
C.6	Detailed PDOS for $\text{Cs}_2\text{Au}_2\text{Cl}_6$ surface A with one B chlorine vacancy at the sub surface (14a-sclvB) computed with SCAN, where the states of each orbital are shown. On the horizontal axis are the $E - E_F$, and on the vertical are states/eV.	72
C.7	Detailed PDOS for $\text{Cs}_2\text{Au}_2\text{Cl}_6$ surface B with one A-type chlorine vacancy at the surface (14b-clvA) computed with SCAN, where the states of each orbital are shown. On the horizontal axis are the $E - E_F$, and on the vertical are states/eV.	73
C.8	Detailed PDOS for $\text{Cs}_2\text{Au}_2\text{Cl}_6$ surface B with one B type chlorine vacancy at the surface (14b-clvB) computed with SCAN, where the states of each orbital are shown. On the horizontal axis are the $E - E_F$, and on the vertical are states/eV.	74
C.9	Detailed PDOS for $\text{Cs}_2\text{Au}_2\text{Cl}_6$ surface B with two type-A chlorine vacancies at the surface (14b-2clv2A) computed with SCAN, where the states of each orbital are shown. On the horizontal axis are the $E - E_F$ and on the vertical are states/eV.	75
C.10	Detailed PDOS for $\text{Cs}_2\text{Au}_2\text{Cl}_6$ surface B with two type B chlorine vacancies at the surface (14b-2clv2B) computed with SCAN, where the states of each orbital are shown. On the horizontal axis are the $E - E_F$, and on the vertical are states/eV.	76

D.1	SCAN computed work function for $\text{Cs}_2\text{Au}_2\text{Cl}_6$ surface A with one A-type chlorine vacancy (14a-clv). The blue line represents the average potential in the z-direction, and the horizontal red dotted line is the Fermi level E_F	77
D.2	SCAN computed work function for $\text{Cs}_2\text{Au}_2\text{Cl}_6$ surface A with two A-type chlorine vacancies at the surface (14a-2clv). The blue line represents the average potential in the z-direction, and the horizontal red dotted line is the Fermi level E_F	78
D.3	SCAN computed work function for $\text{Cs}_2\text{Au}_2\text{Cl}_6$ surface A with one A-type chlorine vacancy at the sub surface (14a-sclvA). The blue line represents the average potential in the z-direction, and the horizontal red dotted line is the Fermi level E_F	78
D.4	SCAN computed work function for $\text{Cs}_2\text{Au}_2\text{Cl}_6$ surface A with one B type chlorine vacancy at the sub surface (14a-sclvB). The blue line represents the average potential in the z-direction, and the horizontal red dotted line is the Fermi level E_F	79
D.5	SCAN computed work function for $\text{Cs}_2\text{Au}_2\text{Cl}_6$ surface B with one A-type chlorine vacancy at the surface (14b-clvA). The blue line represents the average potential in the z-direction, and the horizontal red dotted line is the Fermi level E_F	79
D.6	SCAN computed work function for $\text{Cs}_2\text{Au}_2\text{Cl}_6$ surface B with one B type chlorine vacancy at the surface (14b-clvB). The blue line represents the average potential in the z-direction, and the horizontal red dotted line is the Fermi level E_F	80
D.7	SCAN computed work function for $\text{Cs}_2\text{Au}_2\text{Cl}_6$ surface B with two type-A chlorine vacancy at the surface (14b-2clv2A). The blue line represents the average potential in the z-direction, and the horizontal red dotted line is the Fermi level E_F	80
D.8	SCAN computed work function for $\text{Cs}_2\text{Au}_2\text{Cl}_6$ surface B with two type B chlorine vacancy at the surface (14b-2clv2B). The blue line represents the average potential in the z-direction, and the horizontal red dotted line is the Fermi level E_F	81

List of Tables

4.1	SCAN computed crystallographic parameters for $\text{Cs}_2\text{Au}_2\text{Cl}_6$ perovskite in comparison with experimental data. The parameters presented are: lattice parameters (a,b,c), lattice angles (α, β, γ), optimal volume, bulk modulus (B_0) and the fractional sites (u,v,w)	22
4.2	Energy formation for each vacancy of $\text{Cs}_2\text{Au}_2\text{Cl}_6$ surface A. (14a-clv) represents the one chlorine vacancy at the surface. (14a-2clv) represents the two chlorine vacancies at the surface. (14a-sclvA) represents the A case of one chlorine vacancy at the subsurface, and (14a-sclvB) represents the B case of one chlorine vacancy at the subsurface.	43
4.3	Work Function (ϕ) for each vacancy of $\text{Cs}_2\text{Au}_2\text{Cl}_6$ surface A.(14a-clv) represents the one chlorine vacancy at the surface. (14a-2clv) represents the two chlorine vacancies at the surface. (14a-sclvA) represents the A case of one chlorine vacancy at the subsurface, and (14a-sclvB) represents the B case of one chlorine vacancy at the subsurface.	43
4.4	Energy formation for each vacancy of $\text{Cs}_2\text{Au}_2\text{Cl}_6$ surface B. (14b-clvA) represents the case A chlorine vacancy at the surface. (14b-clvB) represents the case A chlorine vacancy at the surface. (14b-2clvA) is the vacancy formed by removing two chlorine atoms of case A at the surface B. (14b-2clvB) is the vacancy formed by removing two chlorine atoms of case B at the surface B.	54
4.5	Work Function (ϕ) for each vacancy of $\text{Cs}_2\text{Au}_2\text{Cl}_6$ surface B. (14b-clvA) represents the case A chlorine vacancy at the surface. (14b-clvB) represents the case A chlorine vacancy at the surface. (14b-2clvA) is the vacancy formed by removing two chlorine atoms of case A at the surface B. (14b-2clvB) is the vacancy formed by removing two chlorine atoms of case B at the surface B. . . .	55

Chapter 1

Introduction

In our current society, we depend heavily on non-renewable energy sources such as oil to carry out our activities. However, the growing global energy demand has led to the development of energy sources that are renewable and friendly to the environment. The idea of solar panels that take advantage of sunlight to generate energy is in this field where the study of materials that allow us to maximize energy generation takes special importance⁶⁷.

It is precisely here that it is proposed to use perovskite, a compound with an atomic structure defined in such a way that it has several useful properties for this field. Here is where it is performed the study of Integrated Experimental and Theoretical Approach for Efficient Design and Synthesis of Gold-Based Double Halide Perovskites⁸ on which the present work is based when carrying out a deeper analysis of the results found.

A material is considered perovskite when its atoms follow the $A_2B_2X_6$ ⁹; this is the reason why exist several types of perovskites. Several perovskites are being studied to determine their potential application¹⁰¹¹ such us semiconductors¹² or piezoelectrics, which has aroused interest in the field of materials science. Using computational methods such as DFT has proven to be of special interest to simulate and determine the possible properties of this type of material, which can then be synthesized in the laboratory for use in the desired field of application.

1.1 Problem Statement

Perovskite is a material that has attracted attention lately with its electronics. However, the materials we used to form this compound were toxic and generated damage to the environment¹³.

However, since this arrangement of atoms can be quite useful, new perovskites have been investigated. It was found that it is possible to replace toxic atoms with atoms that do not harm the environment, such as gold, chlorine and cesium, and do not produce as much damage as before the lead⁸. An initial analysis of the properties of this material has been carried out. However, it is considered relevant to deepen the study of this compound to establish a state of the art that complements the previously carried out analysis.

This research contributes to some sustainable development objectives proposed by the UN, such as an action for the climate and affordable and non-polluting energy¹⁴. Therefore, we use DFT to investigate the electronic properties

of $\text{Cs}_2\text{Au}_2\text{Cl}_6$ to explore various surfaces that could be synthesized experimentally and used for new technological developments.

1.2 General and Specific Objectives

The main objective of this thesis is to perform a Density Functional Theory (DFT) study of the atomic and electronic structure of the metal halide double perovskite $\text{Cs}_2\text{Au}_2\text{Cl}_6$ with chlorine vacancy defects using SCAN. For this, we have to fulfill the following objectives:

- Explain the theoretical background of the DFT density functional theory and the use of the SCAN functional.
- Modeling and study of the atomic and electronic structure of $\text{Cs}_2\text{Au}_2\text{Cl}_6$ bulk.
- Study the surfaces of $\text{Cs}_2\text{Au}_2\text{Cl}_6$ considering the possible arrangements and the atomic structures with chlorine defects.
- Perform STM simulation images.
- Perform PDOS spin-polarized simulation images for the most energetically favourable surfaces.
- Perform UPS simulation images.
- Compute the work function and the ionization potential.

Chapter 2

Theoretical Background

2.1 Many-Body Schrödinger Equation

In order to analyze the properties of a material, we have to study how it is composed. If we look at the atomic scale, we have a system with a set of nuclei and electrons, which will determine its properties depending on their arrangement.

We are working in a non-relativistic regime, and understanding the behaviour of the particles is necessary to use and solve the Schrödinger equation. However, for this case, we restrict the region of interest to stationary electronic states, so we have to consider just the time-dependent Schrödinger equation, which has the following form:

$$(\hat{K} + \hat{V})\psi = \hat{E}\psi \quad (2.1)$$

where \hat{K} and \hat{V} are the kinetic and potential energy operators respectively, \hat{E} is the energy operator, and ψ is the wave function, where the position $\psi(r)$ is determined by $r = xu_x + yu_y + zu_z$ in Cartesian coordinates.

This equation works when we take into account one particle, but if we add one more particle to the system, our result will not be accurate due to a repulsion force created by the electrons. In this case, as it was mentioned before, we have a collection of nuclei and electrons.

Then, to perform the calculations, we have to introduce the many-body wave-function Ψ , which takes into account the position of every electron and nuclei of the system. Considering the case of N electrons and M nuclei, the new position is going to be given by:

$$\Psi = \Psi(r_1, r_2, \dots, r_N; R_1, R_2, \dots, R_M) \quad (2.2)$$

With this is possible to rewrite equation 2.1 in the following way:

$$(\hat{K} + \hat{V})\Psi = E_{tot}\Psi \quad (2.3)$$

Developing each term of this equation, we have that the kinetic energy has the contribution of the electrons and the nucleus. Therefore it is possible to express it as:

$$K = - \sum_{i=1}^N \frac{\hbar^2}{2m_e} \nabla_i^2 - \sum_{I=1}^N \frac{\hbar^2}{2M_I} \nabla_I^2 \quad (2.4)$$

where m_e is the mass of the electron, M_I represents the mass of the I -th nucleus and ∇^2 are the Laplace operators acting on the coordinates of electrons and nuclei, respectively.

The potential energy is given by the contribution of all the possible Coulomb interactions, which are:

- The repulsive electron-electron (e-e) Coulomb interaction, due to the charge of the electrons, which is given by:

$$V_{e-e} = \frac{1}{2} \sum_{i \neq j} \frac{e^2}{4\pi\epsilon_0} \frac{1}{|r_i - r_j|} \quad (2.5)$$

Here, e is the electron charge, ϵ_0 represents the permeability of free space, and $|r_i - r_j|$ is the distance between each pair of electrons. In this case, i could not be equal to j due to the Coulomb repulsion. Something important is the $\frac{1}{2}$ that is there to consider just one energy per electron pair.

- The Coulomb repulsion between pairs of nuclei (n-n), due to the repulsion between nuclei, is described as:

$$V_{n-n} = \frac{1}{2} \sum_{I \neq J} \frac{e^2}{4\pi\epsilon_0} \frac{Z_I Z_J}{|R_I - R_J|} \quad (2.6)$$

$Z_I Z_J$ represent the atomic numbers of the atoms I and J ; the indices run similarly to the previous case.

- Finally, the Coulomb attraction between electrons and nuclei (e-n), generated by their opposite charges, could be written as:

$$V_{e-n} = - \sum_{i,I} \frac{e^2}{4\pi\epsilon_0} \frac{Z_I}{|r_i - R_I|} \quad (2.7)$$

If we put the equations 2.3 to 2.7 together, we obtain the many-body Schrödinger equation, which has the following form:

$$\left[- \sum_{i=1}^N \frac{\hbar^2}{2m_e} \nabla_i^2 - \sum_{I=1}^N \frac{\hbar^2}{2M_I} \nabla_I^2 + \frac{1}{2} \sum_{i \neq j} \frac{e^2}{4\pi\epsilon_0} \frac{1}{|r_i - r_j|} + \frac{1}{2} \sum_{I \neq J} \frac{e^2}{4\pi\epsilon_0} \frac{Z_I Z_J}{|R_I - R_J|} - \sum_{i,I} \frac{e^2}{4\pi\epsilon_0} \frac{Z_I}{|r_i - R_I|} \right] \Psi = E_{tot} \Psi \quad (2.8)$$

where E_{tot} is the total energy of the system in the quantum state specified by the many-body wave-function Ψ , which for a specific set of coordinates cannot be measured experimentally due to it is not a physical observable.

The complexity of equation 2.8 is so big that it increases exponentially with the size of the system, which leads to unsolvable matrix operations. Therefore, many researchers have been working on different approximations to equation 2.8 and some of their findings will be described in the next sections.

2.2 Atomic Units

It is possible to simplify the many-body Schrödinger equation considering the following fundamental physical constants. These constants were determined experimentally and did not depend on any particular material.¹³

$$\begin{aligned}
 \hbar &= 1.05457163 \cdot 10^{-34} \text{ J} \cdot \text{s}, \\
 m_e &= 9.10938291 \cdot 10^{-31} \text{ kg}, \\
 m_p &= 1.67262164 \cdot 10^{-27} \text{ kg}, \\
 e &= 1.60217649 \cdot 10^{-19} \text{ C}, \\
 \epsilon_0 &= 8.85418782 \cdot 10^{-12} \text{ F/m}, \\
 a_0 &= 0.529 \text{ \AA}
 \end{aligned} \tag{2.9}$$

This is the simplified many-body Schrödinger equation using Hartree units.

$$\left[-\sum_{i=1} \frac{1}{2} a_0^2 \nabla_i^2 - \sum_{I=1} \frac{1}{2(M_I/m_e)} a_0^2 \nabla_I^2 + \frac{1}{2} \sum_{i \neq j} \frac{a_0}{|r_i - r_j|} + \frac{1}{2} \sum_{I \neq J} Z_I Z_J \frac{a_0}{|R_I - R_J|} - \sum_{i,I} Z_I \frac{a_0}{|r_i - R_I|} \right] \Psi = \frac{E_{tot}}{E_{Ha}} \Psi \tag{2.10}$$

However, it is possible to simplify it a little more using these units:

$$\begin{aligned}
 1 \text{ Ha} &= 27.2114 \text{ eV} = 4.3597 \cdot 10^{-18} \text{ J}, \\
 1 \text{ bohr} &= 0.529177 \text{ \AA} = 0.529177 \cdot 10^{-10} \text{ m} \\
 1 \text{ a.u. of mass} &= 9.10938291 \cdot 10^{-31} \text{ kg} \\
 E_{Ha} &= \frac{e^2}{4\pi\epsilon_0 a_0}
 \end{aligned} \tag{2.11}$$

With these units, we can go further and simplifying equation 2.10, we obtain the many-body Schrödinger equation in Hartree units:

$$\left[-\sum_{i=1} \frac{\nabla_i^2}{2} - \sum_{I=1} \frac{\nabla_I^2}{2M_I} + \frac{1}{2} \sum_{i \neq j} \frac{1}{|r_i - r_j|} + \frac{1}{2} \sum_{I \neq J} \frac{Z_I Z_J}{|R_I - R_J|} - \sum_{i,I} \frac{Z_I}{|r_i - R_I|} \right] \Psi = E_{tot} \Psi \tag{2.12}$$

This equation is used in first principles materials modeling and shows all the needed parameters.¹³

2.3 The Born-Oppenheimer Approximation

This approximation is also called adiabatic approximation and states that the total electron-nuclear wavefunction (eq. 2.2) could be separated into a wavefunction that depends on the electron coordinates and a wavefunction that depends on the nuclear coordinates.^{15 13}, as follows:

$$\Psi(r_1, r_2, \dots, r_N; R_1, R_2, \dots, R_M) = \Psi_e(r_1, r_2, \dots, r_N) X_n(R_1, R_2, \dots, R_M) \tag{2.13}$$

where Ψ_e is the wavefunction for electron coordinates and X_n is the wavefunction for nuclear coordinates. We can assume that electrons follow the motion of the nuclei almost instantaneously because their mass is smaller than the nuclei's, which could be expressed by kinetic energy. The electronic states are consistently in their ground state on the time scale of nuclear motion.¹⁶

If we consider that Coulomb repulsion between nuclei is constant, we can define the following energy to simplify the equation 2.8.

$$E = E_{tot} - \frac{1}{2} \sum_{I \neq J} \frac{Z_I Z_J}{|R_I - R_J|} \quad (2.14)$$

For convenience, if we consider the nuclear coordinates R_I and Ψ as function of the electron coordinates ignoring its dependence on the nuclear coordinates. We can define the Coulomb potential of the nuclei experienced by the electrons as:¹³

$$V_n(r_i) = - \sum_I \frac{Z_I}{|r_i - R_I|} \quad (2.15)$$

With equations 2.13, 2.14 and 2.15, we have what is necessary to obtain the fundamental equation of electronic structure theory:

$$\left[- \sum_i \frac{\nabla_i^2}{2} + \sum_i V_n(r_i) + \frac{1}{2} \sum_{i \neq j} \frac{1}{|r_i - r_j|} \right] \Psi = E \Psi \quad (2.16)$$

2.4 Density Functional Theory

Density Functional Theory (DFT) is a quantum mechanical method that makes possible the study of many-body systems and obtains results about some properties of materials such as relativistic effects and magnetism¹⁷. The most important principle is that to calculate a system's ground state energy, we use the electron density $n(r)$ instead of the wave function Ψ . DFT is based on the paper of P. Hohenberg and W. Kohn in 1964¹⁸.

The total energy of a many-electron system is given by:¹³

$$E = \langle \Psi | \hat{H} | \Psi \rangle = \int dr_1 \dots dr_N \Psi^*(r_1, \dots, r_N) \hat{H} \Psi(r_1, \dots, r_N) \quad (2.17)$$

$$\hat{H} = (r_1, \dots, r_N) = - \sum_i \frac{\nabla_i^2}{2} + \sum_i V_n(r_i) + \frac{1}{2} \sum_{i \neq j} \frac{1}{|r_i - r_j|}$$

This Hamiltonian does not depend on the particular material; therefore, if E suffers any change, it must be associated with a change in Ψ . It is possible to represent this property by saying that E is a functional of Ψ and mathematically, we use:¹³

$$E = F[\Psi] \quad (2.18)$$

As a brief reminder, a functional is a function that takes a function as input and gives us a number as output.

So, if E is the lowest possible energy of the system, then E is functional of the electron density $n(r)$:¹³

$$\begin{aligned} E &= F[n] \\ n(r) &= \sum_i |\phi_i(r)|^2 \end{aligned} \quad (2.19)$$

Any quantum state's energy is a functional of the wavefunction containing $3N$ variables. However, the ground-state energy depends only on $n(r)$, which is a function of only three variables. This reduction in variables will help greatly reduce computational costs when performing the calculations.¹⁹

2.5 Hohenberg-Kohn theorems

Hohenberg-Kohn establish that the total energy of a many-electron system is a functional of the electron density $E = F[n]$. The proof of this idea is at¹³.

2.5.1 Theorem 1: Uniqueness

This theorem is based on the following premises:^{13 18}

- The ground-state electron density determines the external potential of the nuclei V_n uniquely. $n \rightarrow V_n$
- The external potential V_n in a quantum state determines the many electron-wave function uniquely. $V_n \rightarrow \Psi$
- The total energy E in any quantum state is functional of the wave-function $\Psi \rightarrow E$

The total energy must be a functional of the density $E = F[n]$ because, if we combine the premises, we obtain the relation: $n \rightarrow V_n \rightarrow \Psi \rightarrow E$ that means the electron density could determine the total energy.

2.5.2 Theorem 2: Variational Principle

This theorem mention that the ground-state energy E_0 can be found by using $E = F[n]$, with the electron number density $n(r)$ that minimizes it¹⁸.

2.6 Kohn-Sham theory

The Hohenberg-Kohn theorems show that when we have many electrons in their ground state, the total energy is a functional of the electron density. However, this theorem does not explain how to build a functional.

Kohn and Sham proposed a way to solve this problem. If we use the complete expression for E , it is possible to obtain a general expression for the functionals:¹³

$$E = F[n] = \int dr n(r)V_n(r) - \sum_i \int dr \phi_i^*(r) \frac{\nabla^2}{2} \phi_i(r) + \frac{1}{2} \int \int dr dr' \frac{n(r)n(r')}{|r-r'|} + E_{xc}[n] \quad (2.20)$$

This equation shows the functional as the sum of known contributions, where the first term represents the external potential, the second term is the kinetic energy, the third term is the Hartree energy, and the final term $E_{xc}[n]$ is the exchange and correlation energy. If we know the value of $E_{xc}[n]$, it is possible to calculate the total energy of the system in its ground state $E = F[n]$ using the electron density.¹³ However, it is necessary to determine the electron density n_0 ; in this sense, we apply Hohenberg-Kohn variational principle, which has the following form:

$$\frac{\delta F[n]}{\delta n} \Big|_{n_0} = 0 \quad (2.21)$$

This equation states that the functional derivative must be zero, which leads to the construct of the density using an equation for the wavefunctions $\phi_i(r)$. If we apply the Hohenberg-Kohn variational principle, we have:¹³

$$\left[-\frac{1}{2} \nabla^2 + V_n(r) + V_H(r) + V_{xc}(r) \right] \phi_i(r) = \varepsilon_i \phi_i(r) \quad (2.22)$$

$$V_{xc}(r) = \frac{\delta E_{xc}[n]}{\delta n} \Big|_{n(r)}$$

where V_n represents the external nuclear potential, V_H is the Hartree potential, $-\nabla^2/2$ is the kinetic energy, and V_{xc} is the exchange and correlation potential. With equations 2.19, we can say that there must be a functional E_{xc} that could give us the exact ground state energy. However, we still do not know what this functional is; that is why it is necessary to use some approximations to E_{xc} . The exchange and correlation functional for the energy can be expressed as:¹⁶

$$E_{xc}[n] = \int d^3r n(r) \varepsilon_{xc}[n(r)] \quad (2.23)$$

where $\varepsilon_{xc}[n(r)]$ is the exchange and correlation energy per particle at the point r , but dependent on the whole electron density $n(r)$.

2.7 Exchange-correlation functionals

Over many years, many proposals have been developed to find the functional E_{xc} . In the efforts to find an accurate functional that satisfies most materials systems modeling, there are many non-empirical and semi-empirical density functionals, each with different levels of prediction, sophistication, accuracy, and computational resource costs.²⁰

The simplest proposal is the **Local Spin Density Approximation (LSDA)**, which is used to perform basic calculations of bulk and surface structures. However, it is highly inaccurate for molecular properties.^{21 16}

Another proposal is the **General Gradient Approximation (GGA)**, an improved version of LSDA. This functional achieves a chemical accuracy for various chemical reactions. However, this functional does not describe van der Waals forces and underestimates the band gaps.^{16 21}

The **meta-GGA** is considered a semi-local functional that can identify the different chemical bonds.²¹ One functional that belongs to this group is the **Strongly Constrained and Appropriately Normed Semi-local (SCAN)** density functional, which has the characteristic that is fully constrained, obeying the 17 known constraints that a semi-local functional can fulfill. This functional can predict geometries and energies of many bonded materials, and

its results have more accuracy than the GGAs. However, it cannot describe the properties in a system with non-local interactions because it is a semi-local functional.^{22 23}

This thesis was developed using SCAN functional for all the calculations.

2.8 Vienna ab initio Simulation Package (VASP)

2.8.1 Periodic systems and plane waves

The Kohn-Sham equations have a way of being solved by representing the wavefunctions as Fourier series. This approximation can be used when we have periodic boundary conditions.¹³

We must expand the electron wavefunctions, for which we need to define the primitive vectors of the reciprocal lattice, as:¹³

$$b_1 = \frac{2\pi}{a}u_x, b_2 = \frac{2\pi}{a}u_y, b_3 = \frac{2\pi}{a}u_z \quad (2.24)$$

and the reciprocal lattice vectors (G) as:

$$G = m_1b_1 + m_2b_2 + m_3b_3 \quad (2.25)$$

where m_1 , m_2 , and m_3 are integers.¹³ The complex exponents satisfy the periodic boundary conditions for solids that are established:

$$\phi_i(x + a, y, z) = \phi_i(x, y, z) \quad (2.26)$$

the complex exponents are defined as:

$$\exp(iG \cdot r) \quad (2.27)$$

Let us consider the following example:

$$\exp[iG \cdot (r + au_x)] = \exp(iG \cdot r)\exp(iG \cdot au_x) = \exp(iG \cdot r)\exp(i2\pi m_1) = \exp(iG \cdot r) \quad (2.28)$$

The functions defined by the complex exponents are the plane waves because they can be part of a propagating wave. These waves also satisfy the periodic boundary conditions of a computational cell, and thanks to this, it is possible to write the Kohn-Sham wavefunctions as a linear combination:¹³

$$\phi_i(r) = \sum_G c_i(G)\exp(iG \cdot r) \quad (2.29)$$

the sum runs over all the G vectors. The plane wave coefficients $c_i(G)$ has a relation with the original wavefunctions by a factor of $\exp(-iG' \cdot r)$. The equation 2.30 is possible to be write as:¹³

$$\int \exp(-iG' \cdot r)\phi_i(r)dr = \sum_G c_i(G) \int \exp(-iG' \cdot r)\exp(iG \cdot r)dr = a^3 c_i(G') \quad (2.30)$$

These relationships are known as the plane-wave representation of the Kohn-Sham wavefunctions.

2.8.2 Cut-off energy E_{cut}

The Fourier series of the equation 2.30 is infinite, but the basis set is defined by the set of G vectors that can be truncated. The G-vector defines the level of detail of the description of the computational cell. The kinetic energy cutoff E_{cut} defines the plane waves that form the basis set.¹³

$$E_{cut} = \frac{|G_{max}|^2}{2} \quad (2.31)$$

The truncation induces errors in the computed properties. However, it can be reduced by improving the E_{cut} for the desired accuracy. An important fact is that the all-electron wave-function of a system has an extensive oscillatory behaviour close to the nuclei.²⁴ Therefore, a significant kinetic energy cut-off means a high computational cost. Therefore, we use the pseudo-potential approximation where we consider the separation of core and valence electrons.

In DFT, this parameter is the first step to performing any calculation, so we must start determining the cut-off energy for the system of interest. The calculation of this parameter gives us values of the total energy of the system E and its cut-off energy E_{cut} . If we graph these results, we realize that from a certain range of energies, the energy E converges. The convergence range must be determined where the energy must vary by less than 1 meV/atom.^{25 26}

2.8.3 K-points Sampling

At DFT, we will need to evaluate integrals in the reciprocal space, and this can be solved over a grid of k-points. So, let us consider the following electronic density:²⁷

$$n(r) = 2 \sum_{nk}^{occ} |\psi_{nk}(r)|^2 \quad (2.32)$$

where the summation is performed at the lowest occupied (occ) states nk described by the Kohn-Sham orbitals $\psi_{nk}(r)$.

The density $n(r)$ could be represented for a set of k points, known as k-point sampling. This set is chosen considering the unit cell size and the system point symmetry. If we have a big unit in the cell, the set of k points needed is smaller; in the reciprocal space, the Brillouin zone becomes smaller when the unit cell is bigger.

It is possible to obtain more accuracy if we consider more k-points to sample the Brillouin zone²⁸. However, the complexity scales linearly with the number of k-points when we want to perform an approximation. That is why we need to find a method that allows us to choose the proper set of k points with a reasonable computational cost to perform the calculus.

In VASP, we have several methods: the Monkhorst-Pack, Rk length, or the generalized regular grids.³ Though, the most used method is the Monkhorst-Pack (MP) method²⁹, which is based on: “a regular grid of k-points is generated, and the Brillouin zone integral of a function is approximated by calculating the average value of the function over the k-points.”²⁸

2.8.4 Pseudopotentials

Modeling all electrons calculations requires an extremely high plane-wave cut-off to represent the highly oscillatory states of core electrons. Therefore, we introduce pseudopotentials to reduce the number of plane-waves needed.²⁴

Pseudopotentials reproduce the behavior of the full nuclear potential and core electrons for the outer electrons using a new potential.^{24 30}

The base idea is that electrons that are very near to the nucleus (core electrons) and those which are far apart from the nucleus (valence electrons) determine some of the chemical and physical properties of our structure. Core electrons will have a considerable influence on the Coulomb potential of the nucleus due to they are tightly bonded to the nucleus, and we can approximate the core electrons by pseudopotentials.³¹ Valence electrons will feel a weaker Coulomb potential from the nucleus; that is why the core electrons partially screen them, and therefore their wave functions are diffuse.²⁷

In DFT simulations, pseudopotentials can be classified according to the minimum cutoff energy used in the calculations. Pseudopotentials that require high cutoff energy are known as hard, and those that require lower cutoff energy are called soft²⁴.

The criteria to choose the pseudopotentials is given by the character of the bonding between the ions in the system and how well it reproduces the results of accurate all-electron calculations.³² One problem of pseudopotential calculations are that it needs non-linear core corrections since of the non-linearity of the exchange interaction between core and valence electrons³³. This problem could be eliminated using the projector-augmented wave (PAW) method.

2.8.5 The Projector Augmented-Wave (PAW) Method

The Projector Augmented Wave (PAW) method was proposed by Blöchl³⁴ and is based on the idea of partitioning the wave functions of all electrons instead of considering only the valence electrons, giving access to the full-wave function information.³⁰ This method approximates the accuracy of the full potential linearized method. Augmented plane wave method (FLAPW).³² To describe this method, we use the valence wavefunctions ψ_{nk}^{AE} formed by a linear transformation of pseudo wavefunctions:³²

$$|\psi_{nk}^{AE}\rangle = |\psi_{nk}^{PS}\rangle + \sum_i (|\phi_{nk}^{AE}\rangle - |\phi_i^{PS}\rangle) \langle p_i^{PS} | \psi_{nk}^{PS}\rangle \quad (2.33)$$

we can rewrite the pseudopotentials in the following way:

$$|\psi_{nk}\rangle = |\tilde{\psi}_{nk}\rangle + \sum_i (|\phi_i\rangle - |\tilde{\phi}_i\rangle) \langle \tilde{p}_i | \tilde{\psi}_{nk}\rangle \quad (2.34)$$

where n is the band index, ϕ_i are solutions of the spherical scalar-relativistic Schrödinger equation for a non-spinpolarized atom, and the pseudo-orbitals $\tilde{\psi}_{nk}$ are variational quantities expanded by VASP as plane waves with the following form:

$$\tilde{\psi}_{nk}(r) = \langle r | \tilde{\psi}_{nk}\rangle = \frac{1}{\sqrt{\Omega}} \sum_G c_{nkG} e^{i(G+k)\cdot r} \quad (2.35)$$

This method was implemented in DFT code with a adaptation³²

Chapter 3

Methodology

This thesis was performed using plane-wave Viena ab initio Simulation Package (VASP), where the projector augmented wave method (PAW) was used to describe the core electrons. The potential for the cesium atom has the following electron configuration $[Kr, 4d^{10}]5s^25p^66s^1$, gold is described as $[Kr, 4f^{14}, 4d^{10}]5s^25p^66s^15d^{10}$ and chlorine is $[Ne]3s^23p^5$.

We use the slab model in our calculations, where we consider a certain number of surface layers inside a slab with a determined vacuum space to avoid artificial interactions. Also, the thickness of the slab should be enough so that the internal surface layers simulate the bulk of the crystal. All the calculations in this thesis were made using a slab model fixing the atoms of the bottom layer. The remaining atoms can relax to create a continuous transition from the surface to the bulk region in the slab.²⁷.

3.1 VASP working principle

In this section, there is a short description of the input and output files that are used in VASP to perform DFT calculations. Some examples of the input and output files used in the calculations can be seen in Appendix A.

3.1.1 VASP inputs

These files describe the parameters that must be considered when making the calculations. To perform any calculation, we need four files: INCAR, POSCAR, POTCAR and KPOINTS

INCAR

This file contains information on what calculations to perform and how to do them. This file contains a series of parameters represented by labels and capital letters.¹

POTCAR

It contains the pseudopotentials and specific information of each species we use to perform the calculations. When we have more than one type of atom, we have to concatenate POTCAR files in the atomic order described in the POSCAR and INCAR files. Only VASP could create, provide or modify this type of file.³⁵

KPOINTS

Contains the Bloch vectors (k-points) that will be used to sample the Brillouin zone in the calculation.³

POSCAR

Contains the atomic structure and the lattice parameters used to describe the structure²

3.1.2 VASP outputs

As VASP performs calculations and generates files where certain information is saved, the most important files are:

CONTCAR

Contains the new atomic structure after the calculations; it has a similar structure as POSCAR.³⁶

OUTCAR

This file has detailed information about the performed calculations, such as forces on the atoms, local charges and magnetic moments, local charges, magnetic moments, dielectric properties³⁷

DOSCAR

DOSCAR file has the total density of states, the partial density of states and Fermi energy level⁴

OSZICAR

It has information that summarises the results, such as convergence speed and the current step.⁵

WAVECAR

It is a binary file that contains the wave functions used in the calculations³⁸

3.2 Scanning Tunneling Microscopy STM

Scanning Tunneling Microscopy is one of the most important tools when studying atomic scales because it allows us to obtain ultra-high resolution images. It provides accurate atomic-scale manipulation and the analysis of many physical properties, such as roughness and surface defect, between others.³⁹

STM uses quantum tunneling, which establishes a wave function that can propagate through a potential barrier. The STM's working principle is that a voltage is applied between the tip of our equipment and a sample, separated by a certain vacuum distance that allows us to generate a tunnel effect current. The separation distance between the sample and the tip is very important because if the distance is not adequate, it can lead us to obtain erroneous results. The tip should be at around less than 0.1 Å from the sample.⁴⁰ The tunneling effect can be described as:⁴¹

$$I \propto e^{-2s/\hbar} \sqrt{2m\varphi} \quad (3.1)$$

where m is the mass of the electron, s is the width of the barrier, and φ is the height of the barrier.

We perform a Tersoff-Hamann approximation using bSKAN⁴² and the output files obtained from VASP calculations to compute the simulated constant current mode STM images in order to study the topography of our atomic structures. In these calculations, we have to specify the bias voltage values; these values are chosen based on the electronic structure of the selected surface using the PDOS. After calculating, we interpolate the outcome in a 3D contour plot figure. This figure is the computed STM image.

3.3 Tersoff-Hamann approximation

STM uses a current operator that is given by:¹³

$$M_{ij} = \frac{1}{2} \int dS \cdot (\psi_{T,i}^* \nabla \psi_{S,j} - \psi_{S,j} \nabla \psi_{T,i}^*) \quad (3.2)$$

where $\psi_{T,i}$ and $\psi_{S,j}$ are the single-particle wave functions of electrons in the tip and the sample. If we use the Tersoff-Hamann approximation, that is, considering a spherical tip; the matrix element M_{ij} becomes proportional to the magnitude of the sample's wave function at the center of a sphere r_T ¹³, so we have:

$$M_{ij} = C \cdot \psi_{S,j}(r_T) \quad (3.3)$$

where r_T is the sphere's center, and C is a constant. We can reproduce STM images using the Kohn-Sham eigenstates ϕ_j and its eigenvalues ε_j in the following way:¹³

$$\psi_{S,j}(r) = \phi_j(r) \quad (3.4)$$

3.4 Ultraviolet Photoelectron Spectroscopy UPS

UPS is based on the idea that photons have energy $h\nu$. When it impinges on the surface, it produces photoelectrons that emerge from the surface with an energy spectrum that contains the peaks of all the binding energies.⁴³

UPS is a surface-sensitive technique, and we use it to obtain information on the surface layer of the material. To compute UPS simulated images, we use the density of states (DOS), the Inelastic Mean Free Path (IMFP) and the energy level cross-sections of the studied material that was taken from tabulated data for each atomic orbital at photoexcitation energy from Yeh and Lindau⁴⁴

In order to calculate a simulated UPS spectrum, it is necessary to consider the depth of surface sensitivity to which the incident photon can penetrate the surface sample. This parameter is associated with the Inelastic Mean Free Path (IMFP).⁴⁵ To calculate the inelastic mean free path for the $\text{Cs}_2\text{Au}_2\text{Cl}_6$ surface, we use NIST Electron Inelastic-Mean-Free-Path Database software⁴⁶. After the calculation, we fit the energy and the data from NIST, obtaining Fig. 3.1.

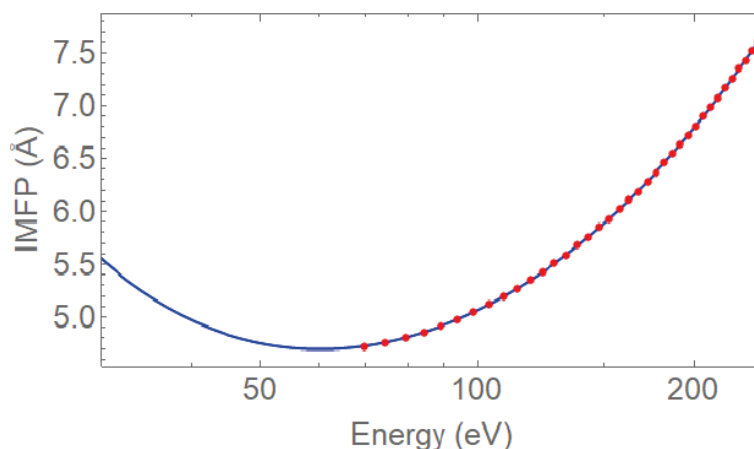


Figure 3.1: Inelastic mean Free Path for $\text{Cs}_2\text{Au}_2\text{Cl}_6$

We used photons with energy of 115 eV we have could penetrate until $\sim 4.7 \text{ \AA}$ that correspond to the surface layer and the information that we are going to obtain is from this layer.

In the results section, you will find UPS simulated images and a brief description of the position of each peak and the element contribution.

3.5 Point Defects in Solids

A point defect in a material is any defect that involves only a single particle or a small set of points. It occurs when an atom is missing from the usual crystalline array and makes a void in the middle of the crystal, called a vacancy. A defect could be produced when we apply external stress to a crystal. Point defects affect materials' physical properties

and, therefore, in the application that will be given to them, being the best known in electronic and optoelectronic devices.⁴⁷ Experimental defect identification is typically difficult and indirect, requiring an ingenious combination of different techniques; one of these techniques is the theoretical modelling of point defects to predict them. This prediction could be made with a DFT approach by the electronic-structure calculations using pseudopotentials or projector augmented wave potentials. This method is most commonly used for first principles defect calculations.⁴⁸ The formation energy of a point defect in solids is defined as:^{48 49 50}

$$E^f[X^q] = E_{tot}[X^q] - E_{tot}[bulk] - \sum_i n_i \mu_i + qE_F + E_{corr} \quad (3.5)$$

where $E_{tot}[X^q]$ is the total energy of the supercell containing the defect X, $E_{tot}[bulk]$ is the total energy for the supercell without defects. The integer n_i indicates the number of atoms that have been added ($n_i > 0$) or removed ($n_i < 0$) to create the defect, the μ_i is the corresponding chemical potentials of chlorine that is the specie that we are removing to create the vacancies. In this thesis, we are considering that we are working with neutral defects; in other words, $q = 0$ and therefore, the term qE_f is 0. Finally, the term E_{corr} represents the correlation energy; it is a correction term that accounts for finite k-point sampling in the case of shallow impurities⁴⁸, but in the calculations, we do not consider impurities, which is why we neglect this term.

In the results section, you will find the Table 4.2 and Table 4.4 with the results of the formation energy of each of the proposed vacancies.

Chapter 4

Results & Discussion

4.1 Bulk metal halide double perovskite $\text{Cs}_2\text{Au}_2\text{Cl}_6$

In this section, there is a description of the DFT simulations of the perovskite $\text{Cs}_2\text{Au}_2\text{Cl}_6$. Its crystal has an fcc structure, as it is shown in its atomic structure at Fig. 4.1

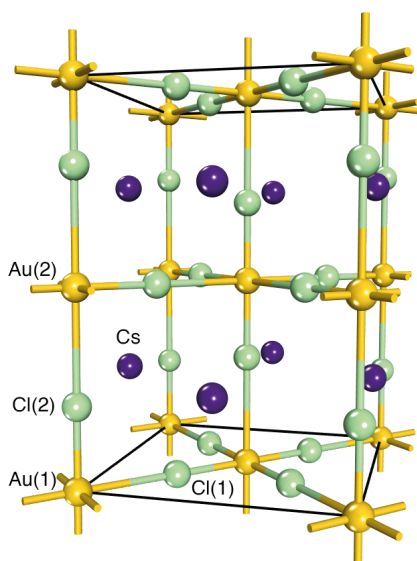


Figure 4.1: Simulated crystal structure of $\text{Cs}_2\text{Au}_2\text{Cl}_6$ perovskite. In this figure, the yellow, green and violet spheres represent the Au, Cl and Cs atoms, respectively. Two gold atoms are not equivalent, the atom identified as Au(1) has a +1 oxidation state, and the atom identified as Au(2) has a +3 oxidation state. The atoms are identified according to the positions presented in Table 4.1. The black line represents the unit cell.

The system's calculations start with the convergence of the cut-off Energy and the K-points, as is seen in the Fig 4.2 and Fig 4.3.

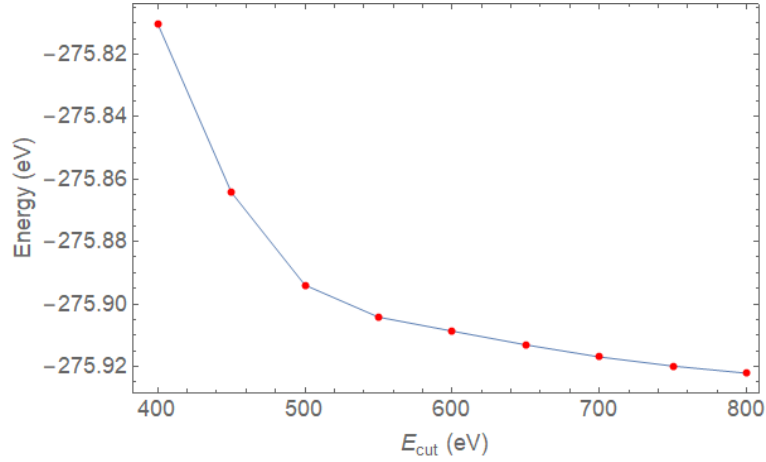


Figure 4.2: Cut-off energy for bulk $\text{Cs}_2\text{Au}_2\text{Cl}_6$. The energies start to converge at 650 eV, according to the $< 1\text{meV/atom}$ criteria.

It was chosen cut-off energy of 650 eV to perform our calculations.

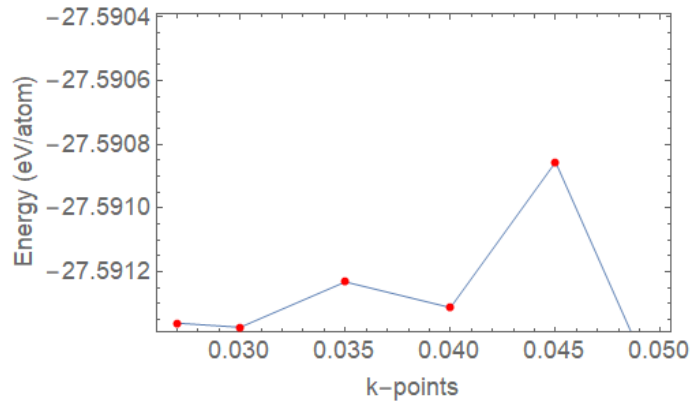


Figure 4.3: k-points mesh convergence for bulk $\text{Cs}_2\text{Au}_2\text{Cl}_6$. The energies begin to converge at $0.035 \text{ } 2\pi \text{ \AA}^{-1}$ according to the $< 1\text{meV/atom}$ criteria. However, it is possible to use upper k points to get more accurate results.

It was chosen $\Delta k = 0.04 \text{ } 2\pi \text{ \AA}^{-1}$ of separation length that correspond to the $4 \times 4 \times 5$ k-points. After this calculations, we fit the $\text{Cs}_2\text{Au}_2\text{Cl}_6$ data to the Birch-Murnaghan equation of state as displayed in Fig. 4.4.

The Birch-Murnaghan equation of state (EOS) used was:⁵¹

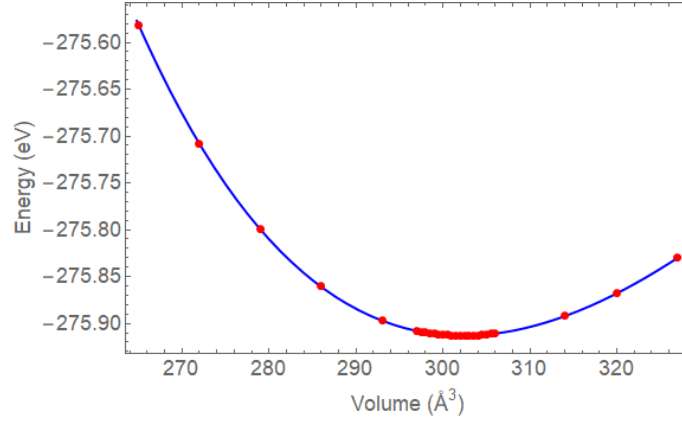


Figure 4.4: SCAN computed equation of state for $\text{Cs}_2\text{Au}_2\text{Cl}_6$. The blue line represents the Birch-Murnaghan equation of state fit, and the red dots represent the computed energies' value.

$$E(V) = E_0 + \frac{9V_0B_0}{16} \left(\left[\left(\frac{V_0}{V} \right)^{\frac{2}{3}} - 1 \right]^3 B'_0 + \left[\left(\frac{V_0}{V} \right)^{\frac{2}{3}} - 1 \right]^2 \left[6 - 4 \left(\frac{V_0}{V} \right)^{\frac{2}{3}} \right] \right) \quad (4.1)$$

where V is the cell volume, E_0 is the ground state energy, V_0 is the ground state volume, B_0 is the bulk modulus and B'_0 is the bulk modulus pressure derivative.

In this plot, the optimal or equilibrium volume of $\text{Cs}_2\text{Au}_2\text{Cl}_6$ perovskite corresponds to the lowest total energy volume. This value and other computed crystallographic parameters are listed in table 4.1. Furthermore, some experimental values⁸ are presented in the same table.

Considering the structure of Fig. 4.1, we computed the Partial Density of States (PDOS) of $\text{Cs}_2\text{Au}_2\text{Cl}_6$ bulk.

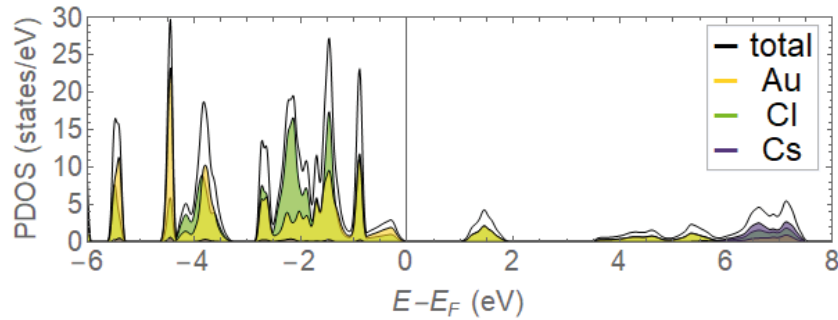


Figure 4.5: SCAN computed PDOS of bulk $\text{Cs}_2\text{Au}_2\text{Cl}_6$ perovskite. The vertical black line represents the Fermi level shifted to 0 eV. The green, yellow and violet represent respectively the chlorine, gold and cesium contribution. The overlapping result in different shades of purple or yellow represents the contribution of more than one atomic species.

Table 4.1: SCAN computed crystallographic parameters for $\text{Cs}_2\text{Au}_2\text{Cl}_6$ perovskite in comparison with experimental data. The parameters presented are: lattice parameters (a, b, c), lattice angles (α, β, γ), optimal volume, bulk modulus (B_0) and the fractional sites (u, v, w)

Property	Calculated (SCAN)	Experiment	
Space Group	I4/mmm	I4/mmm	
$a = b$ (Å)	7.44	7.5	
c (Å)	10.90	10.88	
$\alpha = \beta = \gamma$ (°)	90	90	
Volume (Å ³)	604.49	612.28	
B_0 (GPa)	16.32	15.0	
Fractional sites	u	v	w
Au(1)	0.00	0.00	0.00
Au(2)	0.00	0.00	0.50
Cl(1)	0.72	0.72	0.00
Cl(2)	0.00	0.00	0.21
Cs(1)	0.00	0.50	0.25

The valence band within the energy range -5.60 eV to -5.30 eV approximately is mainly composed of the contribution of Au-d states, a mixture of Cl-s and Cl-d states and a tiny contribution of Cs-p; this band shows a peak at -5.50 eV.

The band ranging from -4.64 eV to -3.30 eV is composed of Au-d and Cl-p states and has two peaks around 4.43 eV and 3.81 eV. Then there is a band from -2.84 eV to near the Fermi level formed principally by Au-d and Cl-p states, and has 4 main peaks located at -2.74 eV, -2.14 eV, -1.44 eV and -0.89 eV. The conduction band appears to range from 1.05 eV to 1.90 eV with contributions Au-d, Cl-p and a peak at 1.45 eV.

As it is possible to see in Fig 4.5 the biggest contribution of cesium is located at the conduction band ranging from 5.90 eV to 7.46 eV and corresponds to the Cs-s and Cs-d states. The orbital contributions of the PDOS can be found in Appendix C.

4.2 The $\text{Cs}_2\text{Au}_2\text{Cl}_6$ (001) surface

This section presents the study of the perovskite $\text{Cs}_2\text{Au}_2\text{Cl}_6$ surface, using slabs with four layers of thickness.

The criteria used to select the optimum thickness is that the slab must be thick enough so that the surface electrons do not feel the interaction of the electrons from the lower layers. For this reason, calculations were made varying the thickness of the slab until a specific thickness was found. In our case, from four layers, the criteria are already met. However, the electronic structure of the system with four and six layers was also analyzed and compared. The result of the PDOS of the surface layer of each of the systems indicates that there is not a very big difference, so four layers

are more than enough to work on the analysis of our material. The PDOS of the four-layer structure is shown in Fig 4.6, and the six-layer structure with its PDOS can be found in Appendix B.

There are two possible arrangements for the surface of our material; it could be finished in gold and chlorine, which will be surface type A, and another finish in cesium and chlorine, which will be called surface type B.

4.3 Four layers thickness surface A (I4a)

The structure was prepared using a thickness of four layers with gold and chlorine atoms at the top, a vacuum of 15 Å, the position of the bottom layer was fixed, and the remaining positions were allowed to relax. It was used an energy cut of 650 eV. and $0.035 \text{ 2}\pi\text{Å}^{-1}$ of separation length, which correspond to the $4 \times 4 \times 1$ k-points and the input files described in the methodology section. The atomic structure used was the following:

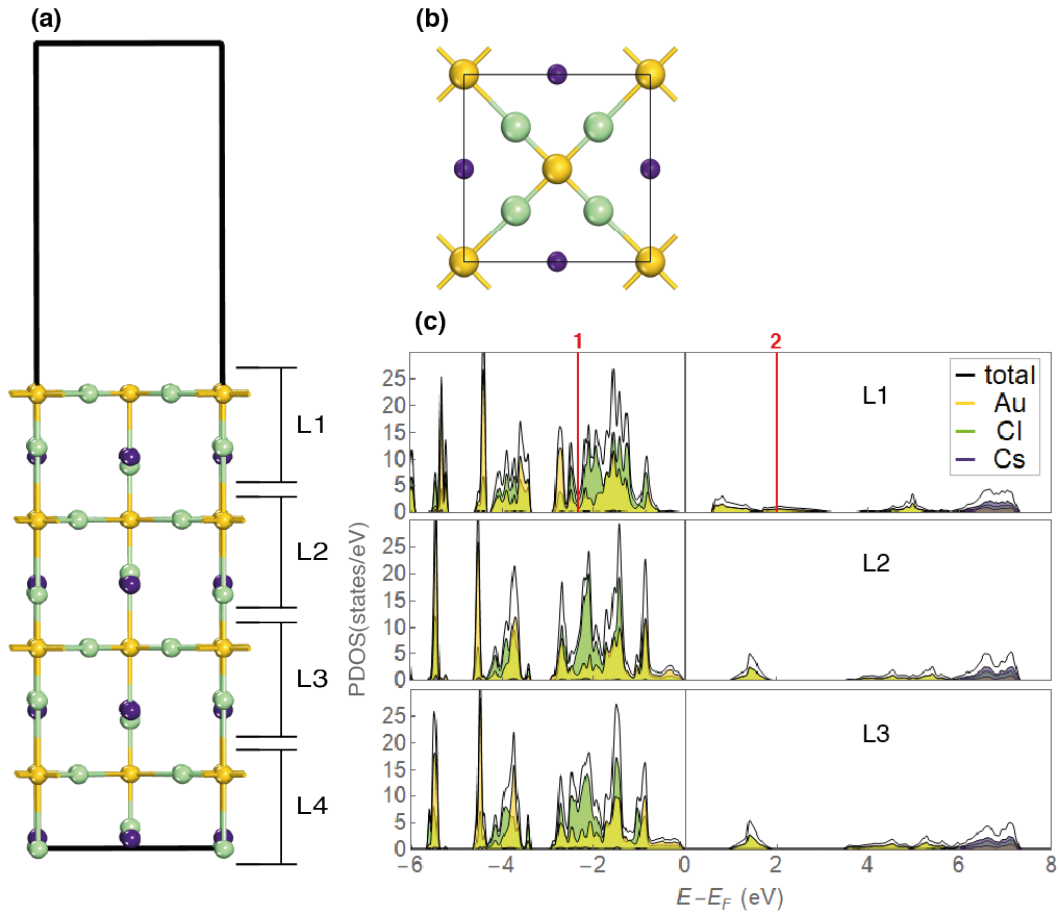


Figure 4.6: Atomic structure and SCAN computed PDOS for outermost layers of $\text{Cs}_2\text{Au}_2\text{Cl}_6$ surface A (14a). a) Side view of the atomic structure with four layers, L1 is the surface layer, and L4 is the last layer. It is important to notice that one layer is composed as shown. b) Top view of the surface layer. The black line represents the unit cell. c) PDOS of the outermost layers. The Fermi level is shifted to 0 eV and is represented by the vertical black line. The red lines (1 and 2) represent the range of integrated energies to obtain the STM images.

The PDOS shows that the surface has insulator behaviour; layer one (L1) presents a valence band with contributions of gold and chlorine, which mainly correspond to Au-d, Cl-p states and in a short amount cesium contribution belongs to Cs-p states. Meanwhile, the conduction band has the gold, chlorine and cesium contributions with the Au-s, Au-d, Cl-p and Cs-d states. The orbital contributions are in Appendix C.

4.3.1 Simulated constant current (STM) images for $\text{Cs}_2\text{Au}_2\text{Cl}_6$ (I4a)

The Tersoff-Hamann approximation was used to compute STM images using a range of energies between -2.34 eV to 2 eV, as shown in Fig. 4.6 part c. STM images are presented in Fig. 4.7 using a negative V_{bias} of -1.10 V and a positive V_{bias} of 1.0 V. Furthermore, it is presented the relative height for each case.

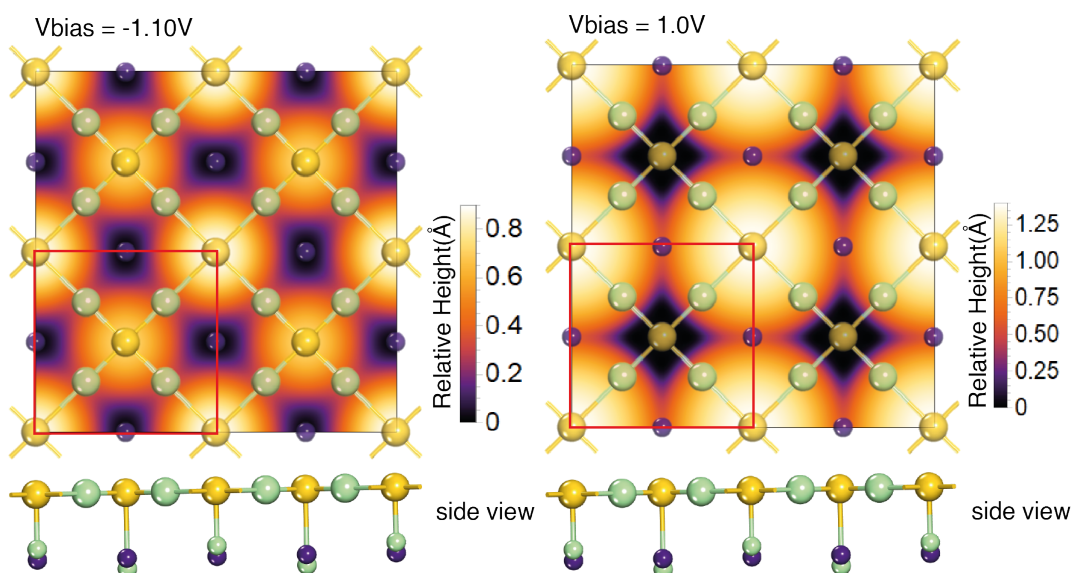


Figure 4.7: Computed STM images, line scan and relative height for $\text{Cs}_2\text{Au}_2\text{Cl}_6$ (I4a) surface. These images were computed for a supercell of $2 \times 2 \times 1$, where $V_{bias} = -1.10$ V (left) and $V_{bias} = 1.0$ V (right) correspond to occupied states and in both images is superimposed the top view of the atomic structure of the surface. The red box represents the unit cell, and at the bottom, there is a side view of the atomic structure of the surface. On the sides of the images it is presented in relative height, which was calculated in the diagonal direction.

The topography for both voltages is similar; in the atomic reconstruction of the surface, the brightest spots represent the position of the superficial atoms. In both cases, it is possible to notice that correspond to gold atoms due to their orbits in the z-direction protrude into the vacuum resulting in the bright spots in the STM image, and the darker spots correspond to the atoms below the surface; such as cesium that is located at the sub surface and does not have a strong contribution as it is possible to check at Fig. 4.6. In the case of chlorine, its atoms are located at the surface. However, the STM images are not visible.

4.3.2 Simulated Ultraviolet Photoelectron Spectroscopy (UPS)

In order to compute the UPS spectrum for $\text{Cs}_2\text{Au}_2\text{Cl}_6$ (14a) surface, we used 115 eV photons which correspond to photoelectrons generated within approximately 4.7 Å of the outermost surface layers, in other words, the first outermost atomic layer.

Fig 4.8 is the computed spectra with the main peak around -1.7 eV, which is mainly composed of chlorine and gold, being the Cl contribution the highest. There is another peak at approximately -3.91 eV, composed of gold and chlorine, but this time there is more contribution of gold. Furthermore, there is a shoulder at -5.75 eV and the last peak at -7.12 eV with a full contribution of cesium.

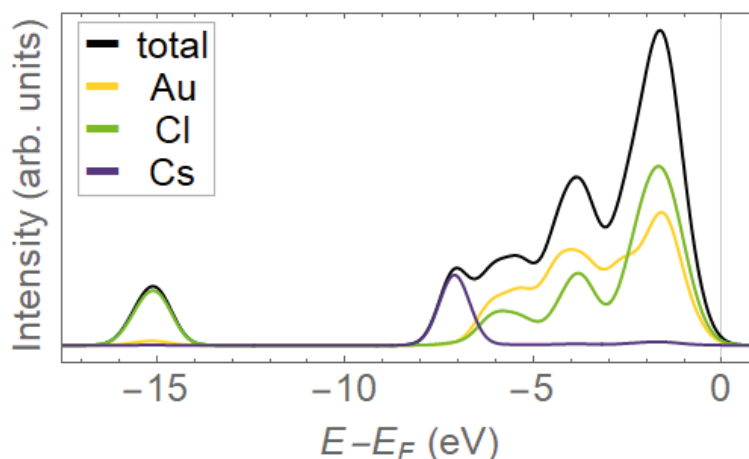


Figure 4.8: Computed UPS spectrum for $\text{Cs}_2\text{Au}_2\text{Cl}_6$ (14a) surface using 115 eV photons. The strongest contribution is from the gold and chlorine atoms, which form the largest peak. The Fermi level is shifted to 0 eV and is represented by the vertical black line.

4.3.3 Work Function (ϕ) and Ionization potential

To calculate the work function, we perform a DFT calculation of the total local potential of a structure in the z-direction. For this, we used the tag LVTOT and obtained an output file called LOCPOT. We use the script called MacroDensity⁵² developed by WMD-group to analyse the potential grid of the LOCPOT file. Finally, we plotted the total local potential averaged on the xy plane along the z-direction; the plateau of the plot indicates the location of the vacuum level above the surface.

The work function (ϕ) for $\text{Cs}_2\text{Au}_2\text{Cl}_6$ (14a) was computed subtracting the value of the Fermi level E_F that is shown with the red horizontal line and the value of the first plateau of the potential in the z-direction that is represented by the blue line. The work function had a value of 6.13 eV and is represented in the following figure with a black line, as shown in Fig. 4.9.

To calculate the ionization potential, we use the formula⁵³:

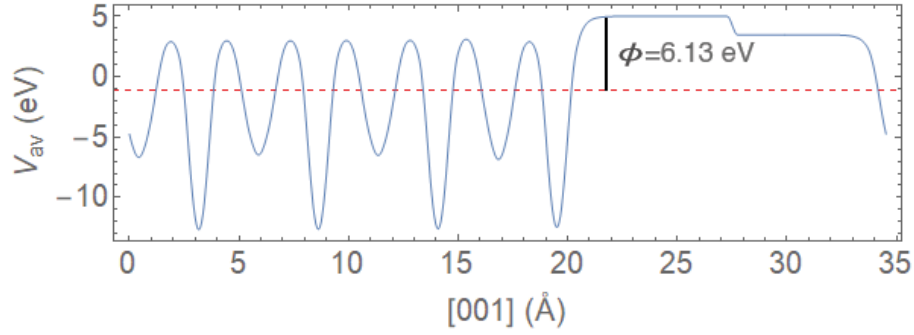


Figure 4.9: SCAN computed work function for $\text{Cs}_2\text{Au}_2\text{Cl}_6$ surface A (14a). The blue line represents the average potential in the z-direction, and the horizontal red dotted line is the Fermi level E_F

$$IP = D_s - E_{vbm} \quad (4.2)$$

where D_s is the surface dipole and E_{vbm} is the Fermi energy at the pristine structure. To get the surface dipole D_s , we compute the difference between the potential (green line) of each plateau represented with black arrows as displayed in Fig. 4.10.

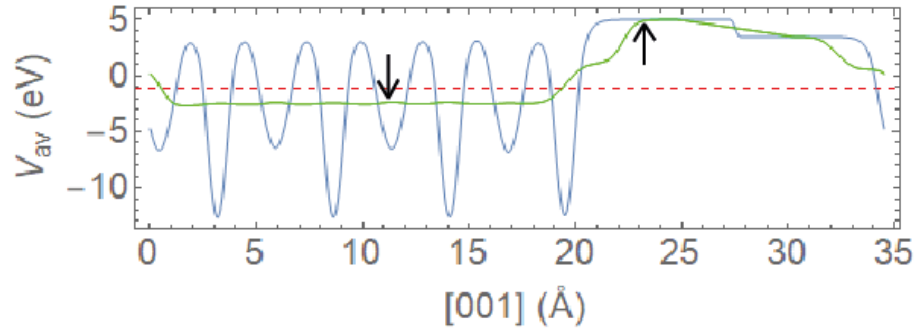


Figure 4.10: Work Function and the potential inside the material for $\text{Cs}_2\text{Au}_2\text{Cl}_6$

Using this we have $D_s = 4.88 - (-2.32) = 7.2$ eV and with this the ionization potential is $IP = 7.2 - 0.76 = 6.6$ eV.

4.4 Four layers thickness surface B (14b)

The structure was built with a thickness of 4 layers. However, this time we made a surface of cesium and chlorine, a vacuum of 15 Å, fixing the position of the bottom layer and allowing for relaxing the remaining ones.

As, in the previous case it was used an energy cut of 650 eV and $0.035 \text{ } 2\pi\text{\AA}^{-1}$ of separation length, which corresponds to the $4 \times 4 \times 1$ k-points and the corresponding input files. The atomic structure used has the following form:

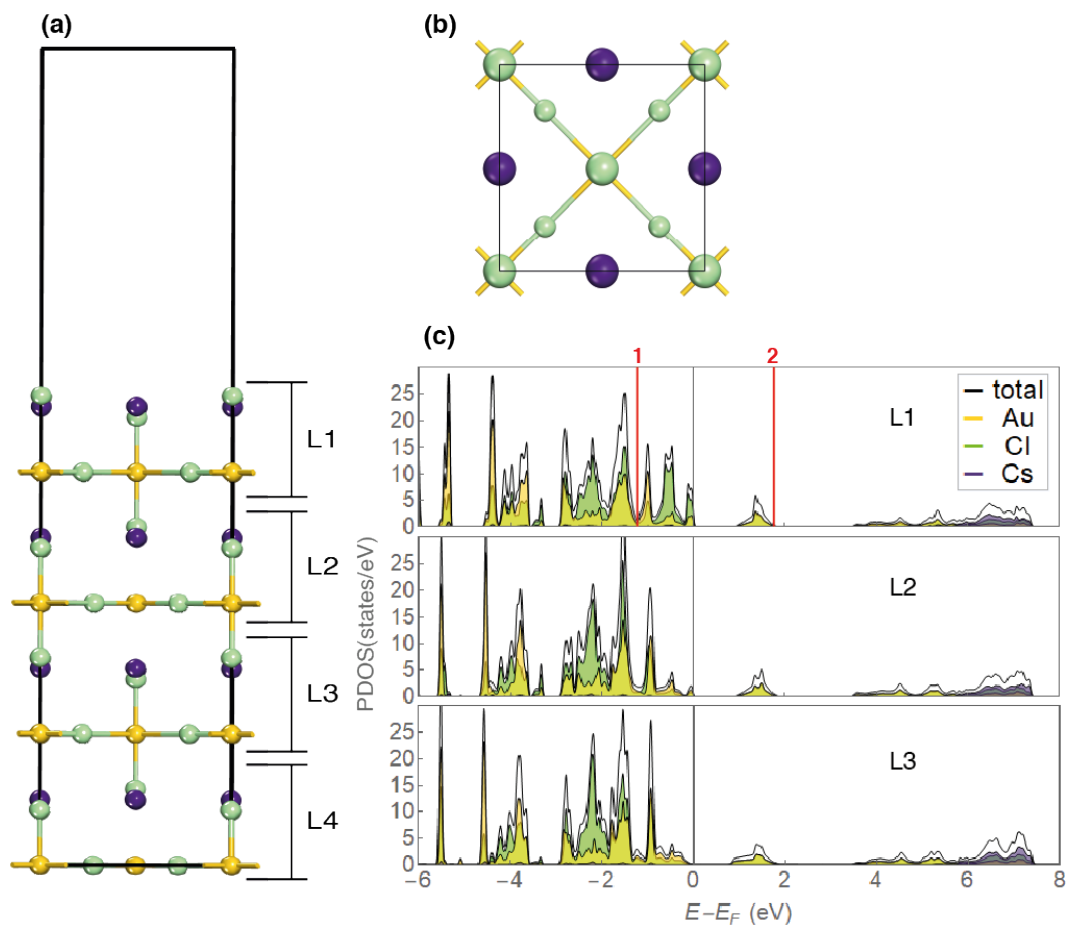


Figure 4.11: Atomic structure and SCAN computed PDOS for outermost layers of Cs₂Au₂Cl₆ surface B (14b). a) Side view of the atomic structure with four layers, L1 is the surface layer, and L4 is the last layer. It is important to notice that one layer is composed as shown. b) Top view of the surface layer. The black line represents the unit cell. c) PDOS of the outermost layers. The Fermi level is shifted to 0 eV and is represented by the vertical black line. The red lines (1 and 2) represent the range of integrated energies to obtain the STM images.

The PDOS shows that the surface has metallic behaviour; layer one (L1) presents a valence band with contributions of gold and chlorine, which mainly correspond to Au-d, Cl-p states and in a short amount cesium contribution to Cs-p states. Meanwhile, the conduction band has the gold, chlorine and cesium contributions with the Au-s, Au-d, Cl-p, Cs-s and Cs-d states. In the deeper layers (L3), the gap band opens, with which, at a certain depth, the material becomes an insulator, as it is possible to see in Fig 4.11 c). As in the previous case, the orbital contributions are in appendix C.

4.4.1 Simulated constant current (STM) images for $\text{Cs}_2\text{Au}_2\text{Cl}_6$ (14b)

In order to compute the STM images, a range of energies was used between -1.20 eV to 1.80 eV, as shown in Fig 4.11 part c). STM images are presented in Fig. 4.12 using a negative V_{bias} of -0.85 V. and a positive V_{bias} of 1.80 V. Furthermore, it is presented the relative height for each case.

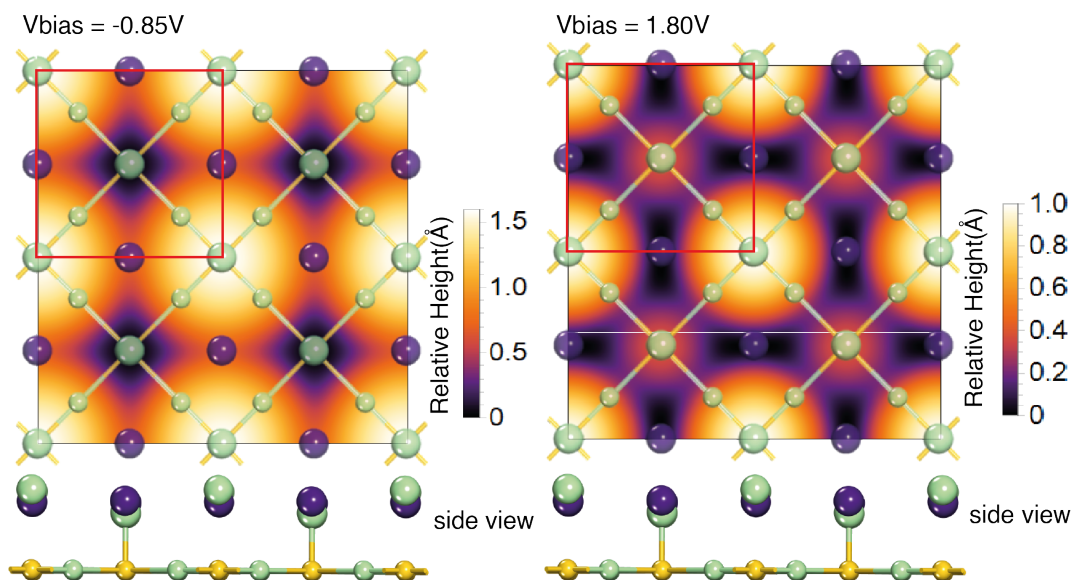


Figure 4.12: Computed STM images, line scan and relative height for $\text{Cs}_2\text{Au}_2\text{Cl}_6(14a)$ surface (14b). These images were computed for a supercell of $2 \times 2 \times 1$, where $V_{bias} = -0.85$ V (left) correspond to an occupied state and the $V_{bias} = 1.80$ V (right) is at an unoccupied state. In both images is superimposed the top view of the atomic structure of the surface. The red box represents the unit cell, and at the bottom, there is a side view of the atomic structure of the surface. On the sides of the images it is presented in relative height, which was calculated in the diagonal direction.

In the case of $V_{bias} = -0.85$ V (left), the brightest spots represent the position of the superficial atoms and, in this case, correspond to the chlorine atoms, cesium atoms do not have a strong contribution as it is possible to check at Fig.4.11 part c). It is impossible to see the gold atoms because they are at the subsurface and covered by the surface chlorine atoms. On the other hand, with a $V_{bias} = 1.80$ V (right), the brightest spots represent the chlorine atoms,

and the darkest spots are the cesium atoms. Like the previous case, it is impossible to see the gold atoms because they are at the subsurface and covered by the surface chlorine atoms.

4.4.2 Simulated Ultraviolet Photoelectron Spectroscopy (UPS)

It was used 115 eV photons to simulated UPS spectrum for $\text{Cs}_2\text{Au}_2\text{Cl}_6$ surface B (14b) which correspond to photoelectrons generated within approximately 4.7 Å of the outermost surface layers, in other words, the first outermost atomic layer.

Fig. 4.13 is the computed spectra with the main peak around -1.66 eV, mainly composed of chlorine and gold. There are two peaks around -4.03 eV and -5.70 eV, respectively, which are also composed of gold and chlorine, but the gold contribution is the highest. Furthermore, the last peak is located at -7.28 eV and has a full contribution of cesium.

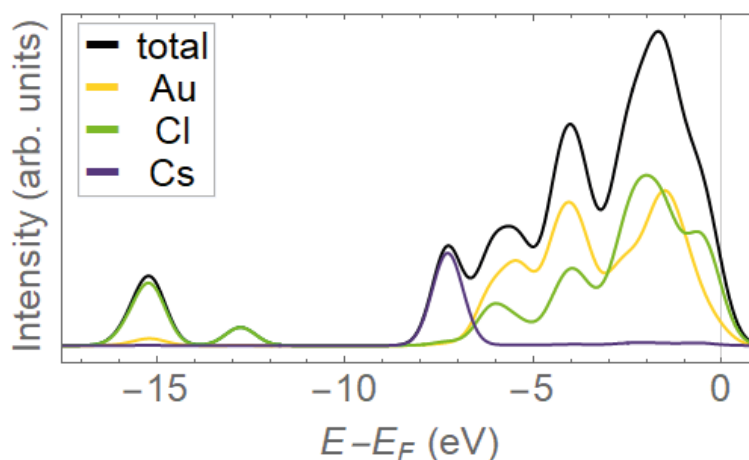


Figure 4.13: Computed UPS spectrum for $\text{Cs}_2\text{Au}_2\text{Cl}_6$ (14b) surface using 115 eV photons. The strongest contribution is from the gold and chlorine atoms. The Fermi level is shifted to 0 eV and is represented by the vertical black line.

4.4.3 Work Function (ϕ)

The work function (ϕ) for the case of $\text{Cs}_2\text{Au}_2\text{Cl}_6$ (14b), is 5.58 eV and is represented with a black line at Fig. 4.14. This result was obtained by subtracting the value of the Fermi level E_F shown with the red horizontal line and the value of the first plateau of the potential in the z-direction by the blue line.

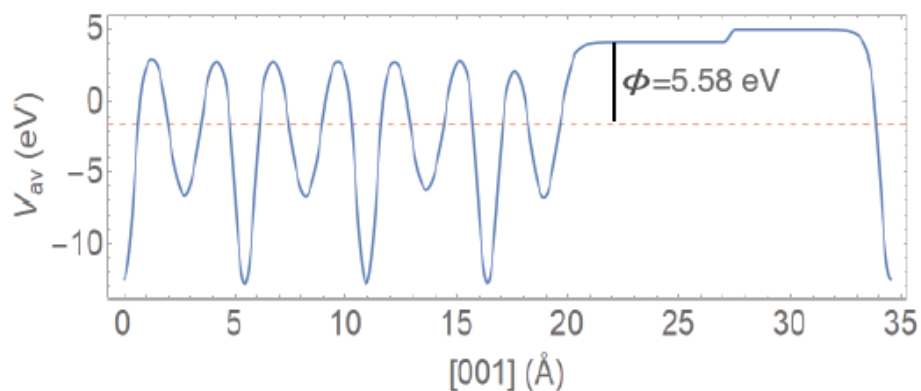


Figure 4.14: SCAN computed work function for $\text{Cs}_2\text{Au}_2\text{Cl}_6$ surface B (14b). The blue line represents the average potential in the z -direction, and the horizontal red dotted line is the Fermi level E_F

4.5 Chlorine Vacancies for $\text{Cs}_2\text{Au}_2\text{Cl}_6$ surface A

In this section, the study of the behaviour of $\text{Cs}_2\text{Au}_2\text{Cl}_6$ surface A with four layers changes when it is removed chlorine atoms from its structure is presented. It was chosen chlorine because it is the smaller atom, and it would need less energy to remove if we compare it with gold and cesium atoms. These vacancies can produce that the structure ends up with an odd number of atoms, and it is possible to suffer magnetization. So, we perform spin-polarized calculations to determine the magnetization of the structure.

To start the calculations, the unit cell was redefined through a linear combination of the lattice parameters. So, the new lattice parameters are: $a' = a + b$, $b' = -a + b$ and $c' = c$.

4.5.1 Surface A with one chlorine vacancy (14a-clv)

The structure was prepared with a thickness of 4 layers, with gold and chlorine atoms at the top. This time, one chlorine atom was removed from the surface; as the chlorine atoms in this arrangement are equivalents, we chose the atom randomly. The vacuum used was 15 \AA , and the position of the bottom layer was fixed, allowing for the relaxing of the remaining atoms. It was used cut off energy of 650 eV . and $0.035 \text{ } 2\pi \text{ \AA}^{-1}$ of separation length, which correspond to the $3 \times 3 \times 1$ k-points. The surface structure is displayed in Fig. 4.15.

Removing a chlorine atom produced a readjustment of the structure, which led to the position and bonds of the atoms changing. This change can be seen in Fig. 4.15 a), wherein the side view, it can be seen that a chlorine atom (2) protrudes from the surface and a gold atom (1) is bottom right of its original position. This change can also be seen in Fig. 4.15 b) where is a top view of the surface layer, where the most important things are that the central gold atom (1) moves to the right of its original position; this moves the chlorine atom (2), which is the one that protrudes from the surface. In addition, it can be seen that several atoms that were present at the beginning are now no longer

visible. Therefore, losing a chlorine atom modifies the atomic structure notably.

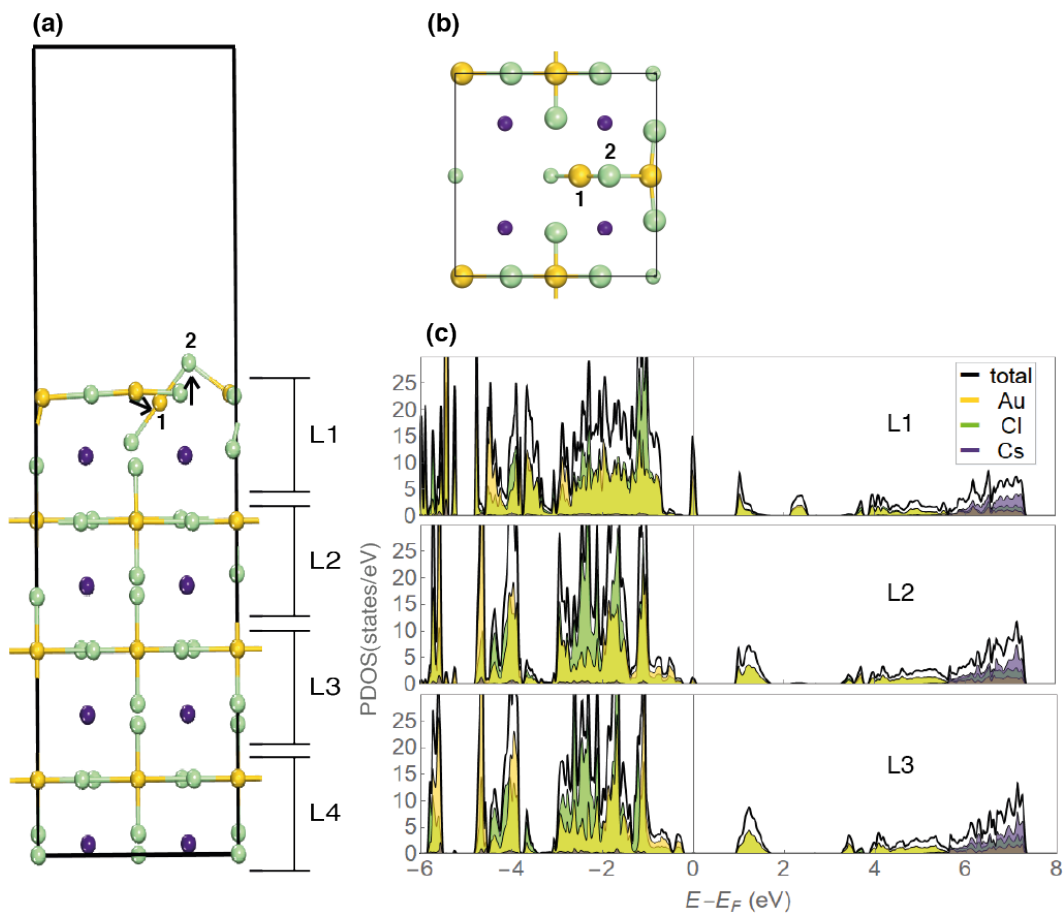


Figure 4.15: SCAN computed atomic and electronic structure for outermost layers of $\text{Cs}_2\text{Au}_2\text{Cl}_6$ with four layers of thickness and one chlorine vacancy (l4a-clv). a) Side view of the atomic structure after relaxation, L1 is the surface layer, and L4 is the last layer. b) Top view of the surface. The black line represents the unit cell. c) PDOS of the outermost layers. The Fermi level is shifted to 0 eV and is represented by the vertical black line.

The PDOS shows that the surface has metallic behaviour, which continues to layer 3 (L3), where a band gap opens; this is different from the pristine l4a case where the surface and deeper layers were insulators.

The outermost layer presents a valence band with contributions of gold and chlorine, which mainly correspond to Au-d, Cl-p states and in a short amount cesium contribution that belongs to Cs-p states, as the pristine case Fig. 4.6 but this time in a larger contribution. Meanwhile, the conduction band has the gold, chlorine and cesium contributions that have the Au-s, Au-d, Cl-p and Cs-d states. As in the previous case, the orbital contributions are in appendix C.

Spin-polarized calculations

The system with four layers should have 80 atoms. However, since we removed one chlorine atom to create the vacancy, it has 79 atoms, so to check if it has magnetic properties, a spin-polarized calculation was performed, and the Fig.4.16 shows the obtained results.

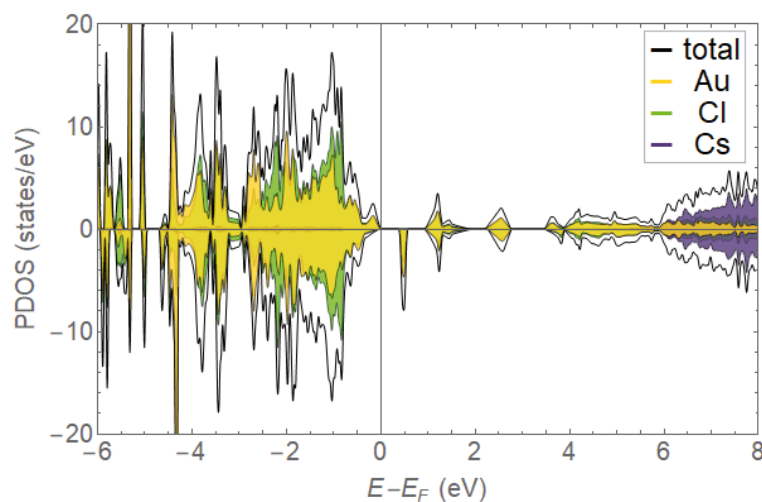


Figure 4.16: SCAN computed spin-polarized PDOS of the surface layer for $\text{Cs}_2\text{Au}_2\text{Cl}_6$ surface A with one chlorine vacancy (l4a-clv). The Fermi level is shifted to 0 eV and is represented by the vertical black line.

It was found that this structure has a magnetization of $1.01 \mu_B$, that correspond to the gold atoms. The contribution of gold is mainly given by Au-f and Au-d states, chlorine contribution is given by Cl-p and Cl-d states, and cesium is represented by Cs-d and Cs-f states.

Simulated Ultraviolet Photoelectron Spectroscopy (UPS)

It was used 115 eV photons to compute UPS spectra for $\text{Cs}_2\text{Au}_2\text{Cl}_6$ surface A with one chlorine vacancy (l4a-clv), which correspond to photoelectrons generated at the first outermost atomic layer.

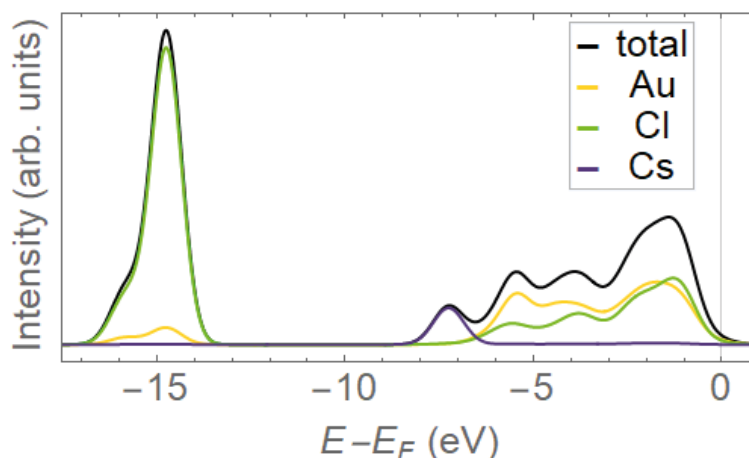


Figure 4.17: Computed UPS spectrum for $\text{Cs}_2\text{Au}_2\text{Cl}_6$ surface A with one chlorine vacancy (14a-clv). The strongest contribution is from the chlorine atoms. The Fermi level is shifted to 0 eV and is represented by the vertical black line.

Fig. 4.17 is the computed spectra with the main peak around -14.80 eV, mainly composed of chlorine and a short contribution of gold. There is a peak at -1.42 eV and other at -7.20 eV, the first one is composed of gold and chlorine, and a full contribution of cesium represents the second.

4.5.2 Surface A with two chlorine vacancies (14a-2clv)

The structure was prepared with a thickness of 4 layers, with gold and chlorine atoms at the top and removing two chlorine atoms from the surface.

The vacuum used was 15 Å, the position of the bottom layer was fixed, allowing to relax remaining atoms. It was used cut off energy of 650 eV and $0.035 \text{ 2}\pi\text{Å}^{-1}$ of separation length, which correspond to the $3 \times 3 \times 1$ k-points. For this case, spin-polarized calculations were not performed because when the two chlorine atoms are removed, the structure has 78 atoms, which is an even number. Instead, it is presented with STM images of the first layer where there is a band gap. Fig. 4.18 shows the atomic structure with the vacancies.

Removing two chlorine atoms produced a readjustment of the structure, which led to the position and bonds of the atoms changing. This change can be seen in Fig. 4.18 a), wherein the side view, it can be seen that a gold atom(1) moves down its original position. Fig. 4.18 b) shows that the top view of the surface has changed; the central gold atom(1) moves to the right of its original position; several of the chlorine and gold atoms that were present at the beginning are now no longer visible.

The PDOS shows that the surface has insulator behaviour, which is similar to the case of our pristine case. However, in layers 2(L2) and 3(L3), the band gap tends to close in the valence band. The surface layer presents a valence band with contributions mainly from gold and chlorine, which correspond to Au-d, Cl-p states and a short

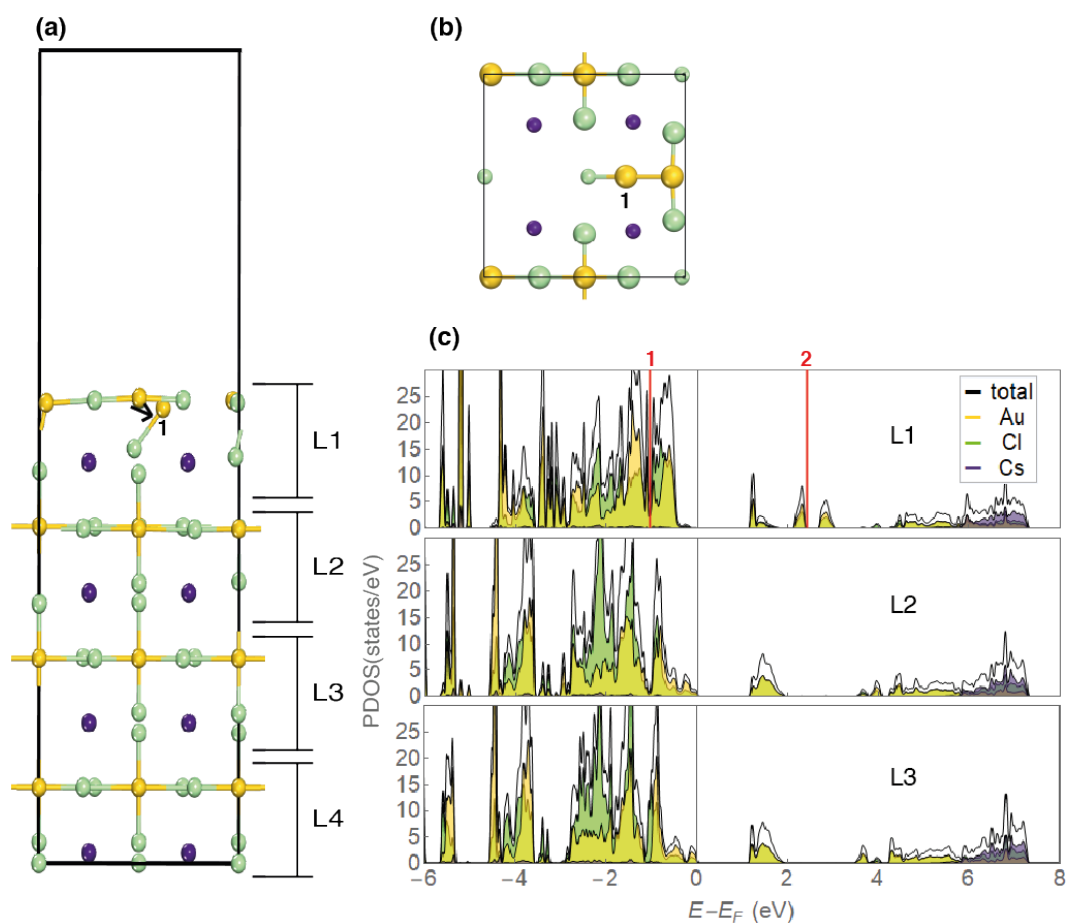


Figure 4.18: SCAN computed atomic and electronic structure for outermost layers of $\text{Cs}_2\text{Au}_2\text{Cl}_6$ with four layers of thickness and two chlorine vacancies (14a-2clv). a) Side view of the atomic structure after relaxation, L1 is the surface layer, and L4 is the last layer. b) Top view of the surface. The black line represents the unit cell. c) PDOS of the outermost layers. The Fermi level is shifted to 0 eV and is represented by the vertical black line. The red lines (1 and 2) represent the range of integrated energies to obtain the STM images.

contribution of Cs-p states, as the pristine case Fig. 4.6. Meanwhile, the conduction band has the gold, chlorine and cesium contributions that have the Au-s, Au-p, Au-d, Cl-p, Cs-s and Cs-d states. See appendix C to find more details on the contribution of each of the atomic orbitals in the PDOS.

Simulated constant current (STM) images for $\text{Cs}_2\text{Au}_2\text{Cl}_6$ (14a-2clv)

The range of energies used to compute the STM images was -1.0 eV to 2.40 eV, as shown in Figure 4.18 part c. STM images presented in Fig. 4.19 were computed using a negative V_{bias} of -0.35 V. and a positive V_{bias} of 2.4 V. Furthermore, it is presented the line scan and relative height for each case.

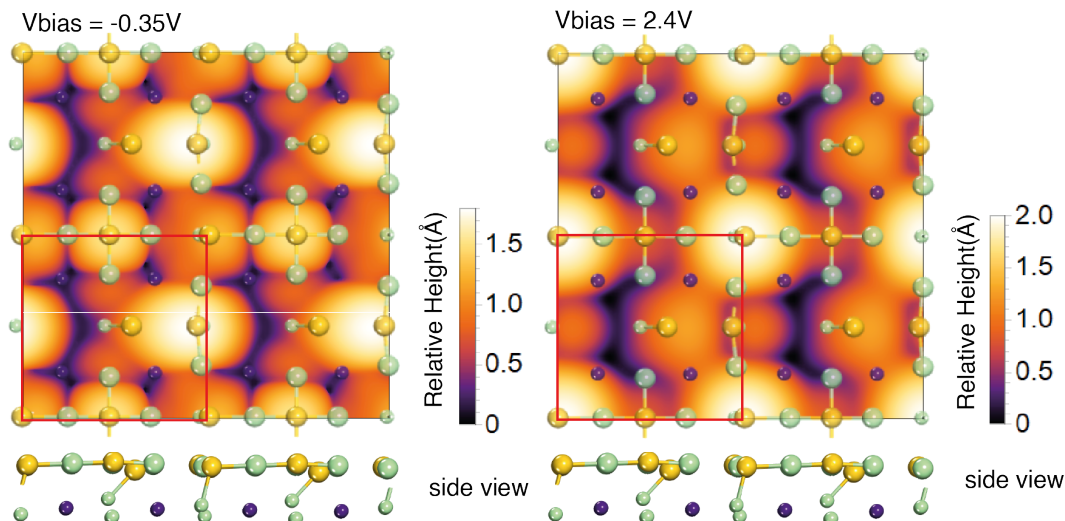


Figure 4.19: Computed STM images, line scan and relative height for $\text{Cs}_2\text{Au}_2\text{Cl}_6$ (14a-2clv). These images were computed for a supercell of $2 \times 2 \times 1$, where $V_{bias} = -0.35$ V. (left) correspond to an occupied state and the $V_{bias} = 2.4$ V. (right) is at an unoccupied state. In both images is superimposed the top view of the atomic structure of the surface. The red box represents the unit cell, and at the bottom, there is a side view of the atomic structure of the surface. On the sides of the images it is presented in relative height, which was calculated in the diagonal direction.

The bright spots represent the position of superficial atoms and, in this case, correspond to the gold atoms due to their orbitals in the z -direction protruding into the vacuum resulting in the bright spots in the STM image. The darker spots correspond to the atoms below the surface or do not have a strong contribution, such as cesium at the sub surface and do not have a strong contribution as it is possible to check at Fig. 4.18. In the case of chlorine, its atoms are located at the surface. However, the STM image is not visible.

Simulated Ultraviolet Photoelectron Spectroscopy (UPS)

In order to compute the UPS spectra, it was used 115 eV photons for $\text{Cs}_2\text{Au}_2\text{Cl}_6$ surface A with two chlorine vacancies (14a-2clv) which correspond to photoelectrons generated at the first outermost atomic layer.

The spectra at Fig 4.20 has a main peak around -1.22 eV, mainly composed of gold and chlorine, with the Au contribution the highest. There is another peak at approximately -5.20 eV, mainly composed of gold and a small quantity of chlorine. Furthermore, there is a small peak at -7.12 eV composed entirely of cesium.

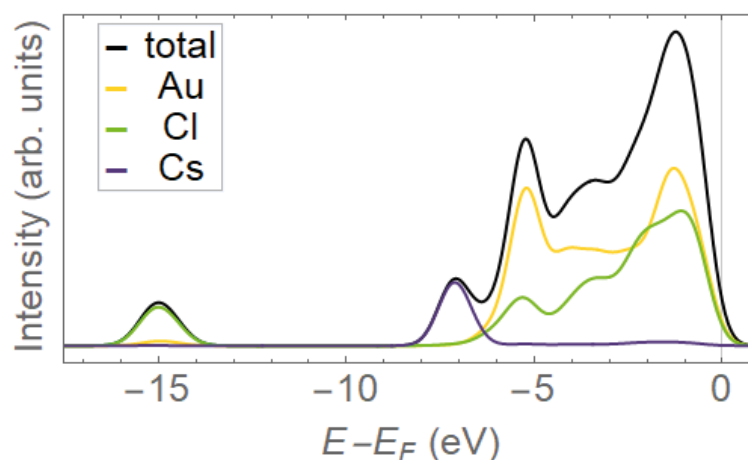


Figure 4.20: Computed UPS spectrum for $\text{Cs}_2\text{Au}_2\text{Cl}_6$ surface A with two chlorine vacancies (14a-2clv). The strongest contribution is from the gold and chlorine atoms. The Fermi level is shifted to 0 eV and is represented by the vertical black line.

4.5.3 Surface A with one A-type chlorine vacancy at the subsurface (14a-sclvA)

As in the previous cases, our slab has four layers of thickness and chlorine atoms will be removed to create the vacancies. At the subsurface, the chlorine atoms can occupy two non-equivalent positions so that both cases will be studied, calling them cases A and B. One chlorine atom will be removed in each case, so our structures will remain with an odd number of atoms. So, in these cases, spin-polarized calculations will be performed to determine the material magnetization.

In this subsection, the A case structure will be studied. The structure was prepared with a thickness of 4 layers, with gold and chlorine atoms at the top. This time it was removed one chlorine atom from the subsurface.

The vacuum used was 15 \AA , and the position of the bottom layer was fixed, allowing to relax remaining atoms. It was used cut off energy of 650 eV and $0.035 \text{ 2}\pi\text{\AA}^{-1}$ of separation length, which correspond to the $3 \times 3 \times 1$ k-points. The surface structure is displayed in Fig. 4.21.

Removing one chlorine atom produced a readjustment of the structure, moving the atomic bonds in the first layer (L1), as it is possible to see in Fig. 4.21 a). The central bond of the structure is broken if we view it from the top, as shown in Fig 4.21 b).

The PDOS shows that the surface has metallic behaviour; however, at layer 3 (L3), the band gap tends to open in the valence band. The surface layer presents a valence band with contributions mainly from gold and chlorine, which correspond to Au-d, Cl-p states and a short contribution of Cs-p states. Meanwhile, the conduction band has the gold, chlorine and cesium contributions that have the Au-s, Au-p, Au-d, Cl-p, Cs-s and Cs-d states. See appendix C to find more details on the contribution of each of the atomic orbitals in the PDOS.

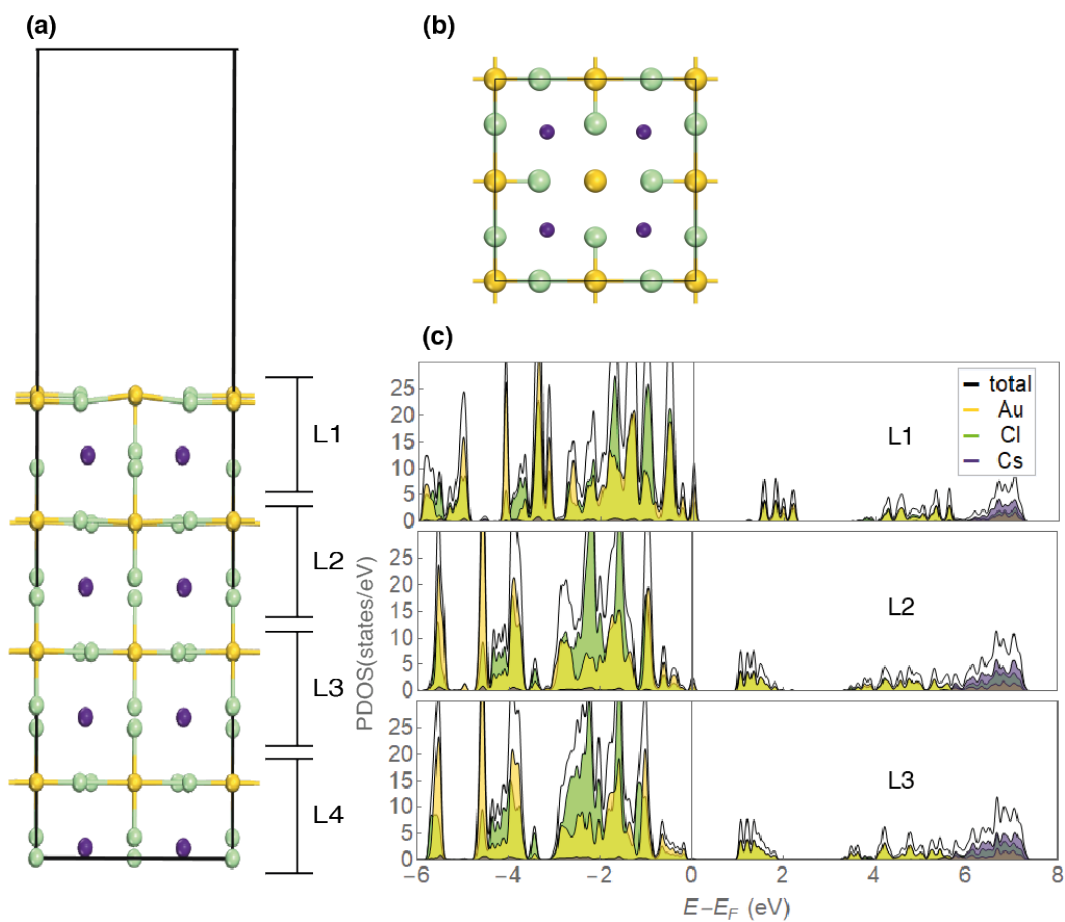


Figure 4.21: SCAN computed atomic and electronic structure for outermost layers of $\text{Cs}_2\text{Au}_2\text{Cl}_6$ with four layers of thickness and one chlorine vacancy at the subsurface (14a-sclvA). a) Side view of the atomic structure after relaxation, L1 is the surface layer, and L4 is the last layer. b) Top view of the surface. The black line represents the unit cell. c) PDOS of the outermost layers. The Fermi level is shifted to 0 eV and is represented by the vertical black line.

Spin-polarized calculations

The system with four layers should have 80 atoms. However, since we removed one chlorine atom at the subsurface to create the vacancy, it has 79 atoms. A spin-polarized calculation was performed to check if it has magnetic properties, and Fig.4.22 shows the obtained results.

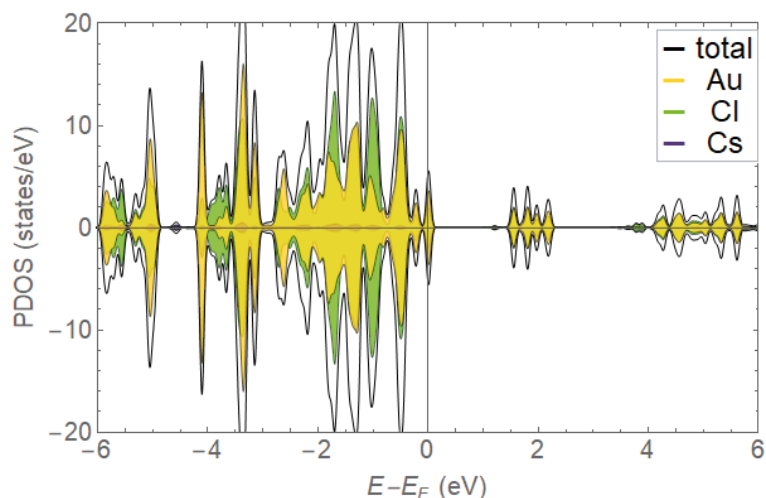


Figure 4.22: SCAN computed spin-polarized PDOS of the surface layer for $\text{Cs}_2\text{Au}_2\text{Cl}_6$ surface A with one chlorine vacancy at the subsurface (14a-sclvA). The Fermi level is shifted to 0 eV and is represented by the vertical black line.

It was found that this structure does not have magnetization, and this could be proved with 4.22 where the positive and the negative part is the same. The contribution of gold is mainly given by Au-d, Au-f states, chlorine contribution is given by Cl-p, Cl-d states and cesium is represented by Cs-d and Cs-f states.

Simulated Ultraviolet Photoelectron Spectroscopy (UPS)

To compute the UPS spectra, they were used 115 eV photons for $\text{Cs}_2\text{Au}_2\text{Cl}_6$ surface A with one chlorine vacancy at the subsurface (14a-sclvA), which corresponds to photoelectrons generated at the first outermost atomic layer.

The spectra has the main peak around -1.46 eV, composed of chlorine and gold. There is another peak at -3.39 eV with the contribution of the same elements. A third peak is at -5.23 eV with gold and chlorine contribution. Finally, the peak is at -6.84 eV, made entirely of cesium

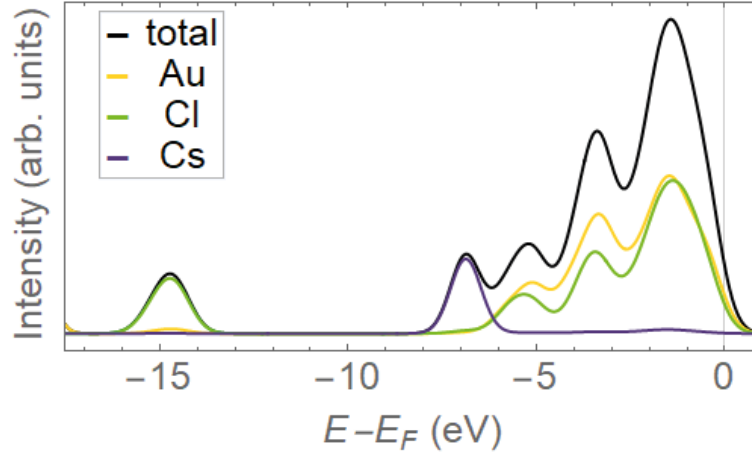


Figure 4.23: Computed UPS spectrum for $\text{Cs}_2\text{Au}_2\text{Cl}_6$ surface A with one chlorine vacancy at the subsurface (14a-sclvA). The strongest contribution is from the gold and chlorine atoms. The Fermi level is shifted to 0 eV and is represented by the vertical black line.

4.5.4 Surface A with one B-type chlorine vacancy at the subsurface (14a-sclvB)

In this subsection, the B case structure will be studied, which is the other case where removing a chlorine atom from the subsurface is possible. This time, one chlorine atom was removed from the subsurface of case B. So, the structure was prepared with a thickness of 4 layers, with gold and chlorine atoms at the top.

The vacuum used was 15 Å, and the position of the bottom layer was fixed, allowing to relax remaining atoms. It was used cut off energy of 650 eV, and $0.035 \text{ 2}\pi\text{Å}^{-1}$ of separation length, which correspond to the $3 \times 3 \times 1$ k-points. The surface structure is displayed in Fig. 4.24.

This time removing one chlorine atom from the subsurface produced a readjustment of the structure with movement at the top part of layer 2 (L2), as it is possible to see in Fig. 4.24 a) and the top view Fig.4.24 b) is not possible to observe a change in the atoms or the bonds.

The PDOS shows that the surface has metallic behaviour that is maintained throughout the structure; this is different from the case (14a-sclvA), where at layer 3 (L3), the band gap tends to open as we could see at 4.21 c). The surface presents a valence band with contributions mainly from gold and chlorine, which correspond to Au-d, Cl-p states and a short contribution of Cs-p states. Meanwhile, the conduction band has the gold, chlorine and cesium contributions that have the Au-s, Au-p, Au-d, Cl-p, Cs-s and Cs-d states. See appendix C to find more details on the contribution of each of the atomic orbitals in the PDOS.

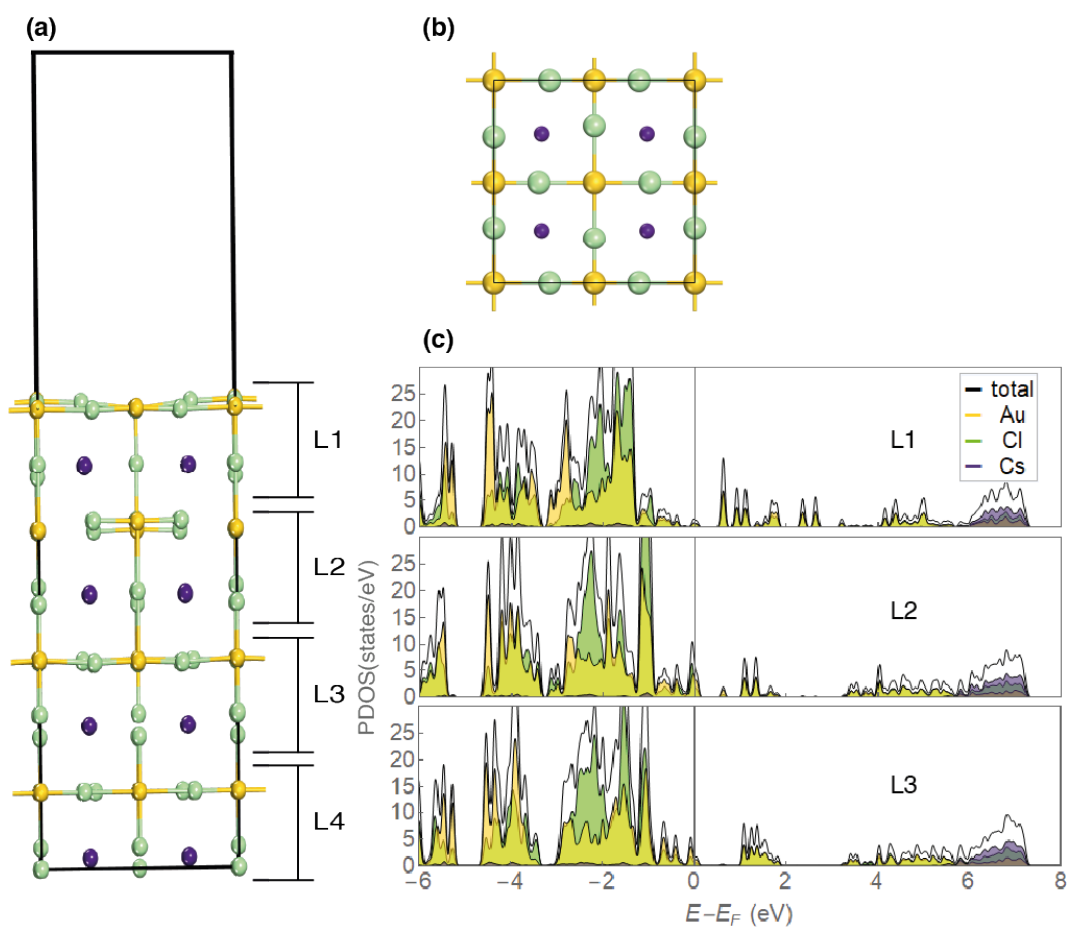


Figure 4.24: SCAN computed atomic and electronic structure for outermost layers of $\text{Cs}_2\text{Au}_2\text{Cl}_6$ with four layers of thickness and one chlorine vacancy at the subsurface of the case B (14a-sclvB). a) Side view of the atomic structure after relaxation, L1 is the surface layer, and L4 is the last layer. b) Top view of the surface. The black line represents the unit cell. c) PDOS of the outermost layers. The Fermi level is shifted to 0 eV and is represented by the vertical black line.

Spin-polarized calculations

The system with four layers should have 80 atoms, but since we removed one chlorine atom at the subsurface to create the vacancy, it has 79 atoms. However, the calculation of the spin-polarized was done for the case (14a-sclvA) because it is more energetically stable than (14a-sclvB).

Simulated Ultraviolet Photoelectron Spectroscopy (UPS)

The UPS spectra was computed using 115 eV photons for $\text{Cs}_2\text{Au}_2\text{Cl}_6$ surface A with one chlorine vacancy at the subsurface (14a-sclvB), which corresponds to photoelectrons generated at the first outermost atomic layer

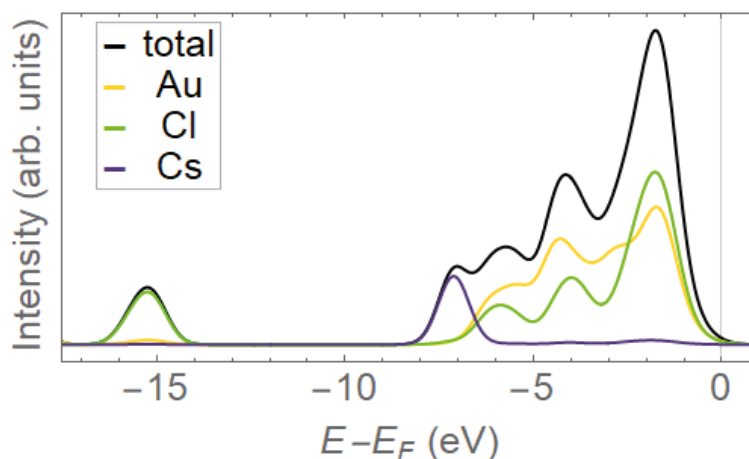


Figure 4.25: Computed UPS spectra for $\text{Cs}_2\text{Au}_2\text{Cl}_6$ surface A with one chlorine vacancy at the subsurface (14a-sclvB). The strongest contribution is from the gold and chlorine atoms. The Fermi level is shifted to 0 eV and is represented by the vertical black line.

The spectra obtained at Fig. 4.25 has a main peak around -1.74 eV, composed of chlorine and gold. There is another peak at -4.03 eV with gold and chlorine contributions. Finally, the peak at -7.08 eV is made entirely of cesium.

4.5.5 Vacancy Energy Formation

This subsection presents Table 4.2 with the results of the vacancy energy formation of a point defect in solids for vacancies in surface A.

From this table, it is possible to see that the vacancy (14a-clv) is the one that needs less energy to be produced, followed by (14a-sclvA), (14a-sclvB) vacancies and the most difficult is the (14a-2clv) vacancy because it is the one that needs the most energy to remove a chlorine atom from its structure. It is also shown that of all the vacancies studied, only the (14a-2clv) vacancy presents insulating behaviour; all the others are metallic.

Table 4.2: Energy formation for each vacancy of $\text{Cs}_2\text{Au}_2\text{Cl}_6$ surface A. (14a-clv) represents the one chlorine vacancy at the surface. (14a-2clv) represents the two chlorine vacancies at the surface. (14a-sclvA) represents the A case of one chlorine vacancy at the subsurface, and (14a-sclvB) represents the B case of one chlorine vacancy at the subsurface.

Vacancy Type	Behaviour	Energy Formation (eV)
14a-clv	metallic	16.26
14a-2clv	insulator	24.83
14a-sclvA	metallic	16.39
14a-sclvB	metallic	17.88

4.5.6 Work Function (ϕ)

Table 4.3 presents a summary of the work function calculated for each case of the vacancies of the finished surface in gold and chlorine. The graphs of the work functions are found in appendix D.

Table 4.3: Work Function (ϕ) for each vacancy of $\text{Cs}_2\text{Au}_2\text{Cl}_6$ surface A. (14a-clv) represents the one chlorine vacancy at the surface. (14a-2clv) represents the two chlorine vacancies at the surface. (14a-sclvA) represents the A case of one chlorine vacancy at the subsurface, and (14a-sclvB) represents the B case of one chlorine vacancy at the subsurface.

Vacancy Type	ϕ (eV)
14a-clv	6.31
14a-2clv	6.74
14a-sclvA	6.96
14a-sclvB	6.28

From this table, the energy necessary to remove an electron from the surface is in the range of 6 eV to 7 eV, where the one that needs less energy is the vacancy (14a-sclvB), followed by (14a-clv), (14a-2clv) and (14a-sclvA) in order from lowest to greatest difficulty to remove an electron.

4.6 Chlorine Vacancies for $\text{Cs}_2\text{Au}_2\text{Cl}_6$ surface B

In this section, we are going to study if the behaviour of $\text{Cs}_2\text{Au}_2\text{Cl}_6$ surface B with four layers changes when chlorine atoms are removed from its structure. These vacancies can end up in a structure with an odd number of atoms. So, spin-polarized calculations will be performed to determine if the material suffers magnetization. We chose chlorine because it is a smaller atom and would need less energy to remove if we compare it with gold and cesium atoms.

To start the calculations, the unit cell was redefined through a linear combination of the lattice parameters. So, the new lattice parameters are: $a' = a + b$, $b' = -a + b$ and $c' = c$.

4.6.1 Surface B with one A-type chlorine vacancy (14b-clvA)

The structure was prepared with a thickness of 4 layers, with cesium and chlorine atoms at the top. In order to create the chlorine vacancy at the surface, it must be taken into account that this atom has two non-equivalent positions, so we will differentiate them by calling them cases A and B. In this subsection, we will study the chlorine vacancy corresponding to case A. The structure was built with a vacuum of 15 Å, and the position of the bottom layer was fixed, allowing to relax remaining atoms. It was used cut off energy of 650 eV and $0.035 \text{ 2}\pi\text{Å}^{-1}$ of separation length, which correspond to the $3 \times 3 \times 1$ k-points. The surface structure is displayed in Fig. 4.26.

Removing one chlorine atom from the surface produced a readjustment of the structure with little movement of the subsurface at layer 1 (L1) as it is possible to see at 4.26 a) if we see the part b) with the top view of the material, it keeps his form after the relaxation.

The PDOS shows that the surface has metallic behaviour, which continues to layer 3 (L3), where a band gap opens. This behaviour is similar to our pristine case Fig 4.11. In this case, the outermost layer presents a valence band with contributions of gold and chlorine, which mainly correspond to Au-d, Cl-p states and in short amount cesium. Meanwhile, the conduction band has the gold, chlorine and cesium contributions that have the Au-s, Au-d, Cl-p and Cs-d states. As in the previous case, the orbital contributions are in appendix C.

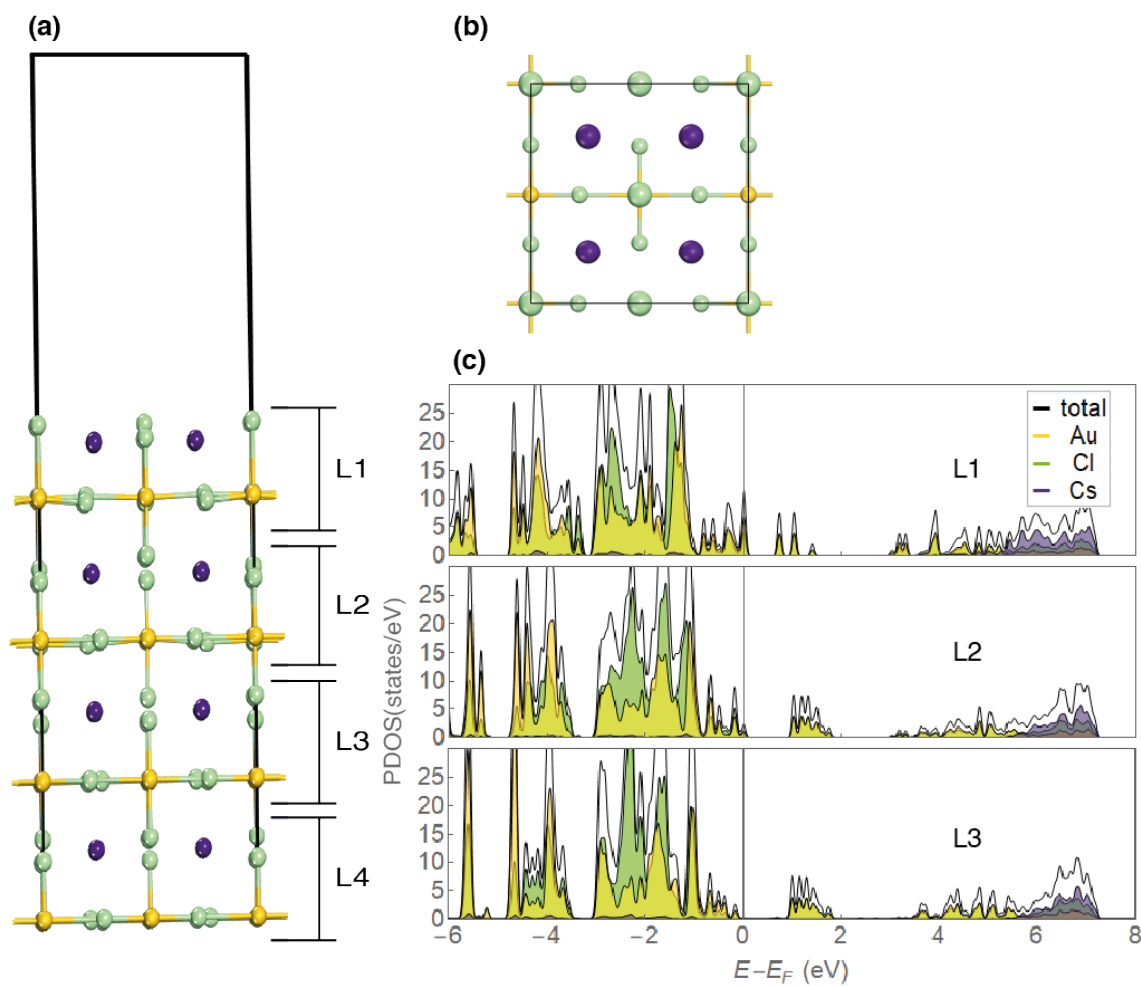


Figure 4.26: SCAN computed atomic and electronic structure for outermost layers of $\text{Cs}_2\text{Au}_2\text{Cl}_6$ with four layers of thickness and one chlorine vacancy (14b-clvA). a) Side view of the atomic structure after relaxation, L1 is the surface layer, and L4 is the last layer. b) Top view of the surface. The black line represents the unit cell. c) PDOS of the outermost layers. The Fermi level is shifted to 0 eV and is represented by the vertical black line.

Spin-polarized calculations

The system with four layers should have 80 atoms, but since we removed one chlorine atom at the surface to create the vacancy, it has 79 atoms. However, the calculation of the spin-polarized was done for case B of one vacancy at the surface (14b-clvB), which is more energetically stable.

Simulated ultraviolet photoelectron spectroscopy (UPS)

The UPS spectra was computed using 115 eV photons for $\text{Cs}_2\text{Au}_2\text{Cl}_6$ surface B with one chlorine vacancy at the surface (14b-clvA), which correspond to photoelectrons generated at the first outermost atomic layer. The spectra of the Fig. 4.27 has a main peak around -1.70 eV, mainly composed of chlorine and gold. There is a peak at -4.07 eV, and other at -5.67 eV, composed of gold and chlorine and the last peak is located at -7.24 eV, represented by a full contribution of cesium.

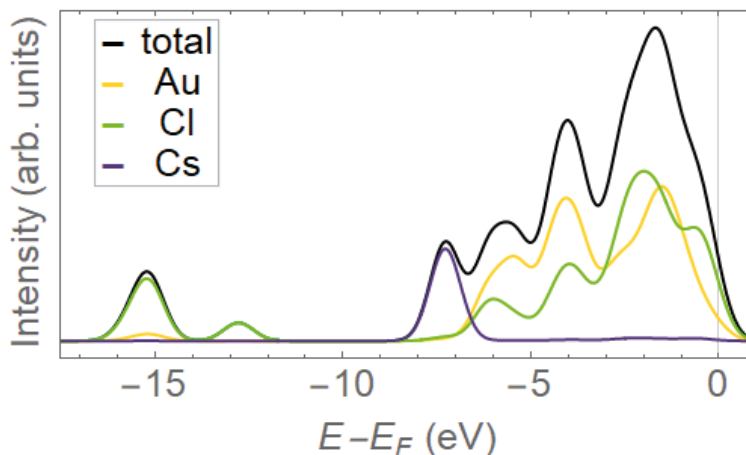


Figure 4.27: Computed UPS spectra for $\text{Cs}_2\text{Au}_2\text{Cl}_6$ surface B with one chlorine vacancy at the surface (14b-clvA). The strongest contribution is from the gold and chlorine atoms. The Fermi level is shifted to 0 eV, and is represented by the vertical black line.

4.6.2 Surface B with one B-type chlorine vacancy (14b-clvB)

The structure was prepared with a thickness of 4 layers, with gold and chlorine atoms at the top and removing one chlorine atom from the second position at the surface. So, this is the analysis of case B.

The vacuum used was 15 Å, and the position of the bottom layer was fixed, allowing to relax remaining atoms. It was used cut off energy of 650 eV and $0.035 \text{ 2}\pi\text{Å}^{-1}$ of separation length, which correspond to the $3 \times 3 \times 1$ k-points. Fig. 4.28 displays the atomic structure with the vacancies.

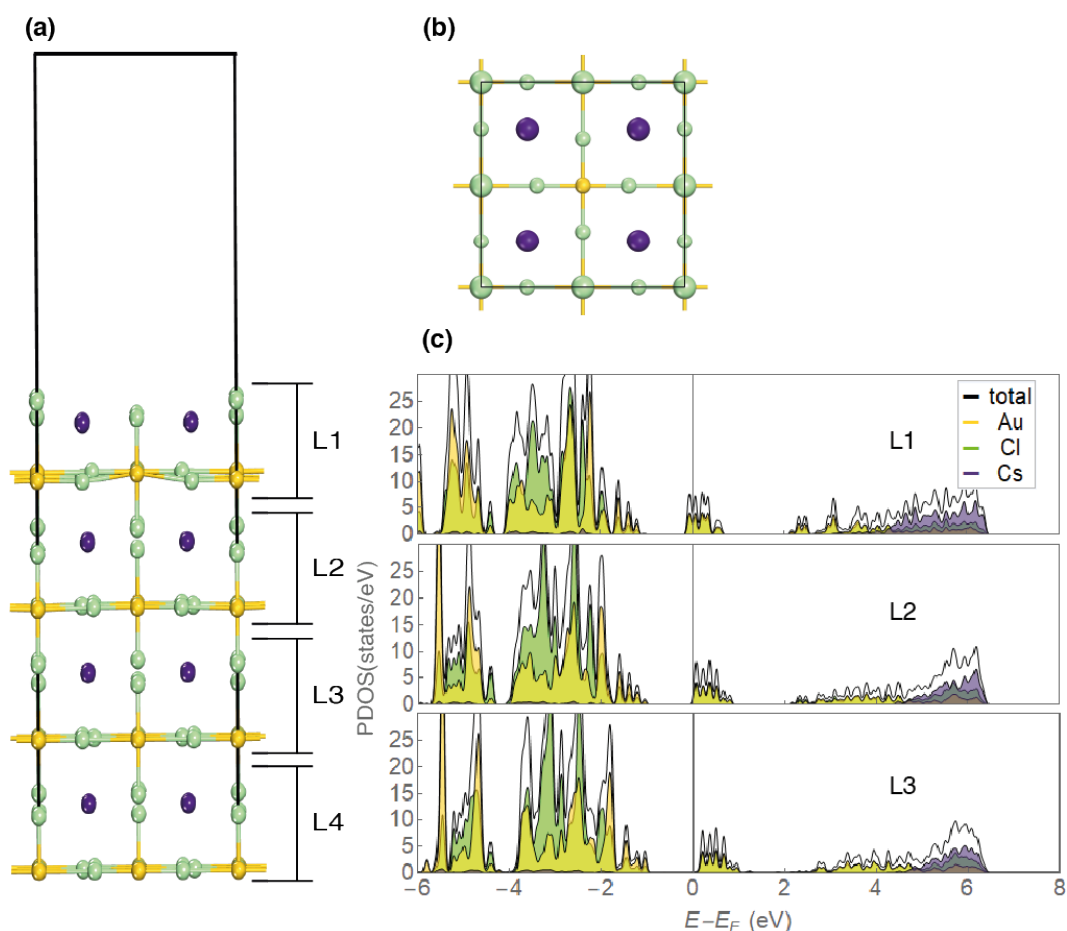


Figure 4.28: SCAN computed atomic and electronic structure for outermost layers of $\text{Cs}_2\text{Au}_2\text{Cl}_6$ with four layers of thickness and one chlorine vacancy (14b-clvB). a) Side view of the atomic structure after relaxation, L1 is the surface layer, and L4 is the last layer. b) Top view of the surface. The black line represents the unit cell. c) PDOS of the outermost layers. The Fermi level is shifted to 0 eV and is represented by the vertical black line.

This time removing the second position chlorine from the surface produced a readjustment of the structure with little movement of the subsurface at layer 1 (L1), as it is possible to see at 4.28 (a) as in the previous case. The surface top view has kept its form and structure, with the rest of the atoms in the structure.

The PDOS shows that the surface has metallic behaviour, which continues to layer 3 (L3), where a band gap opens. This behaviour is similar to our pristine case Fig 4.11. In this case, the outermost layer presents a valence band with contributions of gold and chlorine, which mainly correspond to Au-d, Cl-p states and in a short amount, Cs-p states. Meanwhile, the conduction band has the gold, chlorine and cesium contributions that have the Au-s, Au-d, Cl-p and Cs-d states. As in the previous case, the orbital contributions are in appendix C.

Spin-polarized calculations

The system with four layers should have 80 atoms. However, since we removed one chlorine atom at the surface to create the vacancy, it has 79 atoms, so to check if it has magnetic properties, a spin-polarised calculation was performed, and the Fig.4.29 shows the obtained results.

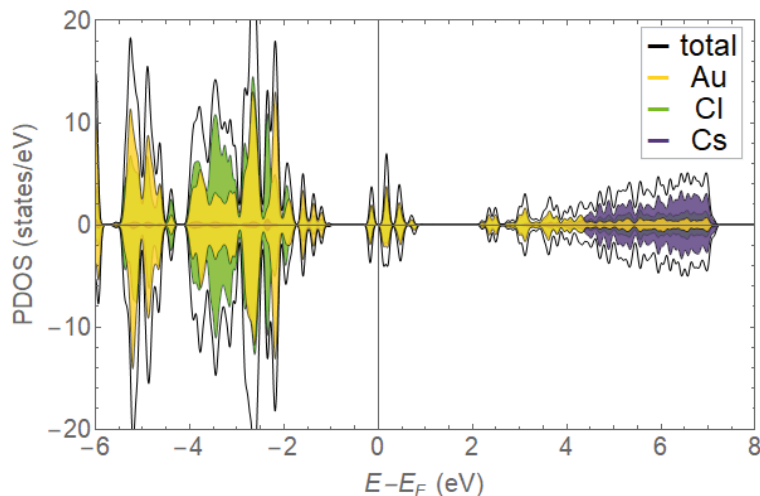


Figure 4.29: SCAN computed spin-polarized PDOS of the surface layer for $\text{Cs}_2\text{Au}_2\text{Cl}_6$ surface B with one chlorine vacancy at the subsurface (l4b-clvB). The Fermi level is shifted to 0 eV and is represented by the vertical black line.

It was found that this structure does not have magnetization, and this could be proved in Fig. 4.29 where the positive and the negative part is the same. Au-d states mainly give the contribution of gold, Au-f states, Cl-p gives chlorine contribution, Cl-d states and cesium is represented by Cs-d and Cs-f states.

Simulated Ultraviolet Photoelectron Spectroscopy (UPS)

The UPS spectra was computed using 115 eV photons for $\text{Cs}_2\text{Au}_2\text{Cl}_6$ surface B with one chlorine vacancy at the surface (l4b-clvB), which correspond to photoelectrons generated at the first outermost atomic layer

The spectra of Fig. 4.30 has a main peak at -2.70 eV, composed of equal parts chlorine and gold. There is a peak at -5.07 eV and another at -6.76 eV formed mainly by gold and a part of chlorine. Finally, cesium is present at -8.80 eV, with a peak done entirely by its contribution.

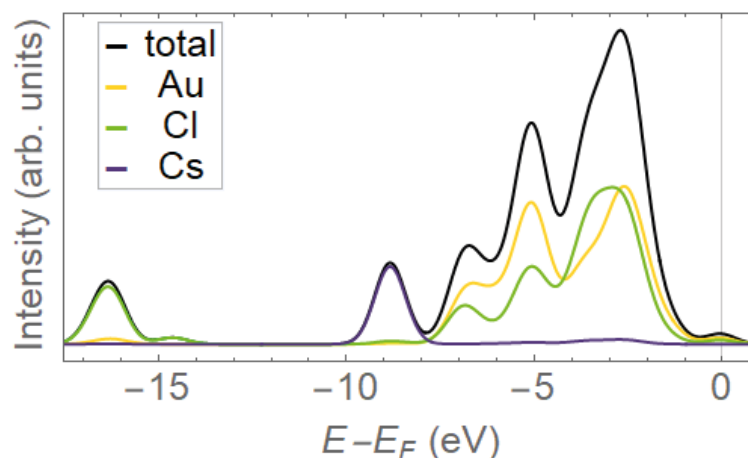


Figure 4.30: Computed UPS spectra for $\text{Cs}_2\text{Au}_2\text{Cl}_6$ surface B with one chlorine vacancy at the surface (l4b-clvB). The strongest contribution is from the gold and chlorine atoms. The Fermi level is shifted to 0 eV, and is represented by the vertical black line.

4.6.3 Surface B with two A-type chlorine vacancies (l4b-2clvA)

The following results are the analysis of the case (l4b-2clvA). The structure was prepared with a thickness of 4 layers, with gold and chlorine atoms at the top and removing two chlorine atoms from the surface of case A. For this case, spin corrections were not calculated because we have a structure with an even number of atoms when removing two atoms.

The vacuum used was 15 Å, and the position of the bottom layer was fixed, allowing to relax remaining atoms. It was used cut off energy of 650 eV, and $0.035 \text{ 2}\pi\text{Å}^{-1}$ of separation length, which correspond to the $3 \times 3 \times 1$ k-points. Fig. 4.31 displays the atomic structure with the vacancies.

This time removing the second position chlorine from the surface produced a readjustment of the structure with little movement of the subsurface at layer 1 (L1), as it is possible to see at 4.31 (a) as in the previous case. The surface has kept its form and structure after the relaxation despite having 2 of its atoms.

The PDOS shows that the surface has metallic behaviour, which continues until layer 3 (L3), where a band gap opens. This behaviour is similar to our pristine case Fig 4.11. In this case, the outermost layer presents a valence band with contributions of gold and chlorine, which mainly correspond to Au-d, Cl-p states and in short amount cesium. Meanwhile, the conduction band has the gold, chlorine and cesium contributions that have the Au-s, Au-d, Cl-p, Cl-d and Cs-d states. As in the previous case, the Fermi level is shifted to 0 eV and is represented by the vertical black line. As in the previous case, the orbital contributions are in appendix C.

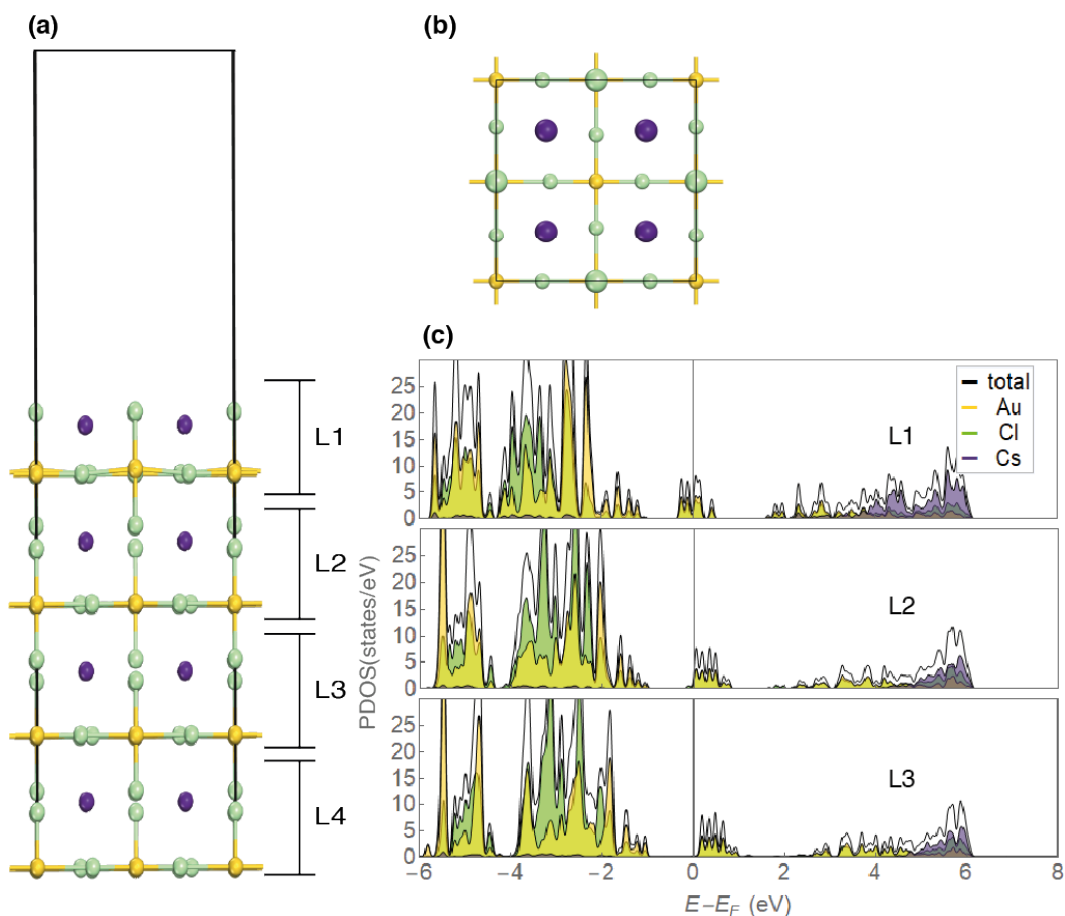


Figure 4.31: SCAN computed atomic and electronic structure for outermost layers of $\text{Cs}_2\text{Au}_2\text{Cl}_6$ with four layers of thickness and two chlorine vacancies (14b-2clvA). a) Side view of the atomic structure after relaxation, L1 is the surface layer, and L4 is the last layer. b) Top view of the surface. The black line represents the unit cell. c) PDOS of the outermost layers. The Fermi level is shifted to 0 eV and is represented by the vertical black line.

Simulated Ultraviolet Photoelectron Spectroscopy (UPS)

The UPS spectra was computed using 115 eV photons for $\text{Cs}_2\text{Au}_2\text{Cl}_6$ surface B with two chlorine vacancies at the surface (14b-2clvA) which correspond to photoelectrons generated at the first outermost atomic layer. The spectra of the Fig. 4.32 has a main peak around -2.90 eV, mainly composed of gold and chlorine. There is a peak at -5.07 eV and another at -6.64 eV, composed of gold and chlorine. The last peak is at -9.41 eV, represented by a full contribution of cesium

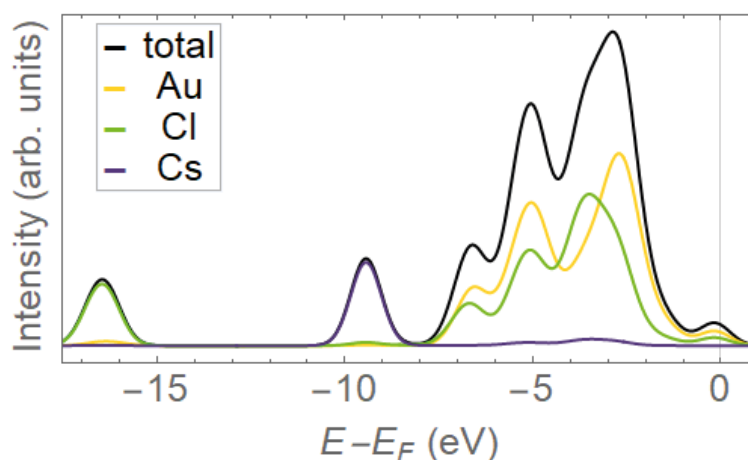


Figure 4.32: Computed UPS spectra for $\text{Cs}_2\text{Au}_2\text{Cl}_6$ surface B with two chlorine vacancies at the surface (l4b-2clvA). The strongest contribution is from the gold and chlorine atoms. The Fermi level is shifted to 0 eV, and is represented by the vertical black line.

4.6.4 Surface B with two B-type chlorine vacancies (l4b-2clvB)

In this subsection, the B case structure will be studied by removing the two chlorine atoms from the other position at the surface. So, the structure was prepared with a thickness of 4 layers, with gold and chlorine atoms at the top.

The vacuum used was 15 Å, and the position of the bottom layer was fixed, allowing to relax remaining atoms. It was used cut off energy of 650 eV, and $0.035 \text{ 2}\pi\text{Å}^{-1}$ of separation length, which correspond to the $3 \times 3 \times 1$ k-points. The surface structure is displayed in Fig. 4.33.

Removing two chlorine atoms from the surface produced a readjustment of the structure. It can be seen in Fig. 4.33 a) and b) that some bonds have been broken in the subsurface.

The PDOS shows that the surface has insulator behaviour, which is different from the pristine case that is metallic Fig 4.11. In this case, the outermost layer presents a valence band with contributions of gold and chlorine, which mainly correspond to Au-d, Cl-p states and in a short amount Cs-p. Meanwhile, the conduction band has the gold, chlorine and cesium contributions that have the Au-s, Au-d, Au-p, Cl-p and Cs-d states. As in the previous case, the orbital contributions are in appendix C.

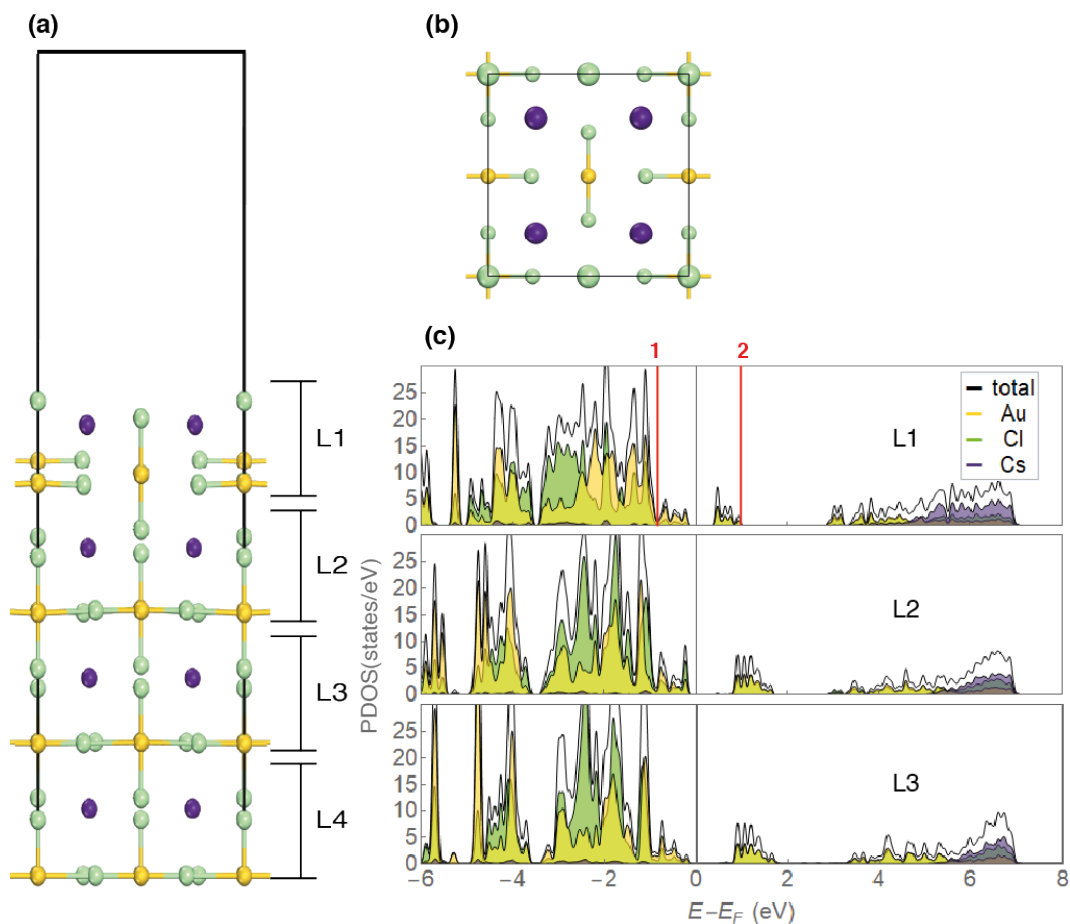


Figure 4.33: SCAN computed atomic and electronic structure for outermost layers of $\text{Cs}_2\text{Au}_2\text{Cl}_6$ with four layers of thickness and two chlorine vacancies (14b-2clvB). a) Side view of the atomic structure after relaxation, L1 is the surface layer, and L4 is the last layer. b) Top view of the surface. The black line represents the unit cell. c) PDOS of the outermost layers. The Fermi level is shifted to 0 eV and is represented by the vertical black line. The red lines (1 and 2) represent the range of integrated energies to obtain the STM images.

Simulated Constant Current (STM) images for $\text{Cs}_2\text{Au}_2\text{Cl}_6$ (14b-2clvB)

The range of energies used to compute the STM images was -0.85 eV to 1.0 eV, as shown in Fig. 4.33 part c. STM images presented in Fig. 4.34 were computed using a negative V_{bias} of -0.85 V. and a positive V_{bias} of 1.0 V. Furthermore, it is presented the relative height for each case.

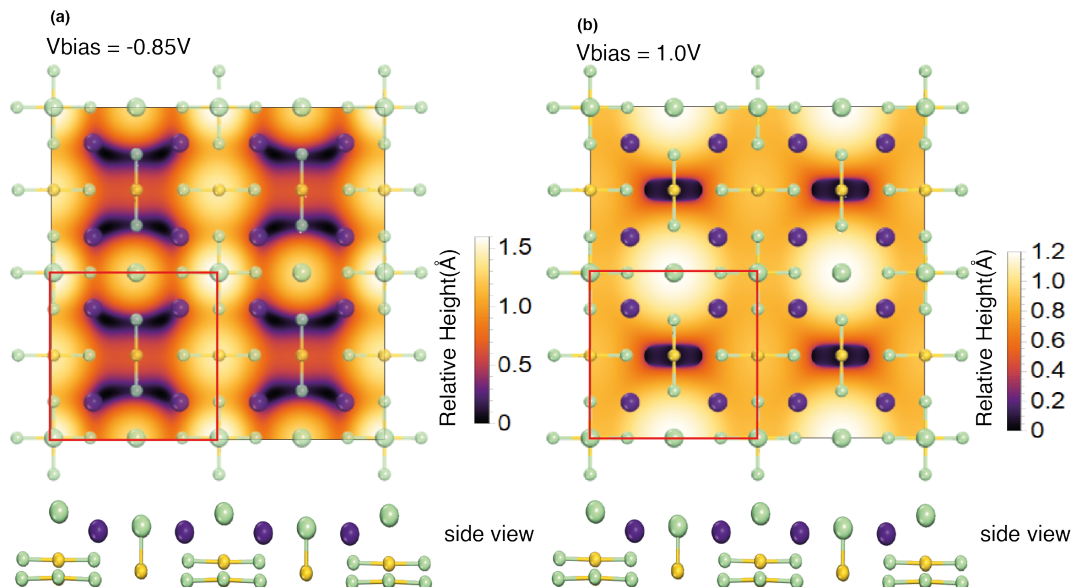


Figure 4.34: Computed STM images, line scan and relative height for $\text{Cs}_2\text{Au}_2\text{Cl}_6$ (14b-2clvB). These images were computed for a supercell of $2 \times 2 \times 1$, where $V_{bias} = -0.85\text{ V}$. (left) correspond to an occupied state and the $V_{bias} = 1.0\text{ V}$. (right) is at an unoccupied state. In both images is superimposed the top view of the atomic structure of the surface. The red box represents the unit cell, and at the bottom, there is a side view of the atomic structure of the surface. On the sides of the images, it is presented the relative height, which was calculated in the diagonal direction.

The bright spots represent the position of the superficial atoms and, in this case, correspond to the chlorine atoms. The darker spots correspond to cesium and the gold atoms below the surface.

Simulated Ultraviolet Photoelectron Spectroscopy (UPS)

The UPS spectra was computed using 115 eV photons for $\text{Cs}_2\text{Au}_2\text{Cl}_6$ surface B with two chlorine vacancies at the surface (14b-2clvB) which correspond to photoelectrons generated at the first outermost atomic layer. The spectra of the Fig. 4.35 has a main peak around -2.22 eV, mainly composed of gold and chlorine. There is a peak at -4.15 eV and a shoulder at -6.04 eV, composed of gold and chlorine. The last peak is at -8.28 eV, represented by a full contribution of cesium.

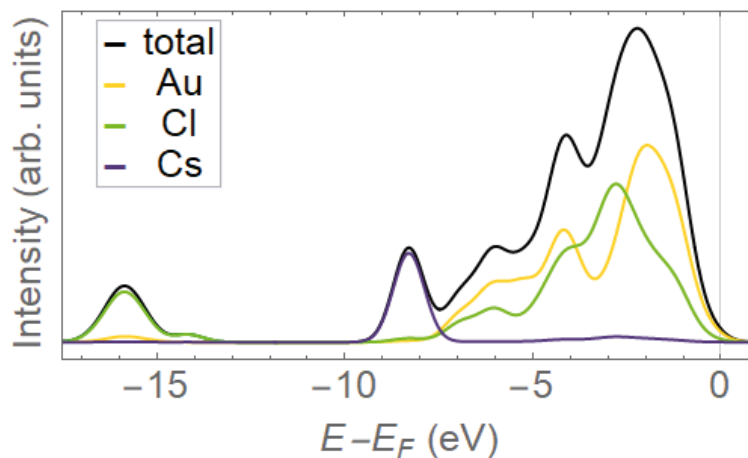


Figure 4.35: Computed UPS spectra for $\text{Cs}_2\text{Au}_2\text{Cl}_6$ surface B with two chlorine vacancies at the surface (14b-2clvB). The strongest contribution is from the gold and chlorine atoms. The Fermi level is shifted to 0 eV and is represented by the vertical black line.

4.6.5 Vacancy Energy Formation

This subsection presents Table 4.4 with the results of the vacancy energy formation of a point defect in solids for vacancies in surface B.

Table 4.4: Energy formation for each vacancy of $\text{Cs}_2\text{Au}_2\text{Cl}_6$ surface B. (14b-clvA) represents the case A chlorine vacancy at the surface. (14b-clvB) represents the case B chlorine vacancy at the surface. (14b-2clvA) is the vacancy formed by removing two chlorine atoms of case A at the surface B. (14b-2clvB) is the vacancy formed by removing two chlorine atoms of case B at the surface B.

Vacancy Type	Behaviour	Energy Formation (eV)
14b-clvA	metallic	18.29
14b-clvB	metallic	17.20
14b-2clvA	metallic	35.33
14b-2clvB	insulator	34.62

From this table, it is possible to see that the vacancy (14b-clvA) is the one that needs less energy to be produced, followed by (14b-clvB), (14b-2clvB) vacancies and the most difficult is the (14b-2clvA) vacancy because it is the one that needs the most energy to remove two chlorine atoms from the structure. It is also shown that of all the vacancies studied, only the (14b-2clvB) vacancy presents insulating behaviour; all the others are metallic.

4.6.6 Work Function (ϕ)

Table 4.5 presents a summary of the work function calculated for each case of the vacancies of the finished surface in cesium and chlorine. The graphs of the work functions are found in appendix D.

Table 4.5: Work Function (ϕ) for each vacancy of $\text{Cs}_2\text{Au}_2\text{Cl}_6$ surface B. (14b-clvA) represents the case A chlorine vacancy at the surface. (14b-clvB) represents the case B chlorine vacancy at the surface. (14b-2clvA) is the vacancy formed by removing two chlorine atoms of case A at the surface B. (14b-2clvB) is the vacancy formed by removing two chlorine atoms of case B at the surface B.

Vacancy Type	ϕ (eV)
14b-clvA	4.68
14b-clvB	3.54
14b-2clv2A	2.31
14b-2clv2B	3.89

From this table, the energy necessary to remove an electron from the surface is in the range of 2 eV to 5 eV. where the one that needs less energy is the vacancy (14b-2clv2A), followed by (14b-clvB), (14b-2clv2B) and (14b-clvA) in order from lowest to greatest difficulty to remove an electron.

Chapter 5

Conclusions & Outlook

In this thesis, we have performed DFT calculations using SCAN to explore the atomic and electronic structure of bulk and several surfaces of the metal halide double perovskite $\text{Cs}_2\text{Au}_2\text{Cl}_6$, including vacancies.

In the first part of the thesis, we studied the electronic properties of pristine bulk face-centered cubic $\text{Cs}_2\text{Au}_2\text{Cl}_6$. Here we determine the appropriate parameters for the calculations, such as the E_{cut} , k-points, and optimal slab thickness. After this, we perform calculations for the surfaces of $\text{Cs}_2\text{Au}_2\text{Cl}_6$ using the two kinds, type A (ended with gold and chlorine), which present an insulator behaviour and surface B (ended with chlorine and cesium) that is metallic. Then we create surfaces with chlorine defects, obtaining four different surface models for each case (type A and B). Of all these surfaces with vacancies, all type A surface vacancies showed a metallic behaviour except for (14a-2clv) structure, which is an insulator. In the same way, the vacancies of the type B surface all showed metallic behaviour, except for the (14b-2clvB) structure, which is an insulator. This conclusion was reached using the PDOS of the superficial layer of each structure, where we could see the contributions of all the atoms in each band (valence and conduction band). The atoms with a stronger contribution are gold and chlorine in all the cases; the contribution of cesium is small compared to the other elements.

We perform STM simulation images using the Tersoff-Hamann approximation of the surfaces where we have a band gap. In these images, it was possible to observe that in the surfaces finished in gold, this element is the dominant one, and in the case where the surface ends in chlorine, this element dominates. Furthermore, accompanying the STM images are relative height.

In the case where we had structures where we were left with an odd number of atoms by removing chlorine atoms, a calculation of the polarized spin was made for the most electronically stable structure. The result obtained from this was that the structures (14a-sclvA), (14b-clvB) with the exception of the structure (14a-clv) that presents a small magnetization whose value is $1.01 \mu_B$. We also made UPS simulations for each structure where gold and chlorine atoms contribute most. In each UPS graph, we talk about the position of each peak and the atomic contribution in each case.

Additionally, the formation energy was calculated for each structure with vacancies, from which it was found that the structures where it is possible to produce a defect are (14b-clvB) and (14a-clv) because they are the ones

that need the least energy. Finally, the work function was calculated for all the structures, of which (4a-sclvB) and (14b-2clv2A) are the ones that need less energy.

The most stable $\text{Cs}_2\text{Au}_2\text{Cl}_6$ surface model is the surface B, which was determined using the energy of the system, and it was found that the most stable is the surface B with a difference in the energy of 0.10 eV. We found that the most stable surfaces with vacancies are the (14a-clv), (14a-sclvB) for the surface A and (14b-clvB), (14b-2clvB) for vacancies for the surface B.

Finally, the results were obtained for metal halide double perovskite $\text{Cs}_2\text{Au}_2\text{Cl}_6$ that may lead to further experiments and DFT calculations. According to the formula $\text{A}_2\text{B}_2\text{X}_6$, there could be several materials that could have the perovskite structure. It is possible to perform the same calculations; for example, in the X_6 position could be elements such as bromine (Br) or iodine(I) and with these results determine which perovskite has the best properties.

Appendix A

Input and output files examples

Examples of input and output files used in the calculations for this work

```
SYSTEM = Cs2AuAuX6, X=Cl double perovskite
##### ELECTRONIC RX #####
ISMEAR = -5 ! -5 insulators&final energy 1 rx in metals
LREAL = auto
PREC = Accurate
ENCUT = 650
ALGO = N !N more accurate, F fast, VF fastest, D damped, A precondition (D,A for HF)
EMIN=-20
EMAX=10
##### FUNCTIONAL #####
METAGGA = SCAN
LMIXTAU = T
LASPH = T !use for LDA+U, hybrid or meta-GGA in f- and 3d-elements
##### DIPOLE CORRECTIONS #####
IDIPOL=3 ! 3 is for surfaces
LDIPOL= T
```

Figure A.1: INCAR file example. It is possible to observe several tags with their assigned value for electronic relaxation, functionals, and dipole corrections to be used in the calculations. These tags determine what to do and how to do the calculations in VASP.¹

```

Au Cl Cs
1.0000000000000000
7.4452999999999996 0.0000000000000000 0.0000000000000000
0.0000000000000000 7.4452999999999996 0.0000000000000000
0.0000000000000000 0.0000000000000000 34.5234999999999985
Au Cl Cs
8 24 8
Selective dynamics
Direct
0.0000000000000000 0.0000000000000000 0.0917000000000032 F F F
0.0000000000000000 -0.0000000000000000 0.4079084322472288 T T T
0.5000000000000000 0.5000000000000000 0.2497064957899165 T T T
0.5000000000000000 0.5000000000000000 0.5670979604799044 T T T
0.0000000000000000 -0.0000000000000000 0.2499479064645471 T T T
0.0000000000000000 -0.0000000000000000 0.5633482794290566 T T T
0.5000000000000000 0.5000000000000000 0.0917000000000032 F F F
0.5000000000000000 0.5000000000000000 0.4079594116785893 T T T
0.7790299999999988 0.7790299999999988 0.0917000000000032 F F F

```

Figure A.2: POSCAR file example. At the top, we have the name of our system. Next is the scaling constant, which scales the lattice vectors. From the third to the fifth line, the lattice vectors are presented. Below we have the species of atoms present in our system; something important point is that the order in which they are presented must be the same order in which they are found in the POTCAR file to avoid errors. The next line shows the number of atoms for each species mentioned in the previous line. The next two lines represent the restrictions on the movement of the atoms and the way the atomic coordinates are presented; in this case, we use direct(fractional) coordinates. Finally, all the atomic positions are presented, accompanied by their respective movement restriction.²

```

kpoints for 001, dk=0.035 1/Ang
0
Gamma
4 4 1
0 0 0

```

Figure A.3: K-POINTS file example. As a first-line, we have our study system. Next, we have that the k points are 0, which will cause the mesh to be generated automatically. Below we have to generate a Gamma-centered mesh. The fourth line shows the number of desired subdivisions for our case. Furthermore, the last line is used when we want to perform a mesh shift.³

```

40 40 0 0
0.4784309E+02 0.7445300E-09 0.7445300E-09 0.3452350E-08 0.5000000E-15
1.000000000000000E-004
CAR
Cs2AuAuX6, X=Cl double perovskite
10.00000000 -20.00000000 301 -1.27500000 1.00000000
-20.000 0.0000E+00 0.8000E+02
-19.900 0.0000E+00 0.8000E+02
-19.800 0.0000E+00 0.8000E+02
-19.700 0.0000E+00 0.8000E+02
-19.600 0.0000E+00 0.8000E+02
-19.500 0.0000E+00 0.8000E+02
-19.400 0.0000E+00 0.8000E+02
-19.300 0.0000E+00 0.8000E+02
-19.200 0.0000E+00 0.8000E+02

```

Figure A.4: DOSCAR file example. DOSCAR file is an output file. In its first line, we have the number of ions (including empty spheres), number of ions, 0 (not partial DOS) or 1 (partial DOS). The next line has the unit cell's volume along with the basis vectors' length (a,b,c). The third line presents the initial temperature. Below we have the system's name as given by the tag SYSTEM in the INCAR file. In the sixth line, values correspond to the energy range given by the DOS, the number of grid points, the Fermi energy level, and 1 as a value. Then all this is followed by the columns energy, DOS, integrated DOS.⁴

N	E	dE	d eps	ncg	rms	rms(c)
DAV: 1	0.591166791722E+04	0.59117E+04	-0.17849E+05	3256	0.167E+03	
DAV: 2	0.554543544348E+03	-0.53571E+04	-0.51068E+04	4200	0.764E+02	
DAV: 3	-0.992533083798E+03	-0.15471E+04	-0.14934E+04	5312	0.446E+02	
DAV: 4	-0.124713441565E+04	-0.25460E+03	-0.24719E+03	4984	0.243E+02	
DAV: 5	-0.127467673230E+04	-0.27542E+02	-0.27020E+02	5480	0.686E+01	0.751E+01
DAV: 6	-0.109944282930E+04	0.17523E+03	-0.39976E+02	5064	0.110E+02	0.439E+01
DAV: 7	-0.110104913178E+04	-0.16063E+01	-0.45381E+01	5192	0.376E+01	0.102E+01
DAV: 8	-0.110071209516E+04	0.33704E+00	-0.52755E+00	5328	0.118E+01	0.513E+00
DAV: 9	-0.110078468202E+04	-0.72587E-01	-0.46818E-01	5072	0.468E+00	0.391E+00
DAV: 10	-0.110076385624E+04	0.20826E-01	-0.19538E-01	4616	0.234E+00	0.205E+00
DAV: 11	-0.110076162562E+04	0.22306E-02	-0.85026E-02	5008	0.158E+00	0.747E-01
DAV: 12	-0.110076020430E+04	0.14213E-02	-0.21626E-02	5000	0.105E+00	0.442E-01
DAV: 13	-0.110075990008E+04	0.30423E-03	-0.70401E-03	4536	0.339E-01	0.234E-01

Figure A.5: OSZICAR file example. OSZICAR file is an output file which gives information about convergence speed and the current step. In the first line, we have N, which represents the number of electronic steps, E is the current free energy, dE is the change in the free energy from the last to the current step and d eps is the change in the band structure energy.⁵

Appendix B

Atomic and electronic structure of $\text{Cs}_2\text{Au}_2\text{Cl}_6$ with 6 layers

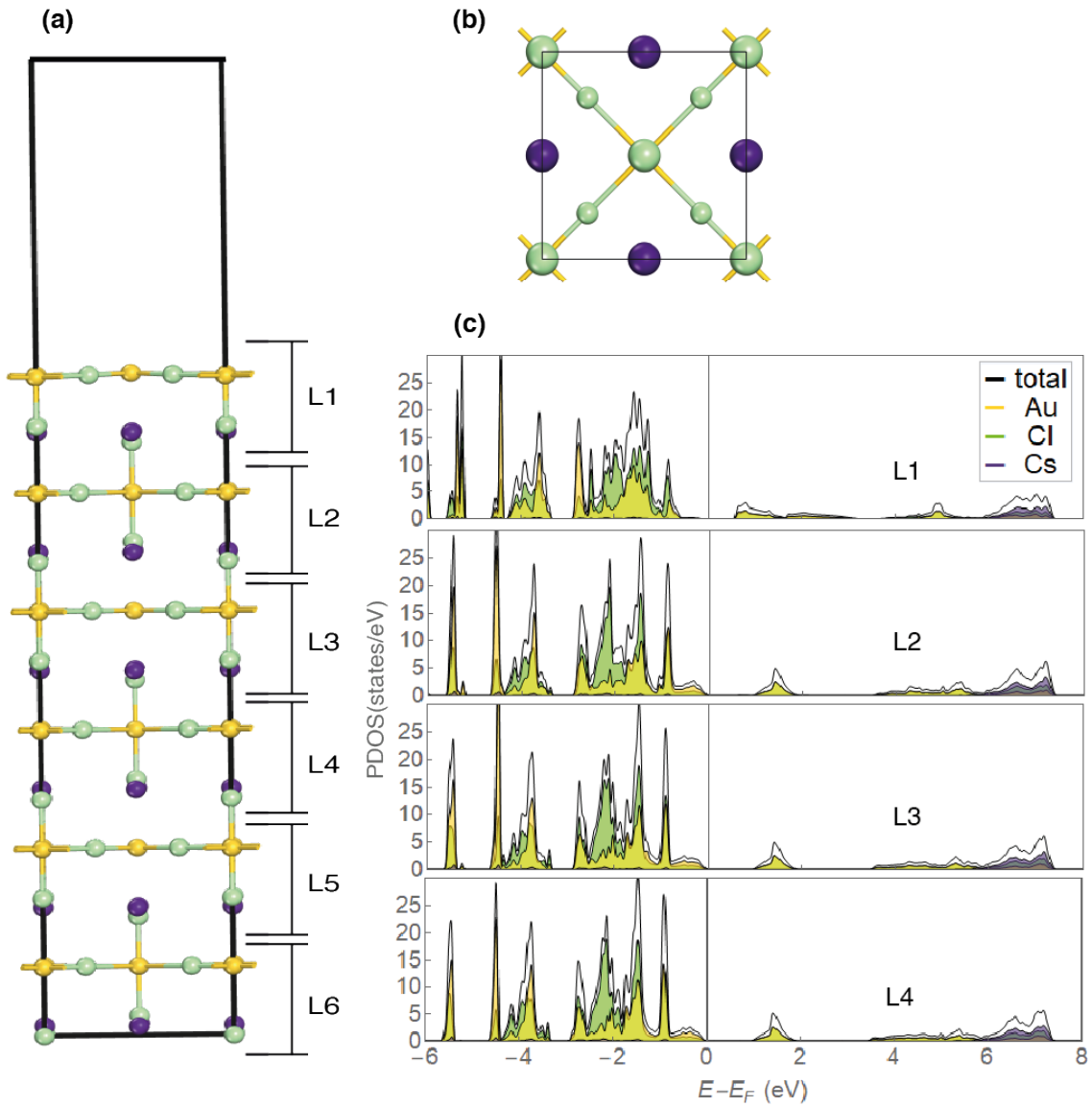


Figure B.1: SCAN computed atomic and electronic structure for outermost layers of $\text{Cs}_2\text{Au}_2\text{Cl}_6$ with six layers thickness type A (16a). a) Side view of the atomic structure after relaxation, L1 is the surface layer, and L4 is the last layer. b) Top view of the surface. The black line represents the unit cell. c) PDOS of the outermost layers. The Fermi level is shifted to 0 eV and is represented by the vertical black line.

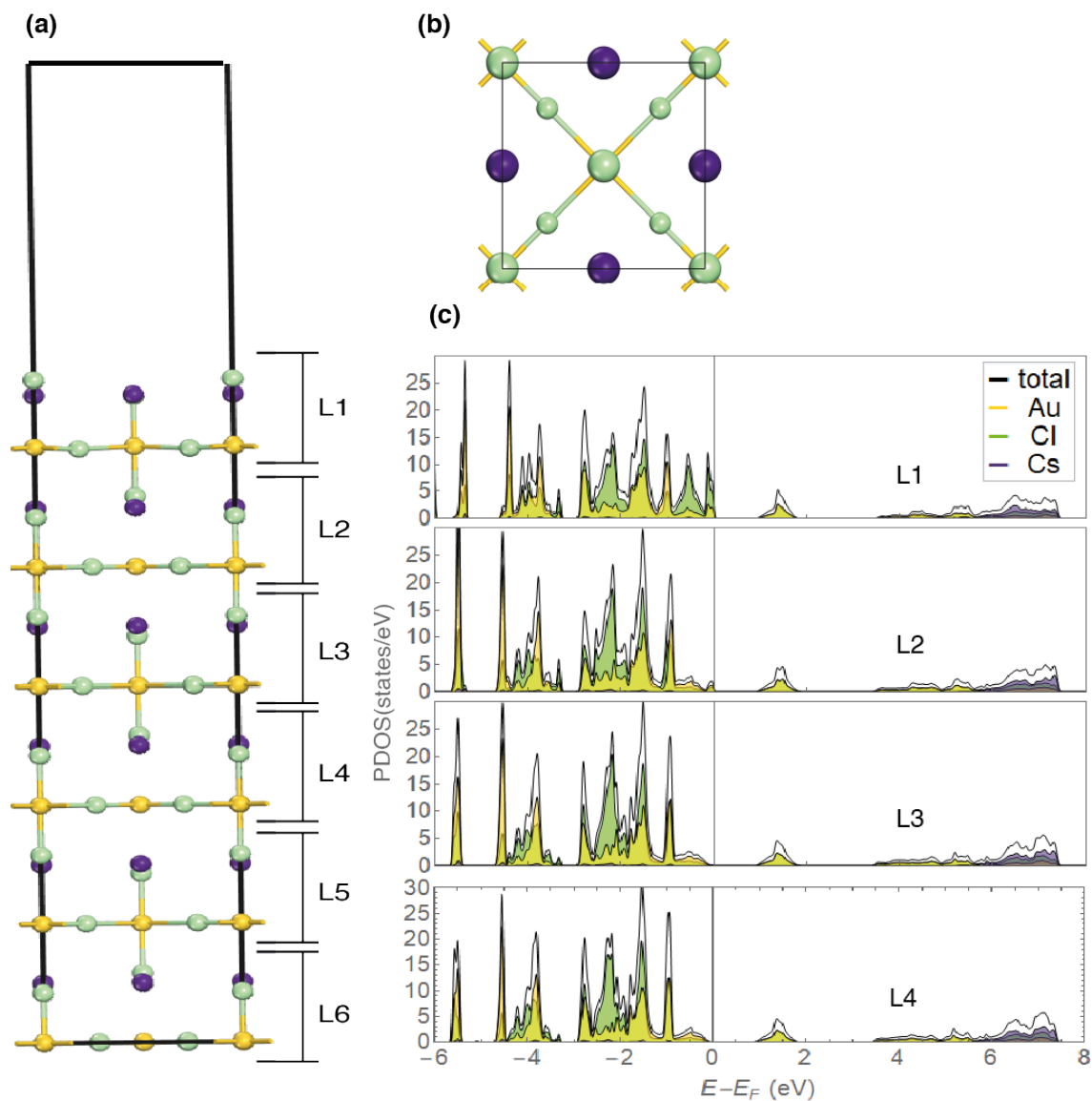


Figure B.2: SCAN computed atomic and electronic structure for outermost layers of $\text{Cs}_2\text{Au}_2\text{Cl}_6$ with six layers thickness type B (16b). a) Side view of the atomic structure after relaxation, L1 is the surface layer, and L4 is the last layer. b) Top view of the surface. The black line represents the unit cell. c) PDOS of the outermost layers. The Fermi level is shifted to 0 eV and is represented by the vertical black line.

Appendix C

Detailed computed PDOS for all the surfaces

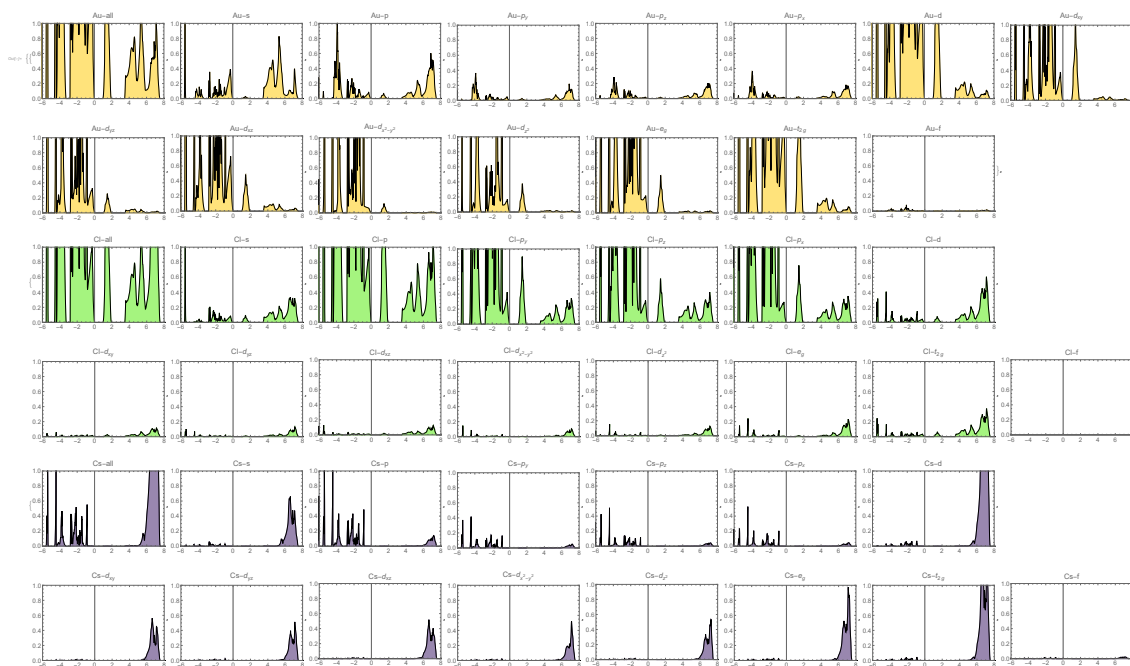


Figure C.1: Detailed PDOS for $\text{Cs}_2\text{Au}_2\text{Cl}_6$ surface A (14a) computed with SCAN, where the states of each orbital are shown. On the horizontal axis are the $E - E_F$, and on the vertical are states/eV.

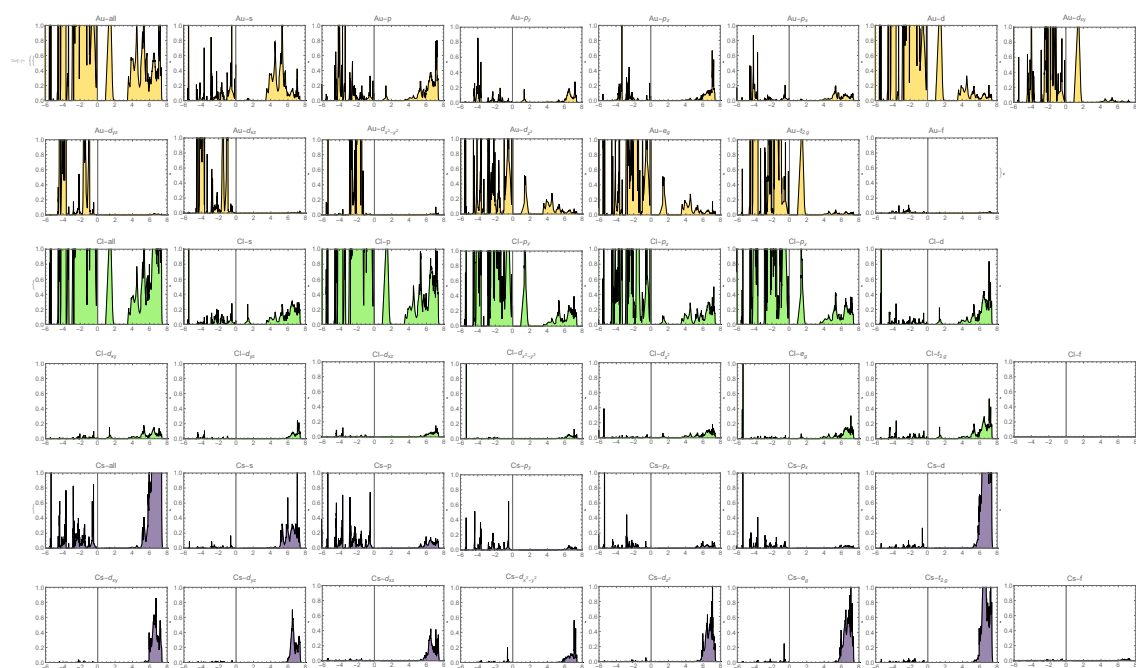


Figure C.2: Detailed PDOS for $\text{Cs}_2\text{Au}_2\text{Cl}_6$ surface B (14b) computed with SCAN, where the states of each orbital are shown. On the horizontal axis are the $E - E_F$, and on the vertical are states/eV.

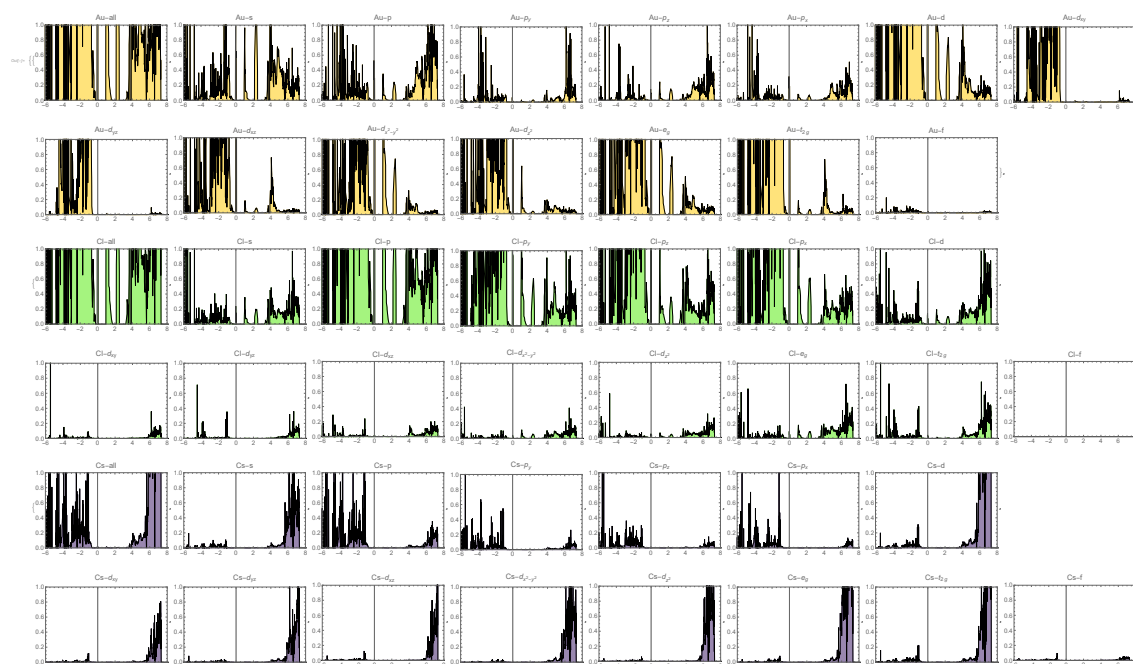


Figure C.3: Detailed PDOS for $\text{Cs}_2\text{Au}_2\text{Cl}_6$ surface A with one A-type chlorine vacancy (14a-clv) computed with SCAN, where the states of each orbital are shown. On the horizontal axis are the $E - E_F$, and on the vertical are states/eV.

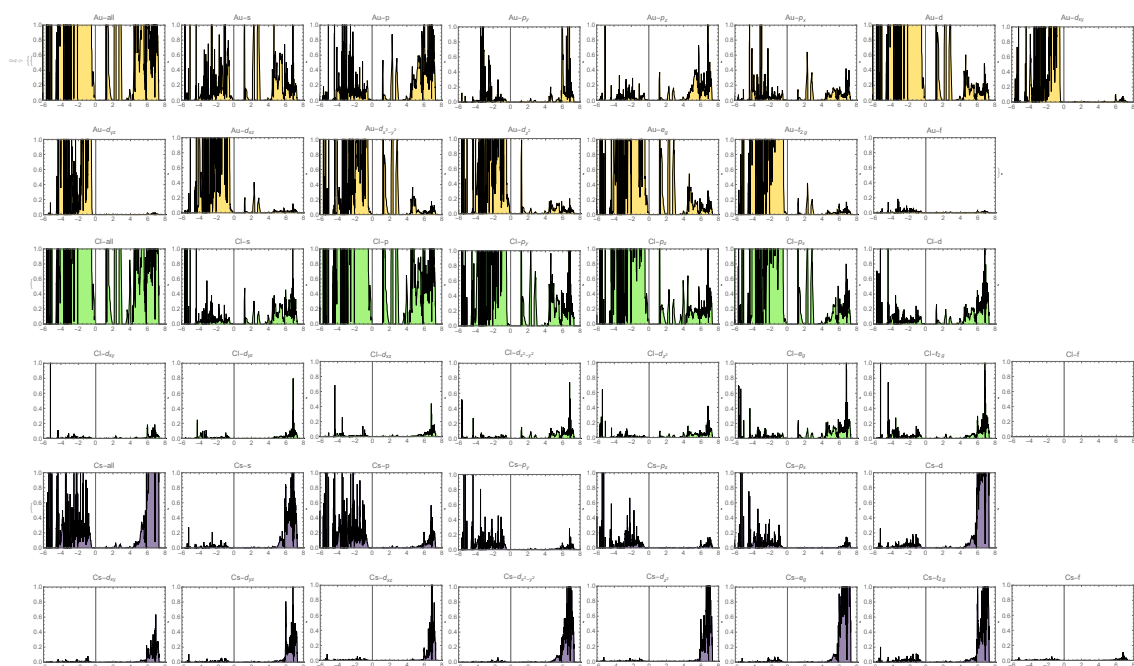


Figure C.4: Detailed PDOS for $\text{Cs}_2\text{Au}_2\text{Cl}_6$ surface A with two A-type chlorine vacancies at the surface (14a-2clv) computed with SCAN, where the states of each orbital are shown. On the horizontal axis are the $E - E_F$ and on the vertical are states/eV.

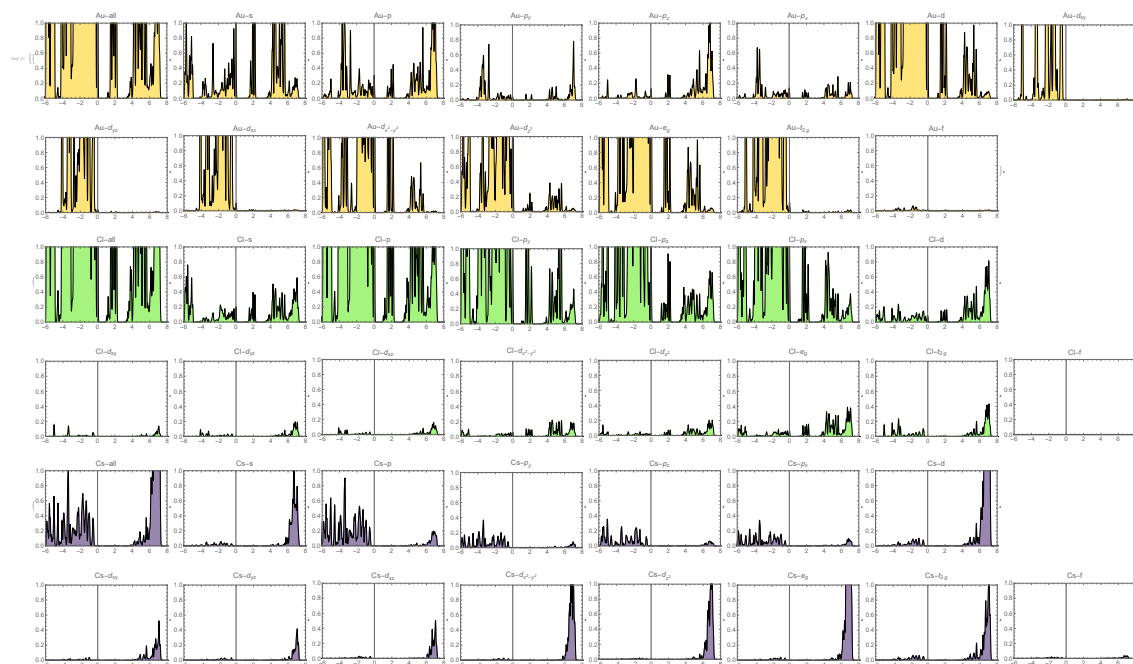


Figure C.5: Detailed PDOS for $\text{Cs}_2\text{Au}_2\text{Cl}_6$ surface A with one A-type chlorine vacancy at the sub surface (14a-sclvA) computed with SCAN, where the states of each orbital are shown. On the horizontal axis are the $E - E_F$, and on the vertical are states/eV.

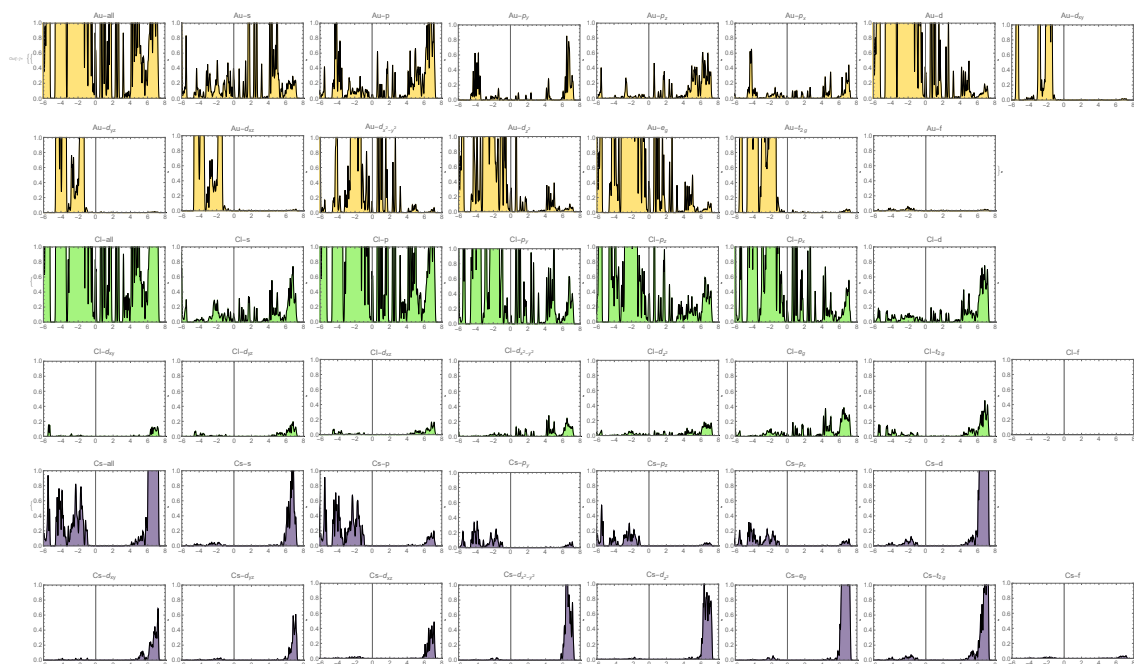


Figure C.6: Detailed PDOS for $\text{Cs}_2\text{Au}_2\text{Cl}_6$ surface A with one B chlorine vacancy at the sub surface (l4a-sclvB) computed with SCAN, where the states of each orbital are shown. On the horizontal axis are the $E - E_F$, and on the vertical are states/eV.

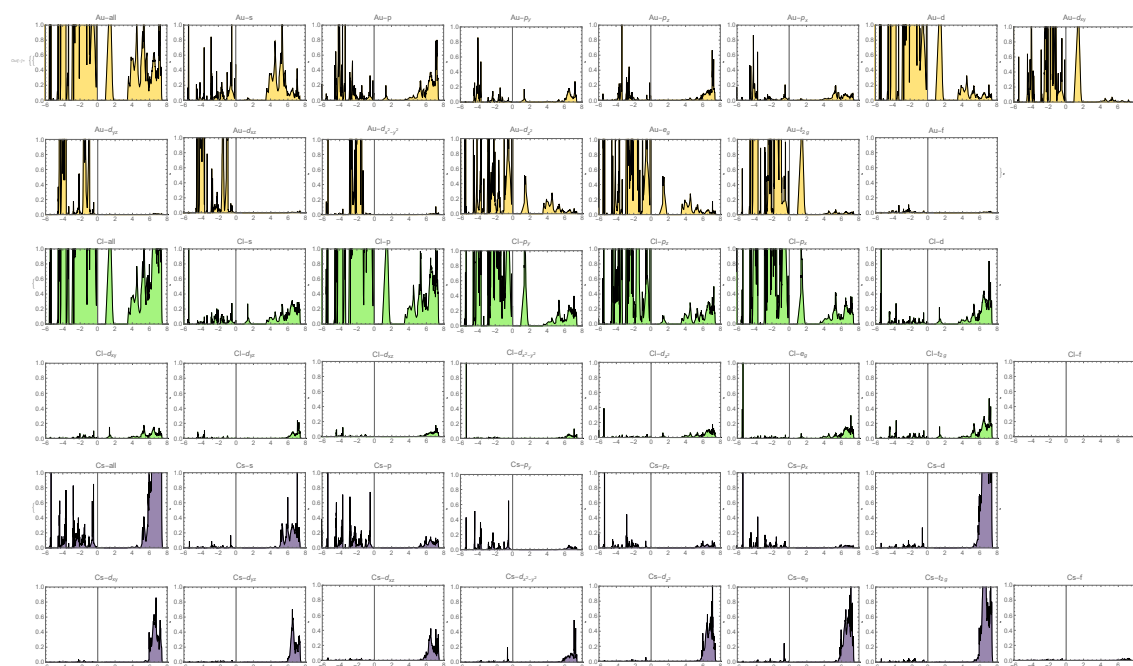


Figure C.7: Detailed PDOS for $\text{Cs}_2\text{Au}_2\text{Cl}_6$ surface B with one A-type chlorine vacancy at the surface (14b-clvA) computed with SCAN, where the states of each orbital are shown. On the horizontal axis are the $E - E_F$, and on the vertical are states/eV.

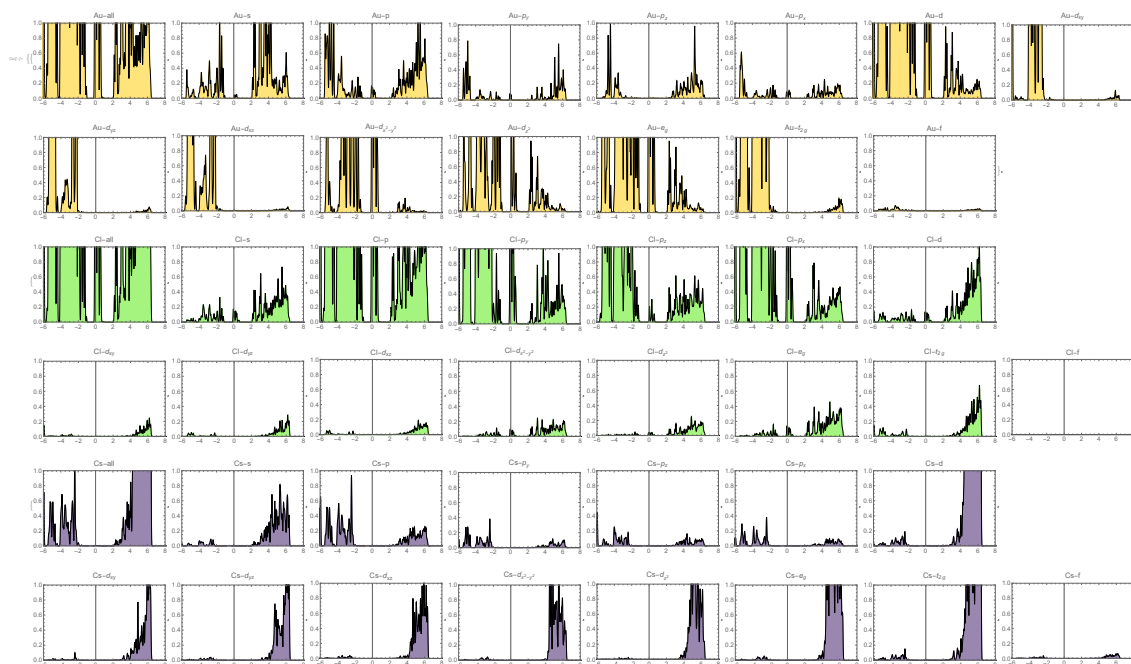


Figure C.8: Detailed PDOS for $\text{Cs}_2\text{Au}_2\text{Cl}_6$ surface B with one B type chlorine vacancy at the surface (14b-clvB) computed with SCAN, where the states of each orbital are shown. On the horizontal axis are the $E - E_F$, and on the vertical are states/eV.

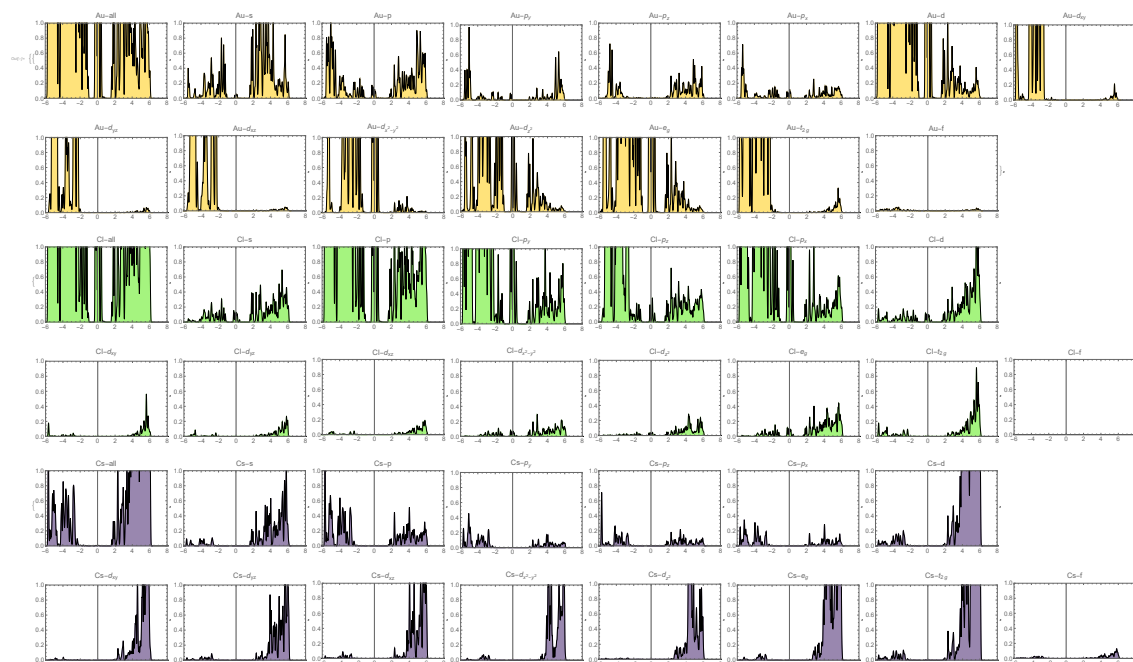


Figure C.9: Detailed PDOS for $\text{Cs}_2\text{Au}_2\text{Cl}_6$ surface B with two type-A chlorine vacancies at the surface (14b-2clv2A) computed with SCAN, where the states of each orbital are shown. On the horizontal axis are the $E - E_F$ and on the vertical are states/eV.

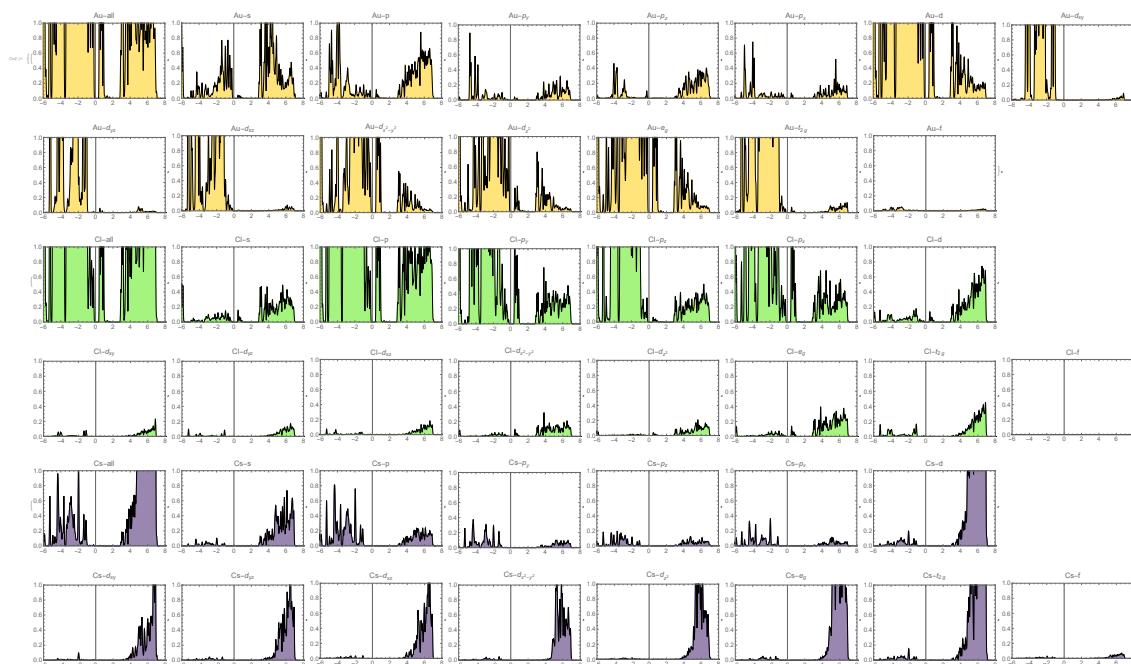


Figure C.10: Detailed PDOS for $\text{Cs}_2\text{Au}_2\text{Cl}_6$ surface B with two type B chlorine vacancies at the surface (14b-2clv2B) computed with SCAN, where the states of each orbital are shown. On the horizontal axis are the $E - E_F$, and on the vertical are states/eV.

Appendix D

Computed work functions (ϕ) for vacancies

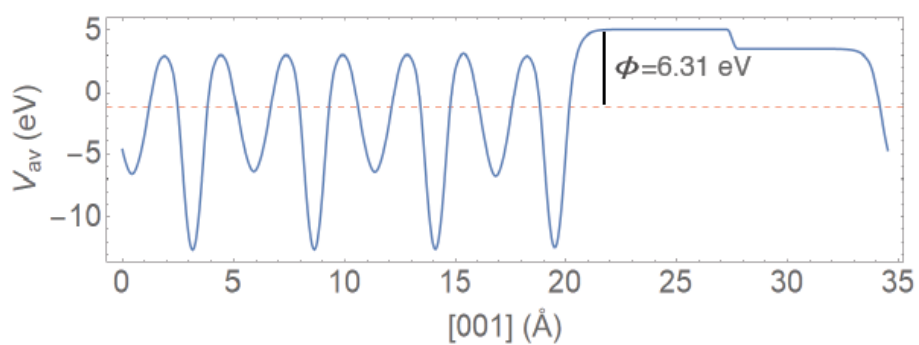


Figure D.1: SCAN computed work function for $\text{Cs}_2\text{Au}_2\text{Cl}_6$ surface A with one A-type chlorine vacancy (14a-clv). The blue line represents the average potential in the z-direction, and the horizontal red dotted line is the Fermi level E_F .

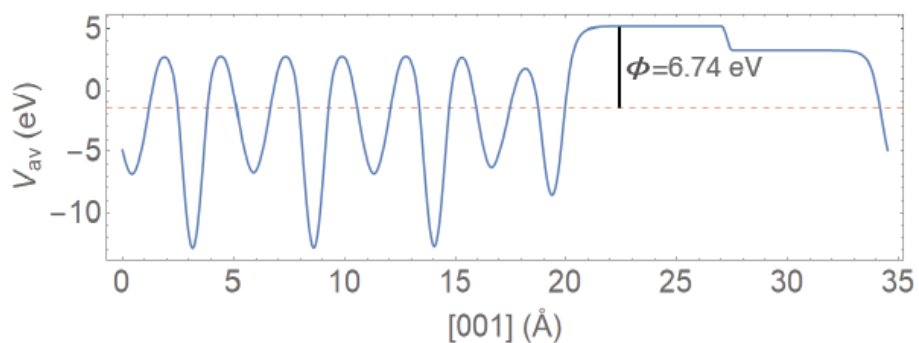


Figure D.2: SCAN computed work function for $\text{Cs}_2\text{Au}_2\text{Cl}_6$ surface A with two A-type chlorine vacancies at the surface (l4a-2clv). The blue line represents the average potential in the z-direction, and the horizontal red dotted line is the Fermi level E_F

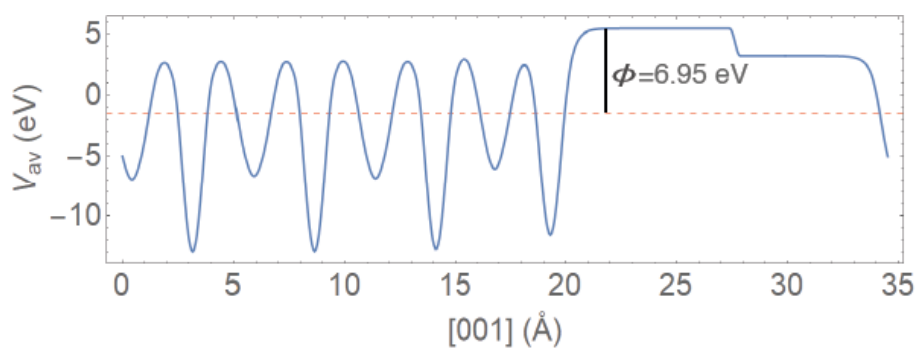


Figure D.3: SCAN computed work function for $\text{Cs}_2\text{Au}_2\text{Cl}_6$ surface A with one A-type chlorine vacancy at the sub surface (l4a-sclvA). The blue line represents the average potential in the z-direction, and the horizontal red dotted line is the Fermi level E_F

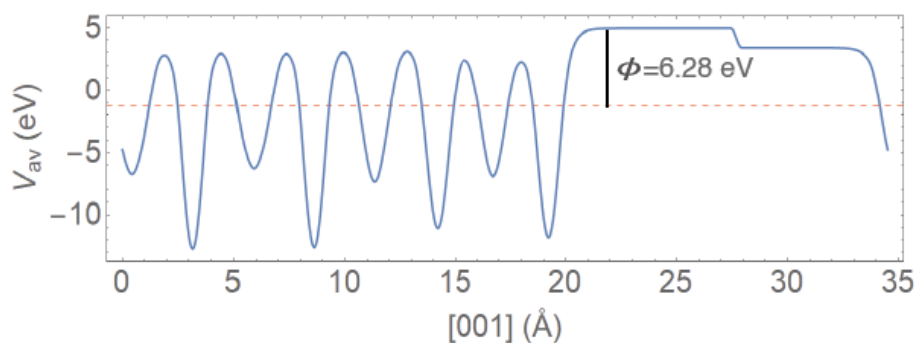


Figure D.4: SCAN computed work function for $\text{Cs}_2\text{Au}_2\text{Cl}_6$ surface A with one B type chlorine vacancy at the sub surface (l4a-sclvB). The blue line represents the average potential in the z-direction, and the horizontal red dotted line is the Fermi level E_F

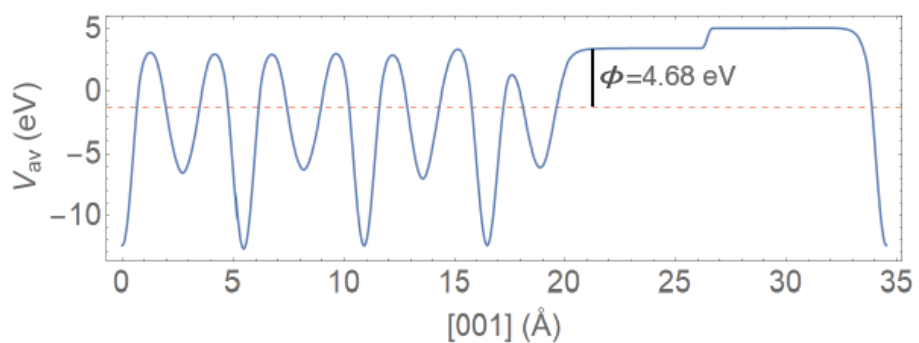


Figure D.5: SCAN computed work function for $\text{Cs}_2\text{Au}_2\text{Cl}_6$ surface B with one A-type chlorine vacancy at the surface (l4b-clvA). The blue line represents the average potential in the z-direction, and the horizontal red dotted line is the Fermi level E_F

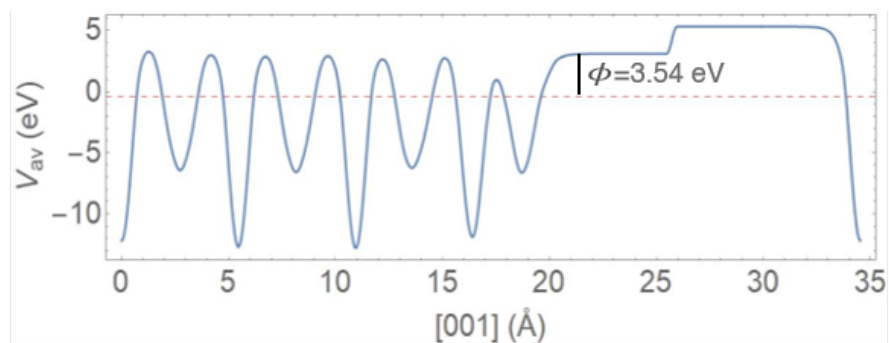


Figure D.6: SCAN computed work function for $\text{Cs}_2\text{Au}_2\text{Cl}_6$ surface B with one B type chlorine vacancy at the surface (14b-clvB). The blue line represents the average potential in the z-direction, and the horizontal red dotted line is the Fermi level E_F

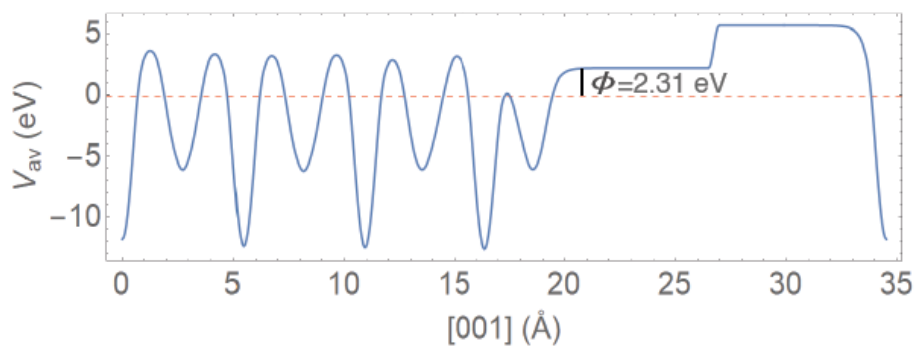


Figure D.7: SCAN computed work function for $\text{Cs}_2\text{Au}_2\text{Cl}_6$ surface B with two type-A chlorine vacancy at the surface (14b-2clv2A). The blue line represents the average potential in the z-direction, and the horizontal red dotted line is the Fermi level E_F

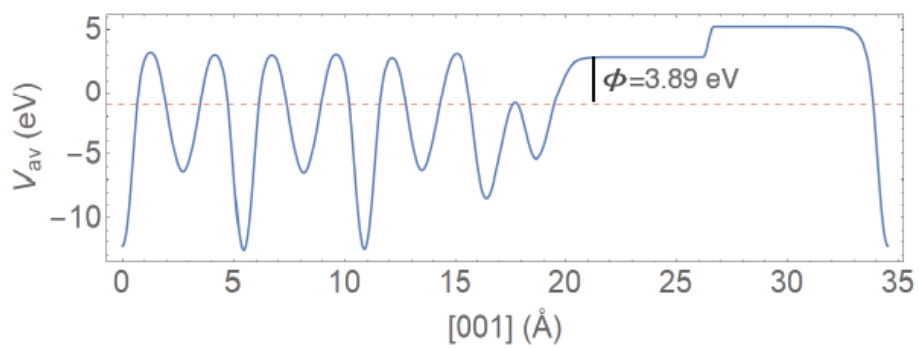


Figure D.8: SCAN computed work function for $\text{Cs}_2\text{Au}_2\text{Cl}_6$ surface B with two type B chlorine vacancy at the surface (14b-2clv2B). The blue line represents the average potential in the z -direction, and the horizontal red dotted line is the Fermi level E_F .

Bibliography

- [1] VASP, INCAR. 2022; <https://www.vasp.at/wiki/index.php/INCAR>, 13 de Abril de 2022.
- [2] VASP, POSCAR. 2022; <https://www.vasp.at/wiki/index.php/POSCAR>, 13 de Abril de 2022.
- [3] VASP, KPOINTS. 2022; <https://www.vasp.at/wiki/index.php/KPOINTS>, 13 de Abril de 2022.
- [4] VASP, DOSCAR. 2022; <https://www.vasp.at/wiki/index.php/DOSCAR>, 13 de Abril de 2022.
- [5] VASP, OSZICAR. 2022; <https://www.vasp.at/wiki/index.php/OSZICAR>, 13 de Abril de 2022.
- [6] Wu, Y.; Wang, P.; Wang, S.; Wang, Z.; Cai, B.; Zheng, X.; Chen, Y.; Yuan, N.; Ding, J.; Zhang, W.-H. Heterojunction Engineering for High Efficiency Cesium Formamidinium Double-Cation Lead Halide Perovskite Solar Cells. *ChemSusChem* **2018**, *11*, 837–842.
- [7] Xiao, Z.; Yan, Y. Progress in theoretical study of metal halide perovskite solar cell materials. *Advanced Energy Materials* **2017**, *7*, 1701136.
- [8] Bajorowicz, B.; Mikolajczyk, A.; Pinto, H. P.; Miodynska, M.; Lisowski, W.; Klimczuk, T.; Kaplan-Ashiri, I.; Kazes, M.; Oron, D.; Zaleska-Medynska, A. Integrated experimental and theoretical approach for efficient design and synthesis of gold-based double halide perovskites. *The Journal of Physical Chemistry C* **2020**, *124*, 26769–26779.
- [9] Moritomo, Y.; Xu, S.; Machida, A.; Akimoto, T.; Nishibori, E.; Takata, M.; Sakata, M. Electronic structure of double-perovskite transition-metal oxides. *Physical Review B* **2000**, *61*, R7827.
- [10] Kobayashi, K.-I.; Kimura, T.; Sawada, H.; Terakura, K.; Tokura, Y. Room-temperature magnetoresistance in an oxide material with an ordered double-perovskite structure. *Nature* **1998**, *395*, 677–680.
- [11] Li, Z.; Yin, W. Recent progress in Pb-free stable inorganic double halide perovskites. *Journal of Semiconductors* **2018**, *39*, 071003.
- [12] Tennyson, E. M.; Doherty, T. A.; Stranks, S. D. Heterogeneity at multiple length scales in halide perovskite semiconductors. *Nature Reviews Materials* **2019**, *4*, 573–587.

- [13] Giustino, F. *Materials modelling using density functional theory: properties and predictions*; Oxford University Press, 2014.
- [14] Nations, U. Sustainable Development Goals. 2022; <https://www.un.org/sustainabledevelopment/es/objetivos-de-desarrollo-sostenible/>, 13 de Abril de 2022.
- [15] Patterson, J. D.; Bailey, B. C. *Solid-state physics: introduction to the theory*; Springer Science & Business Media, 2007.
- [16] Gross, A. Theoretical surface science. *A Microscopic Perspective. Originally published in the series: Advanced Texts in Physics*, **2003**, 132.
- [17] Kohn, W.; Vashishta, P. General density functional theory. *Theory of the Inhomogeneous Electron gas* **1983**, 79–147.
- [18] Hohenberg, P.; Kohn, W. Inhomogeneous electron gas. *Physical review* **1964**, 136, B864.
- [19] Lee, J. G. *Computational materials science: an introduction*; CRC press, 2016.
- [20] Mardirossian, N.; Head-Gordon, M. Thirty years of density functional theory in computational chemistry: an overview and extensive assessment of 200 density functionals. *Molecular Physics* **2017**, 115, 2315–2372.
- [21] Sun, J.; Furness, J. W.; Zhang, Y. *Mathematical Physics in Theoretical Chemistry*; Elsevier, 2019; pp 119–159.
- [22] Sun, J.; Remsing, R. C.; Zhang, Y.; Sun, Z.; Ruzsinszky, A.; Peng, H.; Yang, Z.; Paul, A.; Waghmare, U.; Wu, X.; et al, Accurate first-principles structures and energies of diversely bonded systems from an efficient density functional. *Nature chemistry* **2016**, 8, 831–836.
- [23] Sun, J.; Ruzsinszky, A.; Perdew, J. P. Strongly constrained and appropriately normed semilocal density functional. *Physical review letters* **2015**, 115, 036402.
- [24] Sholl, D.; Steckel, J. A. *Density functional theory: a practical introduction*; John Wiley & Sons, 2011.
- [25] Lejaeghere, K.; Bihlmayer, G.; Björkman, T.; Blaha, P.; Blügel, S.; Blum, V.; Caliste, D.; Castelli, I. E.; Clark, S. J.; Dal Corso, A.; et al, Reproducibility in density functional theory calculations of solids. *Science* **2016**, 351, aad3000.
- [26] Mohr, S.; Ratcliff, L. E.; Genovese, L.; Caliste, D.; Boulanger, P.; Goedecker, S.; Deutsch, T. Accurate and efficient linear scaling DFT calculations with universal applicability. *Physical Chemistry Chemical Physics* **2015**, 17, 31360–31370.
- [27] Kantorovich, L. *Quantum theory of the solid state: an introduction*; Springer Science & Business Media, 2004; Vol. 136.
- [28] Wisesa, P.; McGill, K. A.; Mueller, T. Efficient generation of generalized Monkhorst-Pack grids through the use of informatics. *Physical Review B* **2016**, 93, 155109.

- [29] Monkhorst, H. J.; Pack, J. D. Special points for Brillouin-zone integrations. *Physical review B* **1976**, *13*, 5188.
- [30] Brázdová, V.; Bowler, D. R. *Atomistic computer simulations: a practical guide*; John Wiley & Sons, 2013.
- [31] Cohen, M. L.; Heine, V. *Solid state physics*; Elsevier, 1970; Vol. 24; pp 37–248.
- [32] Hafner, J. Ab-initio simulations of materials using VASP: Density-functional theory and beyond. *Journal of computational chemistry* **2008**, *29*, 2044–2078.
- [33] Louie, S. G.; Froyen, S.; Cohen, M. L. Nonlinear ionic pseudopotentials in spin-density-functional calculations. *Physical Review B* **1982**, *26*, 1738.
- [34] Blöchl, P. E. Projector augmented-wave method. *Physical review B* **1994**, *50*, 17953.
- [35] VASP, POTCAR. 2022; <https://www.vasp.at/wiki/index.php/POTCAR>, 13 de Abril de 2022.
- [36] VASP, CONTCAR. 2022; <https://www.vasp.at/wiki/index.php/CONTCAR>, 13 de Abril de 2022.
- [37] VASP, OUTCAR. 2022; <https://www.vasp.at/wiki/index.php/OUTCAR>, 13 de Abril de 2022.
- [38] VASP, WAVECAR. 2022; <https://www.vasp.at/wiki/index.php/WAVECAR>, 13 de Abril de 2022.
- [39] Liu, M. *Controlled Synthesis and Scanning Tunneling Microscopy Study of Graphene and Graphene-Based Heterostructures*; Springer, 2017.
- [40] Voigtländer, B. *Scanning probe microscopy: Atomic force microscopy and scanning tunneling microscopy*; Springer, 2015.
- [41] Lab, H. Research Overview. 2022; <https://hoffman.physics.harvard.edu/index.html>, 13 de Abril de 2022.
- [42] Hofer, W. A Guide to simulation of STM images and spectra from first principles: bSKAN 3.6. *Surface Science Research Centre, The University of Liverpool, Liverpool, UK* **2005**, 60.
- [43] Woodruff, D. P. *Modern techniques of surface science*; Cambridge university press, 2016.
- [44] Yeh, J.; Lindau, I. Atomic subshell photoionization cross sections and asymmetry parameters: 1 Z 103. *Atomic data and nuclear data tables* **1985**, *32*, 1–155.
- [45] Schaible, M. J.; Pinto, H. P.; McKee, A. D.; Leszczynski, J.; Orlando, T. M. Characterization and simulation of natural pyrite surfaces: a combined experimental and theoretical study. *The Journal of Physical Chemistry C* **2019**, *123*, 26397–26405.
- [46] Tanuma, S.; Powell, C. J.; Penn, D. R. Electron inelastic mean free paths in solids at low energies. *Journal of Electron Spectroscopy and Related Phenomena* **1990**, *52*, 285–291.
- [47] Averill, B.; Eldredge, P. *General chemistry: principles, patterns, and applications*; 2011.

-
- [48] Freysoldt, C.; Grabowski, B.; Hickel, T.; Neugebauer, J.; Kresse, G.; Janotti, A.; Van de Walle, C. G. First-principles calculations for point defects in solids. *Reviews of modern physics* **2014**, *86*, 253.
- [49] Zhang, S.; Northrup, J. E. Chemical potential dependence of defect formation energies in GaAs: Application to Ga self-diffusion. *Physical review letters* **1991**, *67*, 2339.
- [50] Van de Walle, C. G.; Laks, D.; Neumark, G.; Pantelides, S. First-principles calculations of solubilities and doping limits: Li, Na, and N in ZnSe. *Physical Review B* **1993**, *47*, 9425.
- [51] Tyuterev, V.; Vast, N. Murnaghan's equation of state for the electronic ground state energy. *Computational materials science* **2006**, *38*, 350–353.
- [52] WMD-group, MacroDensity. 2021; <https://github.com/WMD-group/MacroDensity>, 13 de Abril de 2022.
- [53] WMD-group, Ionisation potential of a bulk material. 2021; <https://github.com/WMD-group/MacroDensity/blob/master/tutorials/Slab/SlabCalculation.ipynb>, 13 de Abril de 2022.